TGAL-87-4

MISCELLANEOUS STUDIES IN DECOUPLING

I.N. Gupta, K.L. McLaughlin, R.A. Wagner, T.W. McElfresh, and M.E. Marshall

Teledyne Geotech Alexandria Laboratories
314 Montgomery Street
Alexandria, Virginia 22314-1581

NOVEMBER 1987

ANNUAL REPORT: October 1986 - October 1987
ARPA ORDER NO: 4435
PROJECT TITLE: Miscellaneous Discrimination Studies
CONTRACT: F08606-85-C-0022

Prepared For:
DEFENSE ADVANCED RESEARCH PROJECTS AGENCY
1400 Wilson Boulevard
Arlington, VA 22209

Monitored By:
AFTAC/TTR
PATRICK AFB
FLORIDA 32925-6001

UNCLASSIFIED
SECURITY CLASSIFICATION OF THIS PAGE

ADA194991

REPORT DOCUMENTATION PAGE

Form Approved
OMB No. 0704-0188
Exp. Date: Jun 30, 1986

1a. REPORT SECURITY CLASSIFICATION Unclassified	1b RESTRICTIVE MARKINGS N/A
2a SECURITY CLASSIFICATION AUTHORITY N/A	3 DISTRIBUTION / AVAILABILITY OF REPORT Approved for public release; distribution is unlimited.
2b DECLASSIFICATION / DOWNGRADING SCHEDULE N/A	
4 PERFORMING ORGANIZATION REPORT NUMBER(S) TGAL-87-4	5. MONITORING ORGANIZATION REPORT NUMBER(S) N/A
6a NAME OF PERFORMING ORGANIZATION Teledyne Geotech Alexandria Laboratories 6b OFFICE SYMBOL (If applicable)	7a. NAME OF MONITORING ORGANIZATION AFTAC/TTR
6c. ADDRESS (City, State, and ZIP Code) 314 Montgomery Street Alexandria, VA 22314	7b. ADDRESS (City, State, and ZIP Code) Patrick Air Force Base Florida 32925-6001
8a. NAME OF FUNDING / SPONSORING ORGANIZATION DARPA 8b. OFFICE SYMBOL (If applicable) NMRO	9. PROCUREMENT INSTRUMENT IDENTIFICATION NUMBER F08606-85C-0022
8c. ADDRESS (City, State, and ZIP Code) 1400 Wilson Blvd. Arlington, VA 22209	10. SOURCE OF FUNDING NUMBERS PROGRAM ELEMENT NO: 62714E; PROJECT NO.: DT/5121; TASK NO.: 1; WORK UNIT ACCESSION NO.: N/A
11. TITLE (Include Security Classification) Miscellaneous Studies in Decoupling (U)	
12. PERSONAL AUTHOR(S) I.N. Gupta, K.L. McLaughlin, R.A. Wagner, T.W. McElfresh, M.E. Marshall	
13a. TYPE OF REPORT Annual Report 13b. TIME COVERED FROM Mar 85 TO Sep 87	14. DATE OF REPORT (Year, Month, Day) November 1987 15. PAGE COUNT 103
16. SUPPLEMENTARY NOTATION → Keywords:	

17. COSATI CODES		
FIELD	GROUP	SUB-GROUP
08	11	
17	10	

18. SUBJECT TERMS (Continue on reverse if necessary and identify by block number)
Decoupling; Scaled depth; Regional phases; strain and frequency-dependent Lg Q Strain dependent, Contours;

19. ABSTRACT (Continue on reverse if necessary and identify by block number)

A. COMPARISON OF SYNTHETIC AND OBSERVED SEISMOGRAMS

Synthetic responses for plane layered model applicable for paths from Salmon to distances of 16 and 32 km (the same source-receiver distances as for stations 10S and 20S, respectively) are computed by using the wavenumber integration method. Several arrivals in the synthetics agree well with the observed data and the synthetic seismograms help identify the beginning of the S wavetrains on the records at both 10S and 20S. Seismic moment of Salmon, derived by a comparison of the peak amplitudes on the observed and theoretical seismograms, agrees remarkably well with the value obtained from near-field data.

B. ANALYSIS OF PROJECT COWBOY STRONG-MOTION DATA → next page

Near-field data from coupled and decoupled explosions in salt, acquired under Project Cowboy, are analyzed by obtaining the RVP spectra corrected for frequency-dependent

20 DISTRIBUTION / AVAILABILITY OF ABSTRACT ☐ UNCLASSIFIED/UNLIMITED ☒ SAME AS RPT ☐ DTIC USERS	21. ABSTRACT SECURITY CLASSIFICATION Unclassified
22a NAME OF RESPONSIBLE INDIVIDUAL Capt. Donald A. Hirst	22b. TELEPHONE (Include Area Code) (305) 494-5236 22c OFFICE SYMBOL TTR

DD FORM 1473, 84 MAR 83 APR edition may be used until exhausted
All other editions are obsolete

SECURITY CLASSIFICATION OF THIS PAGE
UNCLASSIFIED

(19 Continued)

geometrical spreading. Limited data suggest strain and frequency-dependent attenuation, similar to the results from strong-motion data from Salmon and Sterling.

C. EFFECT OF SCALED DEPTH ON REGIONAL PHASES

Spectral characteristics of the regional phases Pn, Pg, and Lg are studied for several NTS explosions covering a large range of yields and scaled depths. A new parameter, Effective Scaled Depth (ESD), defined as the ratio of shot depth to the estimated elastic radius, is introduced; it is a measure of scaled depth that has been corrected for the variation in overburden pressure with shot depth. Data from a common recording station indicate the mean Pn/Lg and Pg/Lg spectral slopes to be most dependent on ESD, somewhat less on scaled depth, and the least on shot depth. The spectral shapes of Pn and Pg are significantly more dependent on ESD and scaled depth than on shot depth. The enrichment of higher frequencies due to increased ESD (or scaled depth) is the largest in the spectra of Pn, somewhat less for Pg, and the least for Lg. The low-frequency asymptote and the area under the initial pulse of deconvolved Pn also show much greater dependence on scaled depth and ESD than on shot depth.

A comparison of inter-event spectral ratios of Pn, Pg, and Lg for shots with nearly equal yields but different ESD or scaled depths shows significant differences. Similar variations are observed if PSRV response spectra based on Pn and the entire seismogram are compared. These results imply that scaling of the nuclear seismic-source function may vary significantly from one regional phase to another. Therefore, scaling relationships based on the entire seismogram (e.g. Mueller and Murphy, 1971), generally dominated by the Lg wavetrain, may not be appropriate for Pn.

D. DECONVOLUTION AND SPECTRAL RATIOS FROM SOVIET SALT SHOTS

The maximum-likelihood multichannel deconvolution method of Shumway and Der (1985) is applied to teleseismic P waves from ten salt shots in the Astrakhan region of the USSR. The data used came from the GBA array and the four RSTN stations, RSON, RSNT, RSNY, and RSSD. The deconvolved source functions for each shot show clear P and pP arrivals separated by about 1 sec, suggesting large shot depths. There are also several arrivals which consistently show up between the P and pP, similar to those observed for Salmon. These earlier reflections may be due to strong impedance contrasts, such as those in a salt dome environment. Single-station deconvolutions for the four salt shots of October 16, 1982 recorded at the two SRO stations ANMO and KONO are also obtained with similar results. The last shot in the sequence of October 16, 1982 appears to be anomalous with respect to the three earlier shots, as evidenced by comparison of mean amplitude ratios of P and P-coda, spectral ratio slopes of P, and P/P-coda spectral slopes. A possible reason appears to be alteration of shot medium due to close proximity of an earlier shot.

E. ANALYSIS OF DATA FROM SOVIET SALT SHOTS WITH KNOWN YIELDS

Teleseismic P arrivals from three USSR salt explosions with known yields and shot depths and recorded at the LRSM stations NP-NT and RK-ON are analyzed. Of the three Soviet shots, only two (22 April 1966 and 1 July 1968) were very near each other so that the propagation path effects may be considered to be the same. A comparison of their P and P-coda spectral ratios at both stations with von Seggern and Blandford scaling for salt indicates the shot medium to be somewhat "softer" than the Salmon salt. The deconvolution method of Shumway and Der (1985) is applied to the vertical and radial component records at NP-NT of all three USSR shots. The deconvolved source terms for only the two deeper (and larger scaled depth) explosions show clear evidence of P and pP arrivals. The average ratio P/P-coda values are larger for explosions with larger scaled depths, perhaps because an overburied shot is likely to generate less near-source coda than an underburied shot.

MISCELLANEOUS STUDIES IN DECOUPLING

SUMMARY

A. COMPARISON OF SYNTHETIC AND OBSERVED SEISMOGRAMS

Synthetic responses for plane layered model applicable for paths from Salmon to distances of 16 and 32 km (the same source-receiver distances as for stations 10S and 20S, respectively) are computed by using the wavenumber integration method. Several arrivals in the synthetics agree well with the observed data and the synthetic seismograms help identify the beginning of the S wavetrains on the records at both 10S and 20S. Seismic moment of Salmon, derived by a comparison of the peak amplitudes on the observed and theoretical seismograms, agrees remarkably well with the value obtained from near-field data.

B. ANALYSIS OF PROJECT COWBOY STRONG-MOTION DATA

Near-field data from coupled and decoupled explosions in salt, acquired under Project Cowboy, are analyzed by obtaining the RVP spectra corrected for frequency-dependent geometrical spreading. Limited data suggest strain and frequency-dependent attenuation, similar to the results from strong-motion data from Salmon and Sterling.

C. EFFECT OF SCALED DEPTH ON REGIONAL PHASES

Spectral characteristics of the regional phases Pn, Pg, and Lg are studied for several NTS explosions covering a large range of yields and scaled depths. A new parameter, Effective Scaled Depth (ESD), defined as the ratio of shot depth to the estimated elastic radius, is introduced; it is a measure of scaled depth that has been corrected for the variation in overburden pressure with shot depth. Data from a common recording station indicate the mean Pn/Lg and Pg/Lg spectral slopes to be most dependent on ESD, somewhat less on scaled depth, and the least on shot depth. The spectral shapes of Pn and Pg are significantly more dependent on ESD

and scaled depth than on shot depth. The enrichment of higher frequencies due to increased ESD (or scaled depth) is the largest in the spectra of Pn, somewhat less for Pg, and the least for Lg. The low-frequency asymptote and the area under the initial pulse of deconvolved Pn also show much greater dependence on scaled depth and ESD than on shot depth.

A comparison of inter-event spectral ratios of Pn, Pg, and Lg for shots with nearly equal yields but different ESD or scaled depths shows significant differences. Similar variations are observed if PSRV response spectra based on Pn and the entire seismogram are compared. These results imply that scaling of the nuclear seismic-source function may vary significantly from one regional phase to another. Therefore, scaling relationships based on the entire seismogram (e.g. Mueller and Murphy, 1971), generally dominated by the Lg wavetrain, may not be appropriate for Pn.

D. DECONVOLUTION AND SPECTRAL RATIOS FROM SOVIET SALT SHOTS

The maximum-likelihood multichannel deconvolution method of Shumway and Der (1985) is applied to teleseismic P waves from ten salt shots in the Astrakhan region of the USSR. The data used came from the GBA array and the four RSTN stations, RSON, RSNT, RSNY, and RSSD. The deconvolved source functions for each shot show clear P and pP arrivals separated by about 1 sec, suggesting large shot depths. There are also several arrivals which consistently show up between the P and pP, similar to those observed for Salmon. These earlier reflections may be due to strong impedance contrasts, such as those in a salt dome environment. Single-station deconvolutions for the four salt shots of October 16, 1982 recorded at the two SRO stations ANMO and KONO are also obtained with similar results. The last shot in the sequence of October 16, 1982 appears to be anomalous with respect to the three earlier shots, as evidenced by comparison of mean amplitude ratios of P and P-coda, spectral ratio slopes of P, and P/P-coda spectral slopes. A possible reason appears to be

weakening of shot medium due to close proximity of an earlier shot.

E. ANALYSIS OF DATA FROM SOVIET SALT SHOTS WITH KNOWN YIELDS

Teleseismic P arrivals from three USSR salt explosions with known yields and shot depths and recorded at the LRSM stations NP-NT and RK-ON are analyzed. Of the three Soviet shots, only two (22 April 1966 and 1 July 1968) were very near each other so that the propagation path effects may be considered to be the same. A comparison of their P and P-coda spectral ratios at both stations with von Seggern and Blandford scaling for salt indicates the shot medium to be somewhat "softer" than the Salmon salt. The deconvolution method of Shumway and Der (1985) is applied to the vertical and radial component records at NP-NT of all three USSR shots. The deconvolved source terms for only the two deeper (and larger scaled depth) explosions show clear evidence of P and pP arrivals. The average ratio P/P-coda values are larger for explosions with larger scaled depths, perhaps because an overburied shot is likely to generate less near-source coda than an underburied shot.

(THIS PAGE INTENTIONALLY LEFT BLANK)

TABLE OF CONTENTS

LIST OF FIGURES

(THIS PAGE INTENTIONALLY LEFT BLANK)

INTRODUCTION

One of the most difficult problems in the detection and discrimination of underground nuclear explosions is that posed by the evasion possibilities of decoupled detonations. Of crucial importance is the spectral shapes of the decoupled versus coupled or tamped explosions and the mechanism responsible for the differences on their records at regional and teleseismic distances. The Russians have conducted a large number of explosions in salt under their Peaceful Nuclear Explosions (PNE) program. These explosions in salt are still continuing, as evidenced by the two shots of April 19, 1987, in the Urals Mountains region. It is possible that some of the smaller explosions in salt were decoupled. It is therefore important to understand the seismic waves generated by Soviet explosions in salt. With these objectives, we have been carrying out a number of miscellaneous studies related to decoupling. Our earlier work has already been reported in two annual reports (Gupta et al., 1986a, and Gupta et al., 1986b).

In Gupta et al. (1986a), analyses of available data from Salmon, the decoupled shot Sterling, and the high-explosive Sterling Calibration shot recorded at USCGS stations 10S and 20S and the USGS station PL-MS (at shot-receiver distances of 16, 32, and 27 km, respectively) were carried out to further our understanding of the decoupling of explosions in salt. The spectra and spectral ratios were obtained for both P and the surface-wave group, Lg, for signal windows of various lengths. The results confirmed the earlier findings of Blandford and Woolson (1979) indicating: (1) reduced decoupling at higher frequencies for both P and Lg, and (2) relatively greater decoupling for Lg than for P at high frequencies. At each station, the spectral ratio P/Lg was found to have a more positive slope for the decoupled explosion Sterling than for the tamped shot Salmon.

An attempt was made to determine why the decoupling ratio is different for P and the surface-wave group, Lg. The theoretical work of Cisternas (1964) shows that for Rayleigh

waves produced by the application of pressure at the walls of spherical cavities whose centers are at a fixed depth from the free surface, the larger the volume, the greater the enrichment of high frequencies. In other words, for the generation of surface waves, larger volume sources have shallower "effective" source depths. For a fixed source function, one would therefore expect that, in comparison to Sterling, a considerably larger volume around the shot point was involved in the generation of surface waves by Salmon so that Lg (Salmon) should be richer in high frequencies than Lg (Sterling), as observed. Further support for this explanation comes from the observed increase of the spectral ratio Pn/Lg with scaled depth for 7 Pahute Mesa explosions recorded at the LRSM station KNUT.

A comparison of the spectral ratio P/P-coda at teleseismic distances with the spectral ratio Pn/Lg at regional distances, for NTS explosions, shows that the two are similar in their dependence on "effective" scaled depth. Variations in the mean spectral slope of P/P-coda may therefore be diagnostic of variations in the spectral ratio Pn/Lg or P/Lg similar to those observed for the tamped explosion Salmon and the decoupled shot Sterling. Teleseismic P arrivals recorded at RKON and NPNT from 4 Azgir salt explosions covering the magnitude range of m_b = 4.7 to 5.5 were analyzed. The spectral ratios P/P-coda were found to be more positive (indicating P to be richer in high-frequency energy as compared to P-coda) for the two smallest shots than for the other two larger explosions. It is therefore likely that the two smallest shots were overburied or possibly decoupled. These preliminary results suggest a method for distinguishing between decoupled and normal explosions by comparing the spectral ratios Pn/Lg on regional data and/or P/P-coda on teleseismic data.

A summary of work in Gupta et al. (1986b) follows:

An understanding of the frequency dependence of decoupling is essential for monitoring nuclear explosions detonated in large underground cavities. Analysis of available data from the

nuclear explosions Salmon (5.3 kt in salt) and Sterling (0.38 kt shot in the cavity created by Salmon) recorded at shot-receiver distances of 16, 32, and 27 km, confirmed the earlier findings of Blandford and Woolson (1979) indicating: (1) reduced decoupling of Sterling at higher frequencies for both P and "Lg," and (2) relatively greater decoupling of Sterling for Lg than for P at high frequencies. In an attempt to understand why the frequency dependence of the decoupling ratio is different for P and the Lg group, we examined the spectral content of Pn and Lg from 7 Pahute Mesa, NTS explosions covering a wide range of scaled depths and recorded at a common station, KN-UT. The spectral ratio Pn/Lg varied strongly with scaled depth, mainly due to significantly greater dependence on scaled depth of the spectra of Pn than of Lg. These results are in agreement with those from Salmon and Sterling with scaled depths of 475 and 1145 $m/(kt)^{1/3}$, respectively. A possible reason for the decoupling at higher frequencies to be different for P and Lg is therefore the greater scaled depth of decoupled shots. The larger variability of Pn spectra than those of Lg can be due to an explosion (especially those that are not overburied) approximating a pressurized ellipsoid cavity with major axis in the vertical direction so that the source function is more variable for down-going waves comprising Pn than for others making up Lg. The spectral ratio Pn/Lg may be useful in discriminating between decoupled (or overburied) and normal shots.

The amplitude and spectra of teleseismic and regional seismic P waves depend on the material properties in the source region. The effects of strain and frequency dependent attenuation are therefore important for understanding the source characteristics of coupled versus decoupled explosions. Near-field velocity and acceleration data from the Salmon and Sterling explosions in salt were analyzed for strain and frequency dependent attenuation. Attenuation, parameterized as 1/Q, was estimated for various source-receiver distance ranges and frequency bandwidths by using two methods: (a) mean spectral ratio slope and (b) average amplitude spectral ratio. Results from Salmon indicate that (1) in the frequency range of 1-25 Hz, Q is

about 5 to 10; (2) Q increases with source-receiver distance, suggesting lower Q for larger strain levels; (3) Q in the frequency range of 25-50 Hz is substantially higher than in the frequency range of 1-25 Hz, or Q increases with frequency. Analysis of data from Sterling indicates that Q is frequency independent and about one order of magnitude larger than for Salmon. Therefore the near-source attenuation was strain and frequency dependent and hence non-linear for Salmon out to a range of 600 m.

Most of the work during the current year was directed towards the following five tasks:

(A) Comparison of synthetic seismograms for Salmon with the observed data,

(B) Analysis of near-field data from paired cavity-detonated and coupled (tamped) explosions in salt recorded under Project Cowboy,

(C) Effect of scaled depth on regional phases by analyzing data from NTS shots with known yields and depths,

(D) Deconvolution and spectral ratios of P waves from Soviet salt explosions recorded at arrays and stations at teleseismic distances, and

(E) Analysis of teleseismic data from Russian salt explosions of known yields.

A. COMPARISON OF SYNTHETIC AND OBSERVED SEISMOGRAMS

Theoretical Seismograms

Using wavenumber integration, responses for plane layered earth model appropriate for paths within 32 km from Salmon and Sterling were computed (C. A. Langston, written communication). The sampling rate is 20/sec so that the Nyquist frequency is 10 Hz. The earth model (Table A1) was based on Springer's (1966) Model D which is essentially derived from Warren et al.'s (1966) refraction results in the area. The attenuation parameter Q for P waves, Q_P, is assumed to be twice that for S waves, i.e. $Q_P = 2\ Q_S$.

TABLE A1

EARTH MODEL USED FOR SYNTHETIC SEISMOGRAMS

Thickness (km)	P-wave Velocity (km/sec)	Q_P	S-wave Velocity (km/sec)	Q_S	Density (gm/cc)
0.70	2.75	500	1.40	250	1.8
0.40	3.00	500	1.50	250	1.9
0.40	4.00	500	2.00	250	2.3
1.60	3.70	500	1.80	250	2.0
6.00	5.00	500	3.00	250	2.6

The displacement field from the simplest of sources - namely, the unidirectional unit impulse, which is localized precisely in both space and time, is the elastodynamic Green function (Aki and Richards, 1980). Displacement from realistic source models can therefore be obtained by synthesizing appropriate Green's functions. The synthetics for source-receiver distance of 16 km (the same as for records at station 10S) are shown in Figures A1, A2, and A3 for Salmon, Sterling, and Green's function. A seismic moment of 1×10^{20} dyne-cm is assumed for each source. Salmon and Sterling have Brune source functions with corner frequencies of

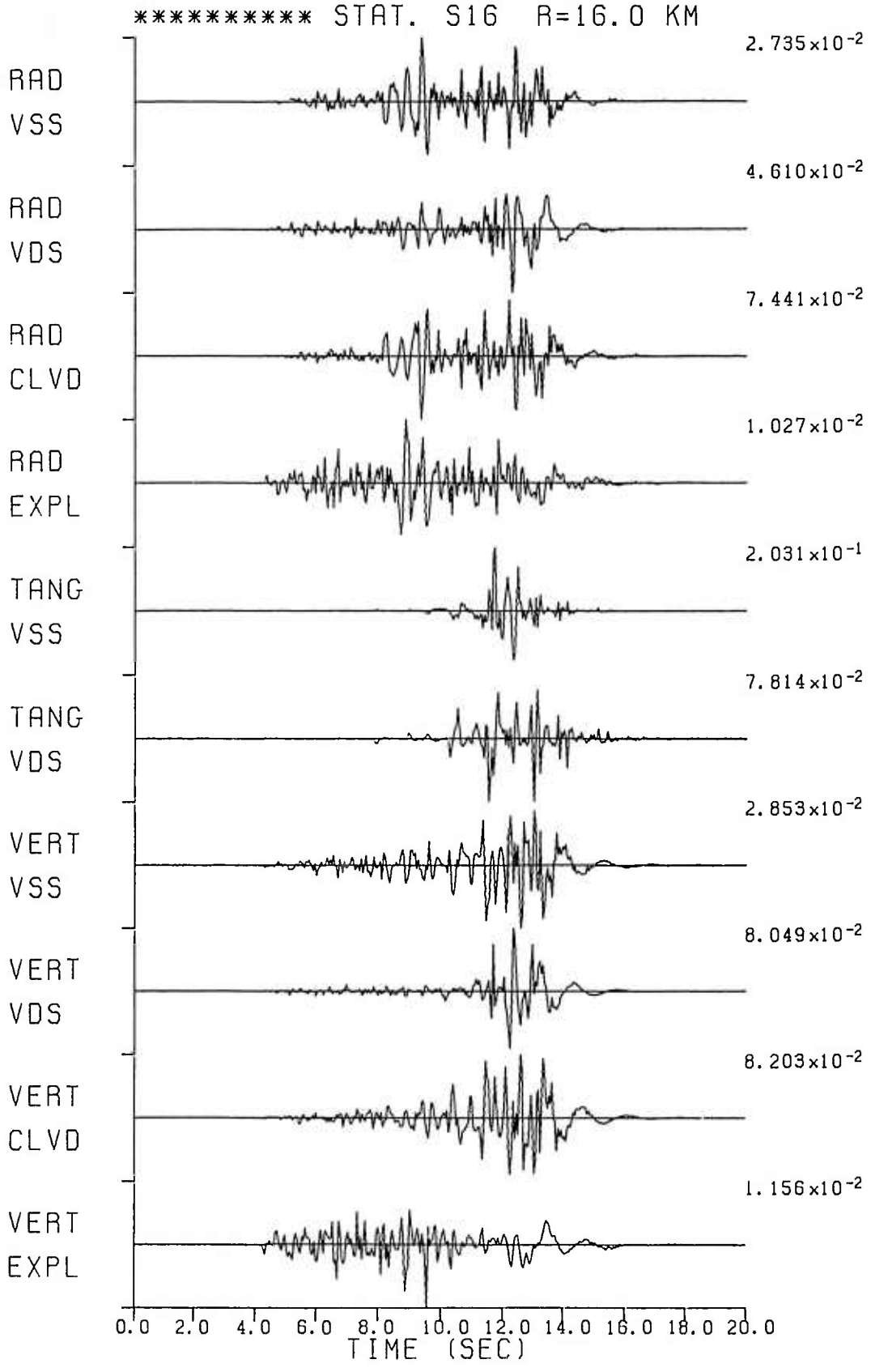

Figure A1. Synthetics for Salmon at 16 km. RAD, TANG, and VERT denote radial, tangential, and vertical components, respectively whereas VSS, VDS, CLVD, and EXPL represent vertical strike-slip, vertical dip-slip, compensated vector-dipole, and explosion sources, respectively.

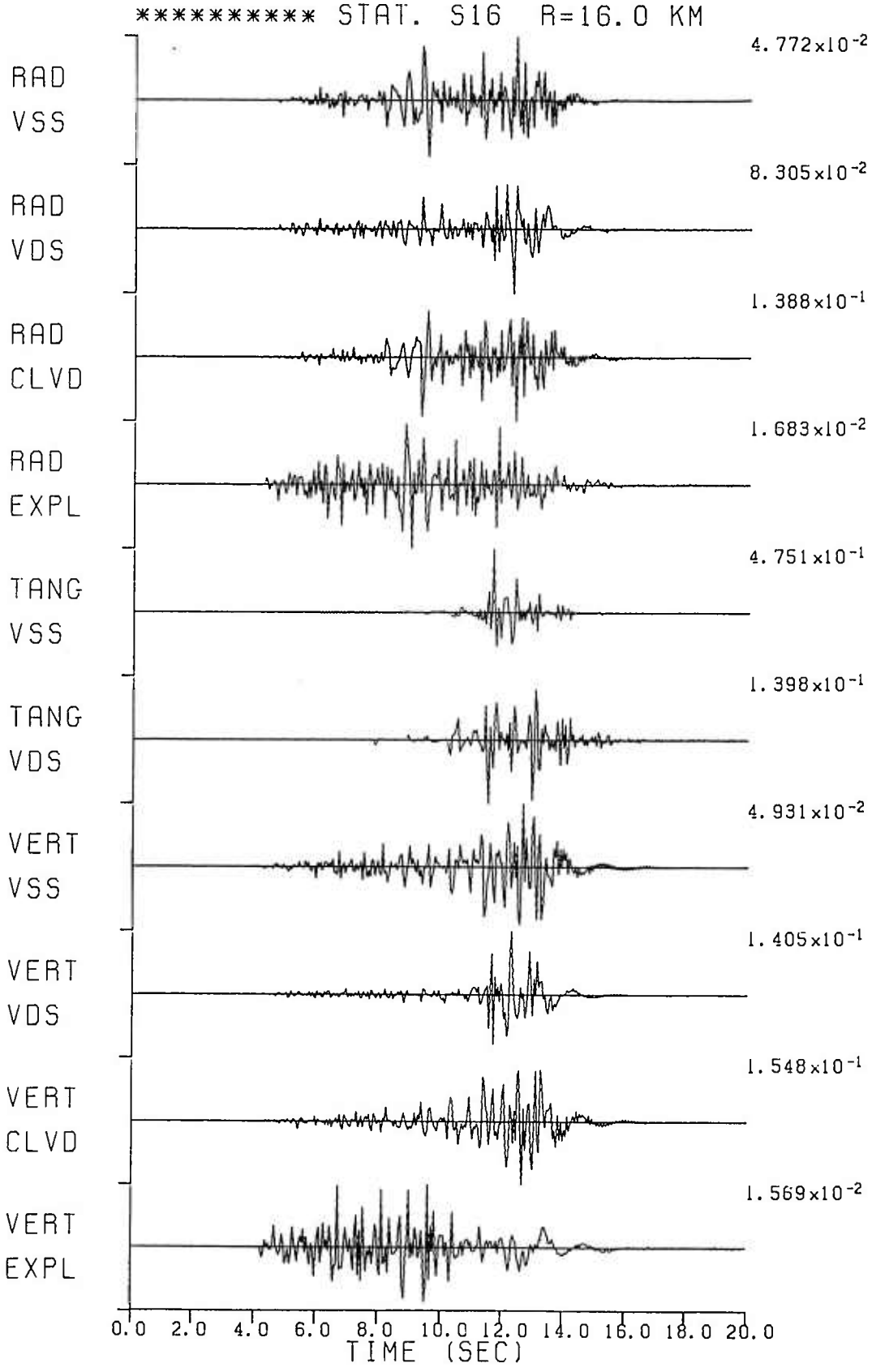

Figure A2. Synthetics for Sterling at 16 km. The abbreviations have the same meaning as in Figure A1.

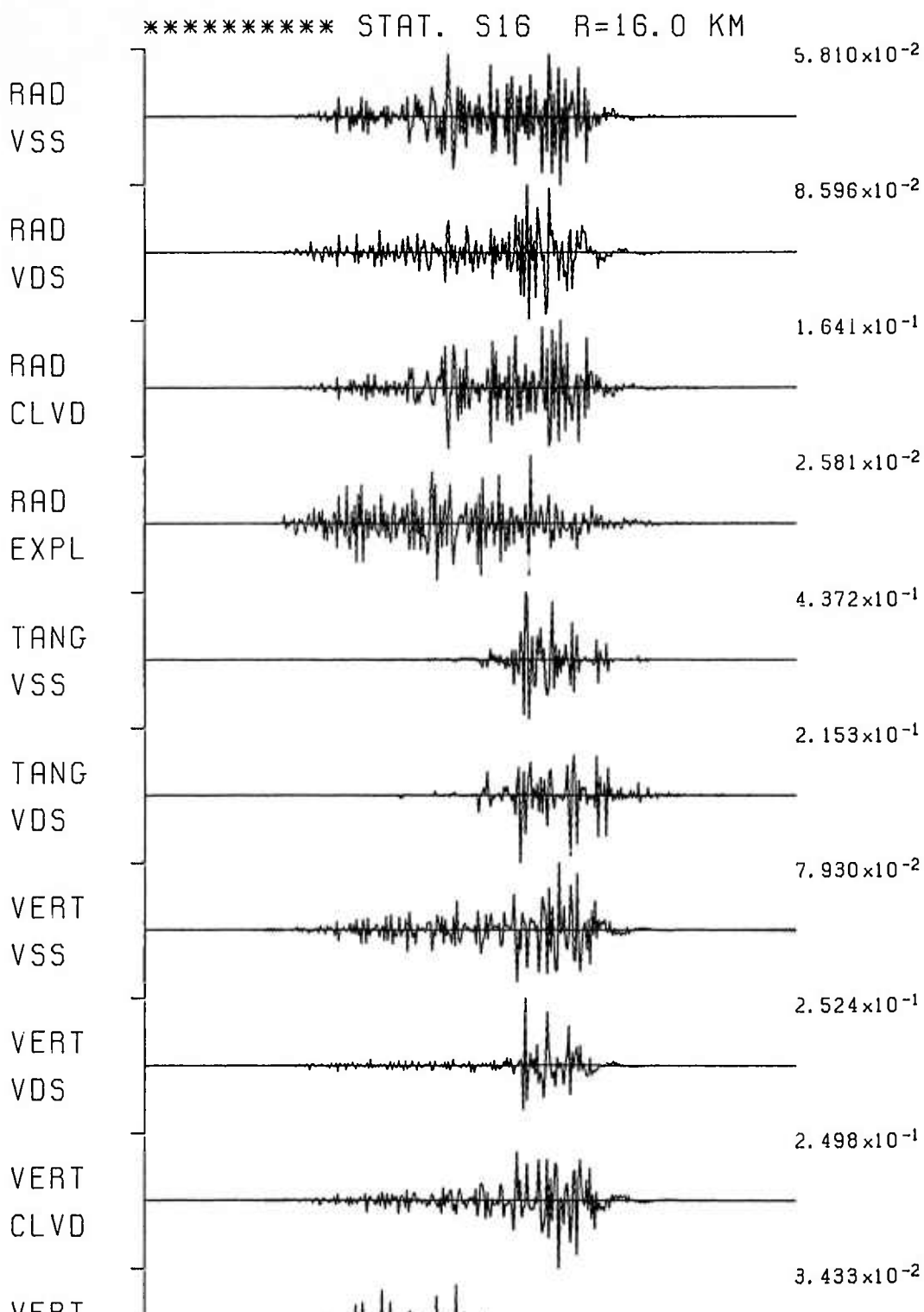

Figure A3. Synthetics for Green's function at 16 km. The abbreviations have the same meaning as in Figure A1.

4 and 10 Hz, respectively. The synthetics represent ground velocity and the peak amplitudes are normalized with the scale factor (cm/sec) shown to the right. The top four traces are the radial (RAD) components for sources needed to construct an arbitrary moment tensor source; VSS, VDS, CLVD, and EXPL denote vertical strike-slip, vertical dip-slip, compensated linear vector dipole, and isotropic sources, respectively. The middle two traces in each figure represent the tangential (TANG) components whereas the last four show the vertical (VERT) component ground velocity. Conventions for the coordinate system are positive radial away from the source, vertical positive downward, and tangential positive clockwise about the source (looking from above). Results for the same four sources at distance of 32 km (the same as for the 20S records) are shown in Figures A4, A5, and A6.

Comparison with Observed Records at Stations 10S and 20S

The instrument response for the recording at 10S is nearly flat in ground velocity over a wide range of frequencies (see Springer et al., 1968, Figure 3). A comparison of the observed vertical component data from Salmon at one of the detectors at station 10S and the synthetic for VERT EXPL (Figure A1), after applying the instrumental response, is shown in Figure A7. Considering the simplicity of the assumed theoretical model, agreement between the theoretical and observed records is good for the first several seconds after the first P arrival. Synthetics for the TANG VDS source (Figure A1), which does not generate direct P but shows a distinct first S arrival, indicate an S-P time of about 3.5 sec. The largest arrival on the observed record is the low-frequency arrival starting about 1.7 sec after the onset of P. This maxima in the wave trains was considered to be the S-wave group by Springer et al. (1968). The synthetics, on the other hand, suggest that this arrival, being too early to be S wave, is due to P waves reverberating within the low velocity sediments. Furthermore, this arrival is too early to be the direct S on the basis of the available three-component data from Salmon and Sterling at

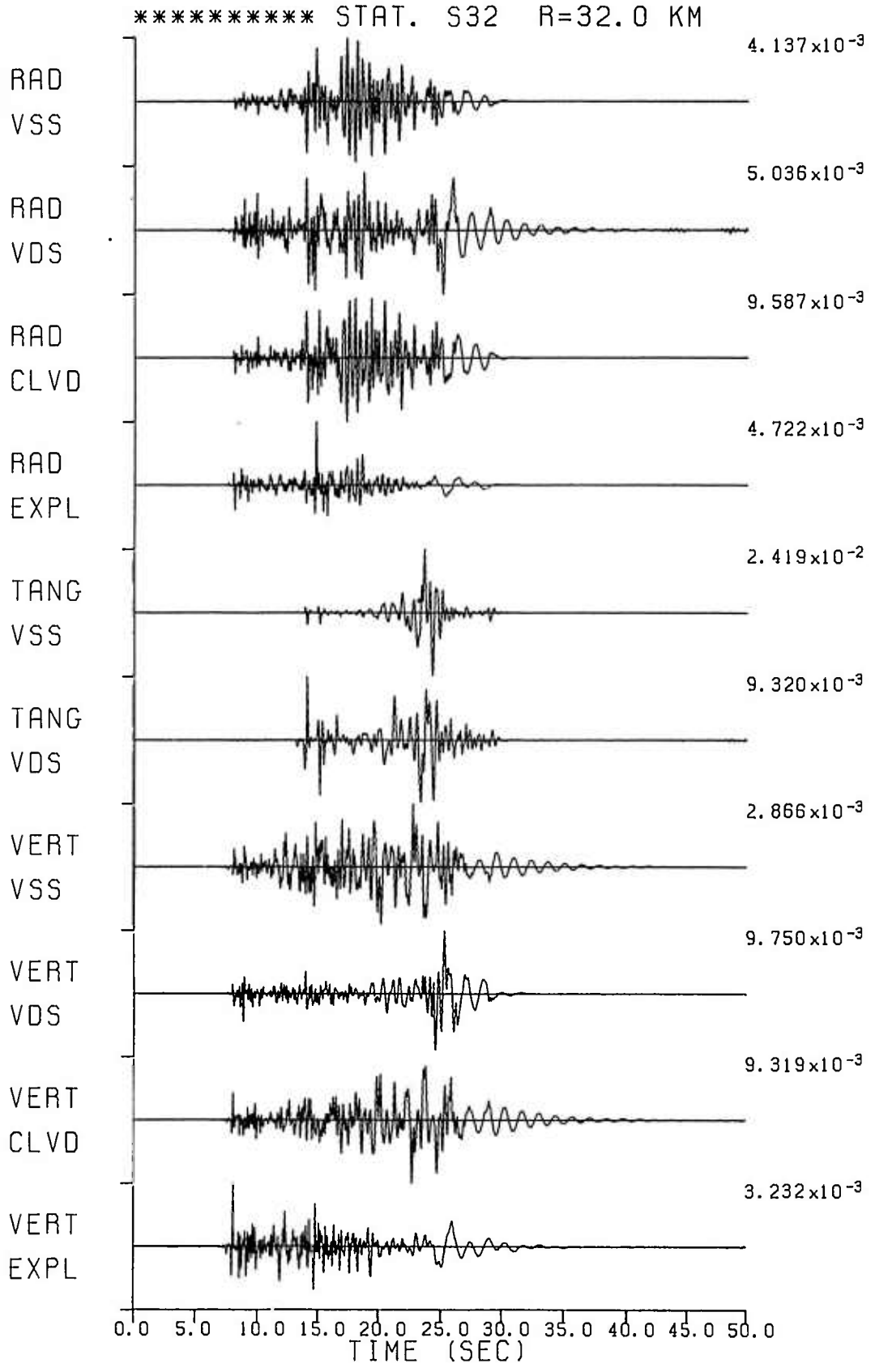

Figure A4. Synthetics for Salmon at 32 km. The abbreviations have the same meaning as in Figure A1.

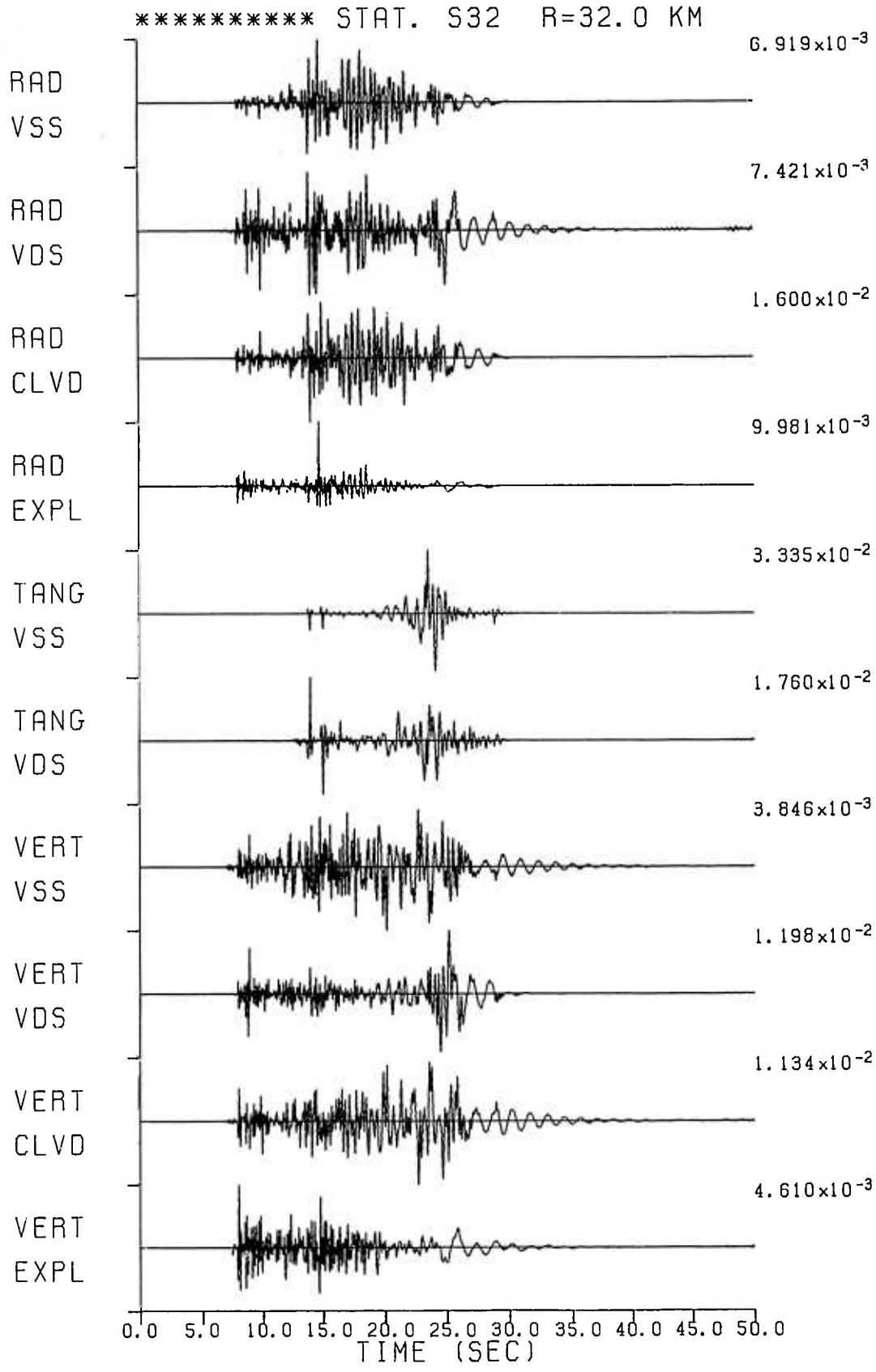

Figure A5. Synthetics for Sterling at 32 km. The abbreviations have the same meaning as in Figure A1.

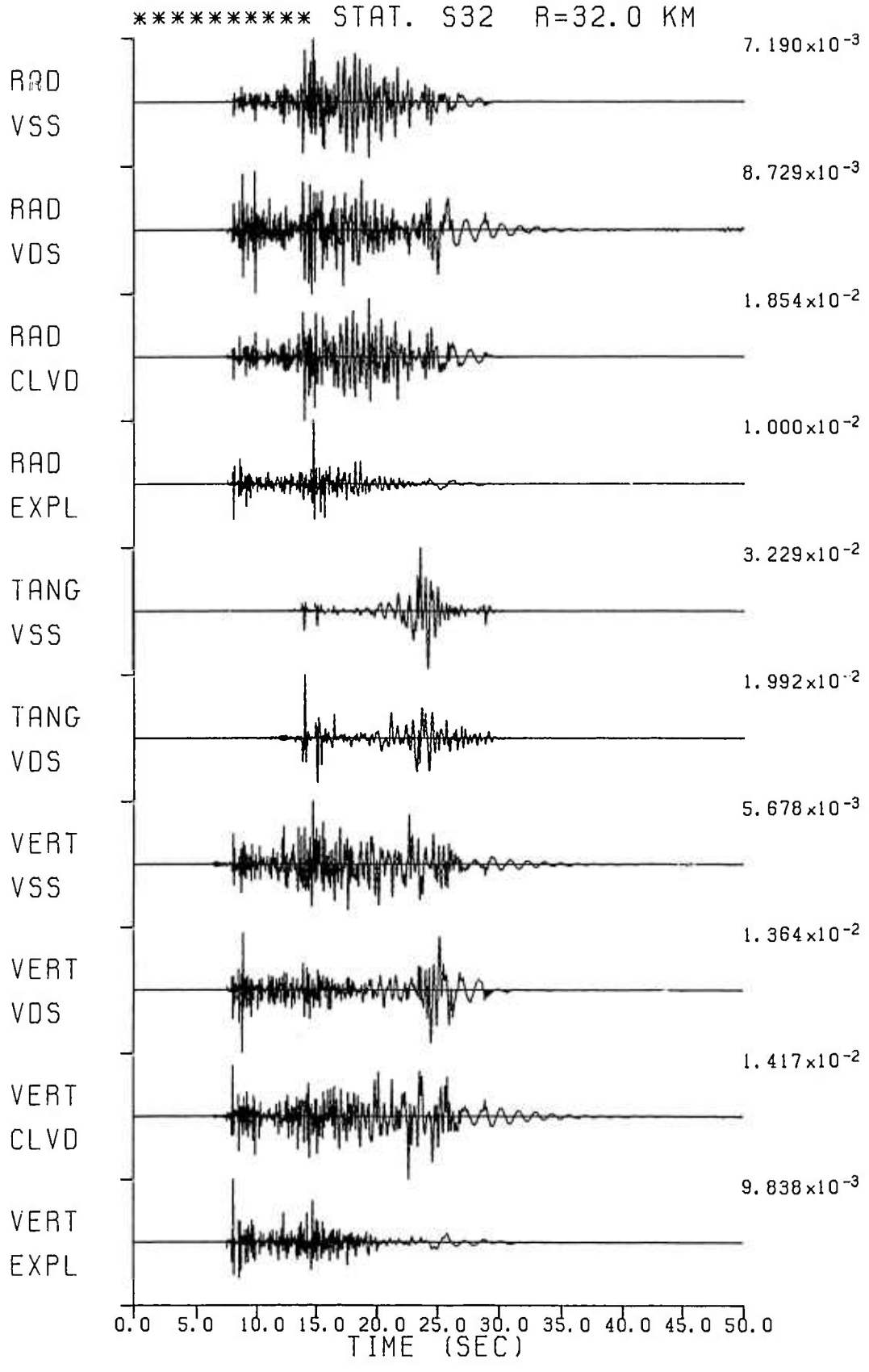

Figure A6. Synthetics for Green's function at 32 km. The abbreviations have the same meaning as in Figure A1.

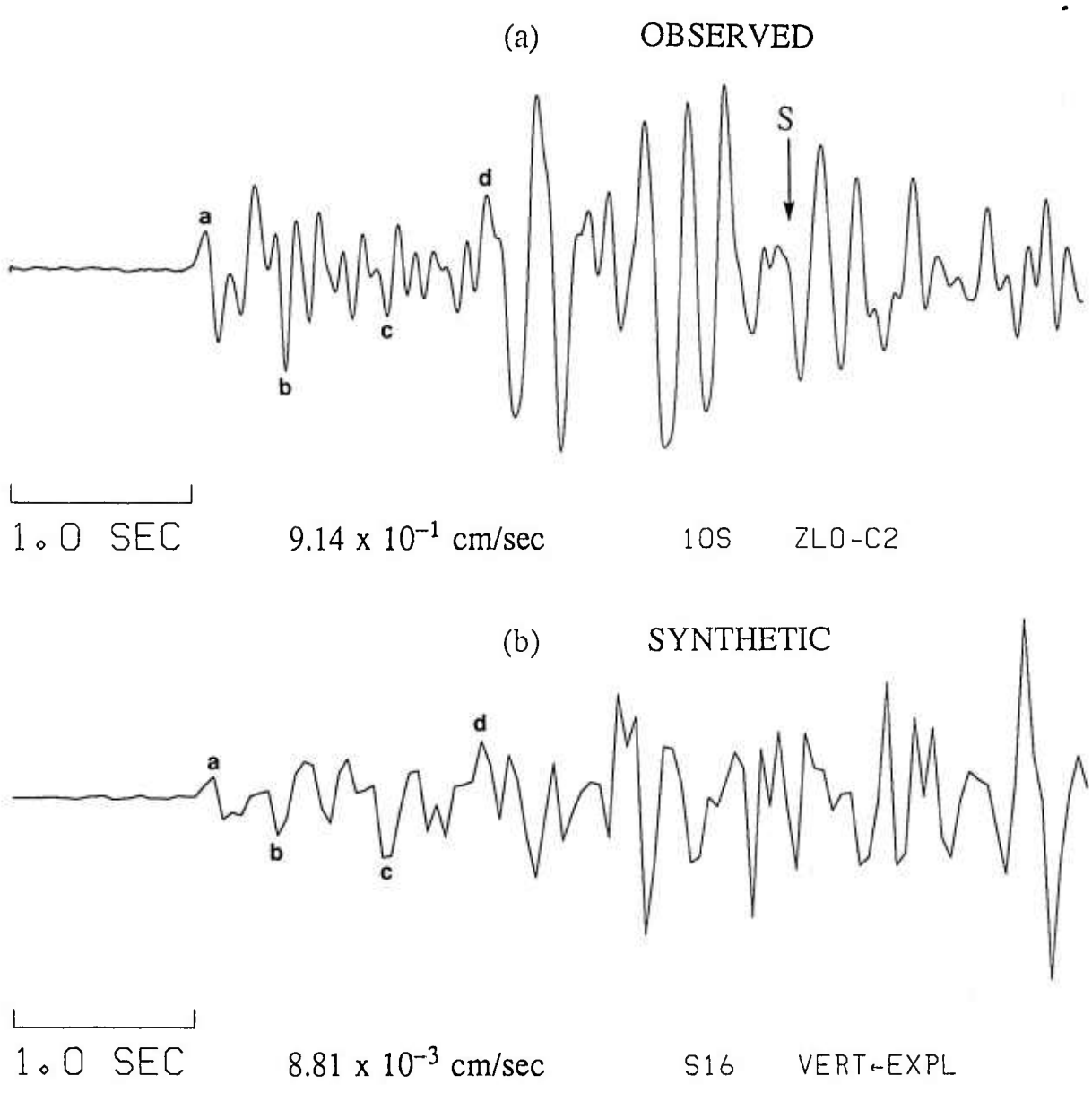

Figure A7. Observed and synthetic (explosion) vertical component records (with up motion representing compression) for Salmon at the same time scale, at a distance of 16 km, showing good agreement between arrivals (such as those marked a, b, c, and d) within the first several seconds. The maximum zero-to-peak amplitude values are given at the bottom of the two traces.

comparable source-receiver distances in Borcherdt et al. (1967). A distinct arrival, about 3.3 sec after the first P, is therefore identified as the beginning of the S wavetrain (denoted by S in Figure A7a). Beyond the arrival of S waves, the synthetic record shows lot more motion than the observed record. This indicates that there may be too many interfaces within the model of sediments and/or that the assumed Q is too high so later arrivals including the surface waves are not attenuated enough at high frequencies.

The observed and corresponding synthetic vertical component records from station 20S are shown in Figure A8. Agreement between the observed and theoretical seismograms is not as good as for the data from station 10S. Synthetics (Figure A4) indicate an S-P time of about 5.8 sec which agrees well with the distinct arrival (denoted by S in Figure A8a) separated from the first P by nearly 5.5 sec.

Both Figures A7 and A8 indicate substantially larger S waves in the observed data than in the synthetics for an explosion source. This means that the source function for Salmon was considerably more complicated than an isotropic point source. A comparison of the zero-to-peak amplitude values in Figures A7 and A8 suggest the ratio observed/synthetic of about 104 and 163, respectively. Since the synthetics are based on a seismic moment of 1×10^{20} dyne-cm, the observed data from 10S and 20S indicate seismic moments of about 1.0×10^{22} and 1.6×10^{22} dyne-cm, respectively. These values agree remarkably well with the Salmon seismic moment value of 2×10^{22} dyne-cm derived from close-in data (Aki et al., 1974).

Conclusion

Synthetic seismograms for Salmon show considerably less S waves than the observed data at both 10S and 20S. This means that the source function was significantly more complicated than an isotropic point explosion source. The synthetics were helpful in the correct identification of the beginning of the S wavetrains.

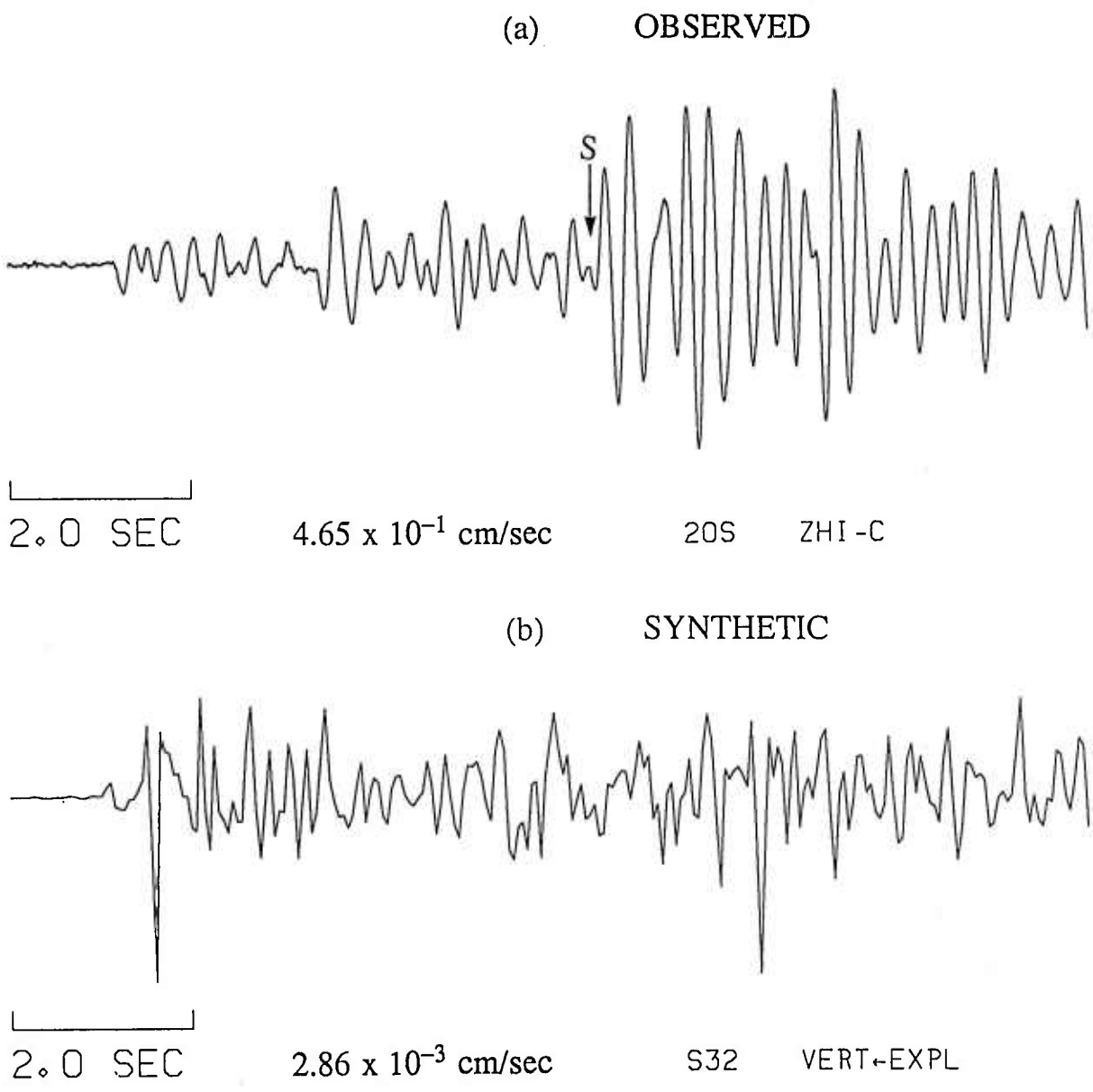

Figure A8. Observed and synthetic (explosion) vertical component records (with up motion representing compression) for Salmon at the same time scale, at a distance of 32 km showing a general lack of agreement between various arrivals. The maximum zero-to-peak amplitude values are given at the bottom of the two traces.

B. ANALYSIS OF PROJECT COWBOY STRONG-MOTION DATA

Introduction

Project Cowboy was an experiment designed to determine to what extent underground explosions could be effectively concealed simply by firing the explosion in a large cavity. Comparative measurements of ground motion were obtained from tamped charges of high explosives and high-explosive charges of similar yield fired in large cavities in halite. The tamped explosions are referred to as coupled shots and the explosions in cavities as decoupled shots. The experiment was conducted at depths near 800 ft in a salt mine near Winnfield, Louisiana. Details of the experiment have been provided by Murphey (1961), Adams and Allen (1960), and many others. Analysis of strong-motion data recorded at distances less than 600 ft was first performed by Murphey (1961). His study was, however, based on peak measurements and did not include spectral analyses.

The Project Cowboy data were digitized at 5000 samples/sec and made available to us (Neil K. Perl, written communication). The measuring devices were two different types of velocity gages with different instrumental responses (Thornbrough et al., 1960). An attempt was made to analyze as much data as possible but a large number of recordings suffered from problems such as clipping and/or poor S/N ratio. Many records of decoupled shots showed high frequency signals, probably due to ringing of the canister containing the gages (Murphey, 1961). Useful data could therefore be obtained from only a rather small number (13) of recordings as listed in Table B1.

TABLE B1

PROJECT COWBOY DATA USED IN THIS STUDY

Record No.	Shot No.	Yield (lb)	Coupled (C) or Decoupled (D)	Distance (m)
Cow-3	2	20	D	11.0
Cow-5	2	20	D	6.3
Cow-12	6	200	D	24.3
Cow-14	6	200	D	61.0
Cow-15	6	200	D	24.4
Cow-23	8	477	D	24.3
Cow-26	8	477	D	61.0
Cow-29	9	500	C	24.3
Cow-30	9	500	C	15.4
Cow-32	9	500	C	112.4
Cow-72	17	200	C	45.7
Cow-73	17	200	C	50.9
Cow-76	17	200	C	83.5

Attenuation from Coupled and Decoupled Shots

By analyzing near-field velocity and acceleration data from the Salmon and Sterling explosions in salt, Gupta et al. (1986b) obtained evidence for strain and frequency dependent attenuation. An attempt was made to carry out similar analysis by obtaining spectral ratios between various receiver locations for both coupled (tamped) and decoupled shots. Before the spectral ratios were taken, it was of course necessary to correct the observed records from identical instruments for the distance and frequency-dependent geometrical spreading. An algorithm for applying this correction (e.g. Larson, 1982) and thereby deriving spectra that correspond to spectra of the Reduced Velocity Potential (RVP) was developed. Four examples are shown in Figures B1, B2, B3, and B4 in which the first two are from a coupled shot (Shot No. 9, 500 lbs) recorded at distances of 15.4 and 24.3 m, respectively. The other two figures

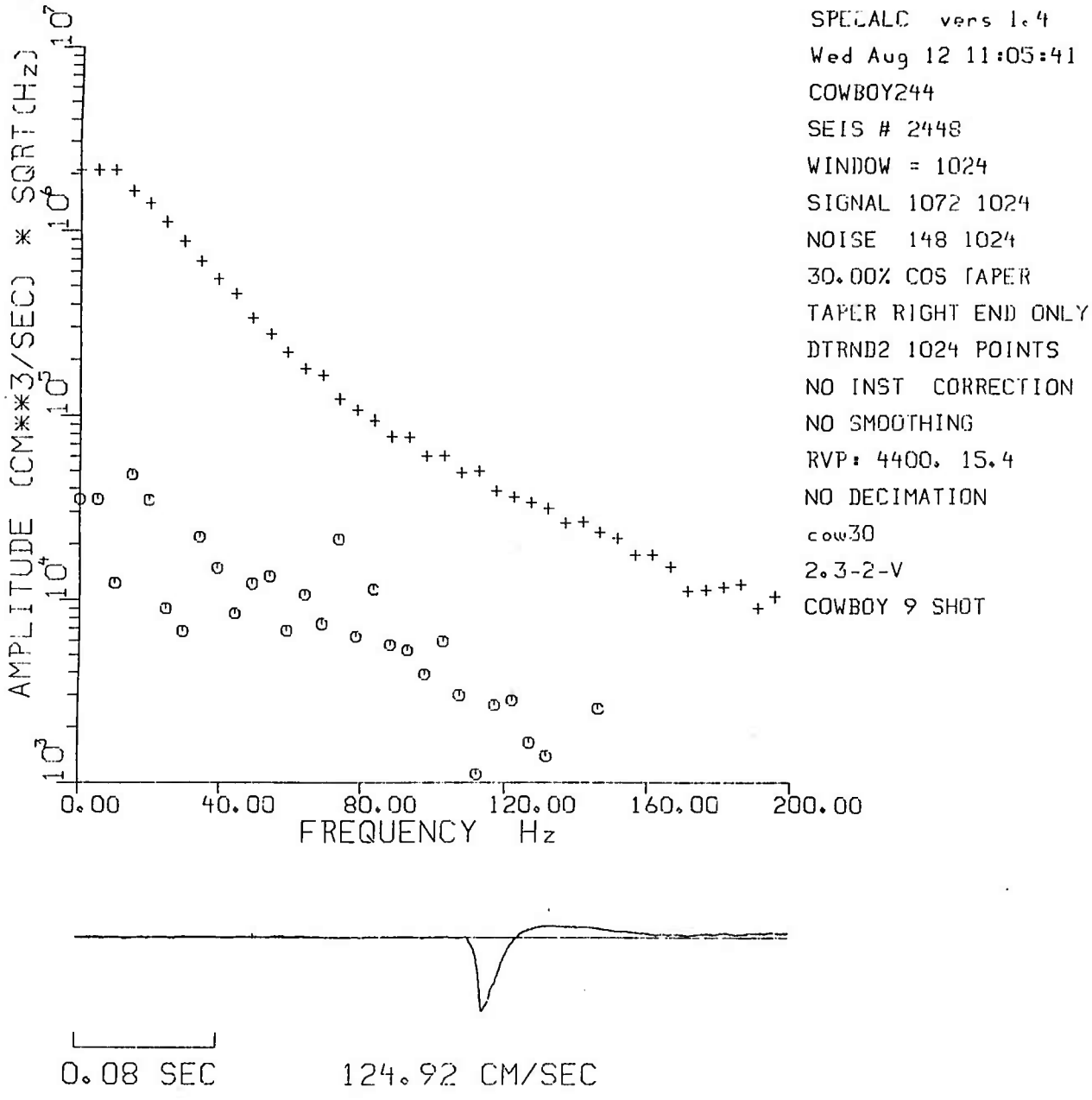

Figure B1. Record Cow-30 (shown at bottom) and the corresponding RVP spectra for Shot No. 9 (500 lbs, coupled) recorded at a distance of 15.4 m. The lower spectra is for noise preceding the signal and of equal window length.

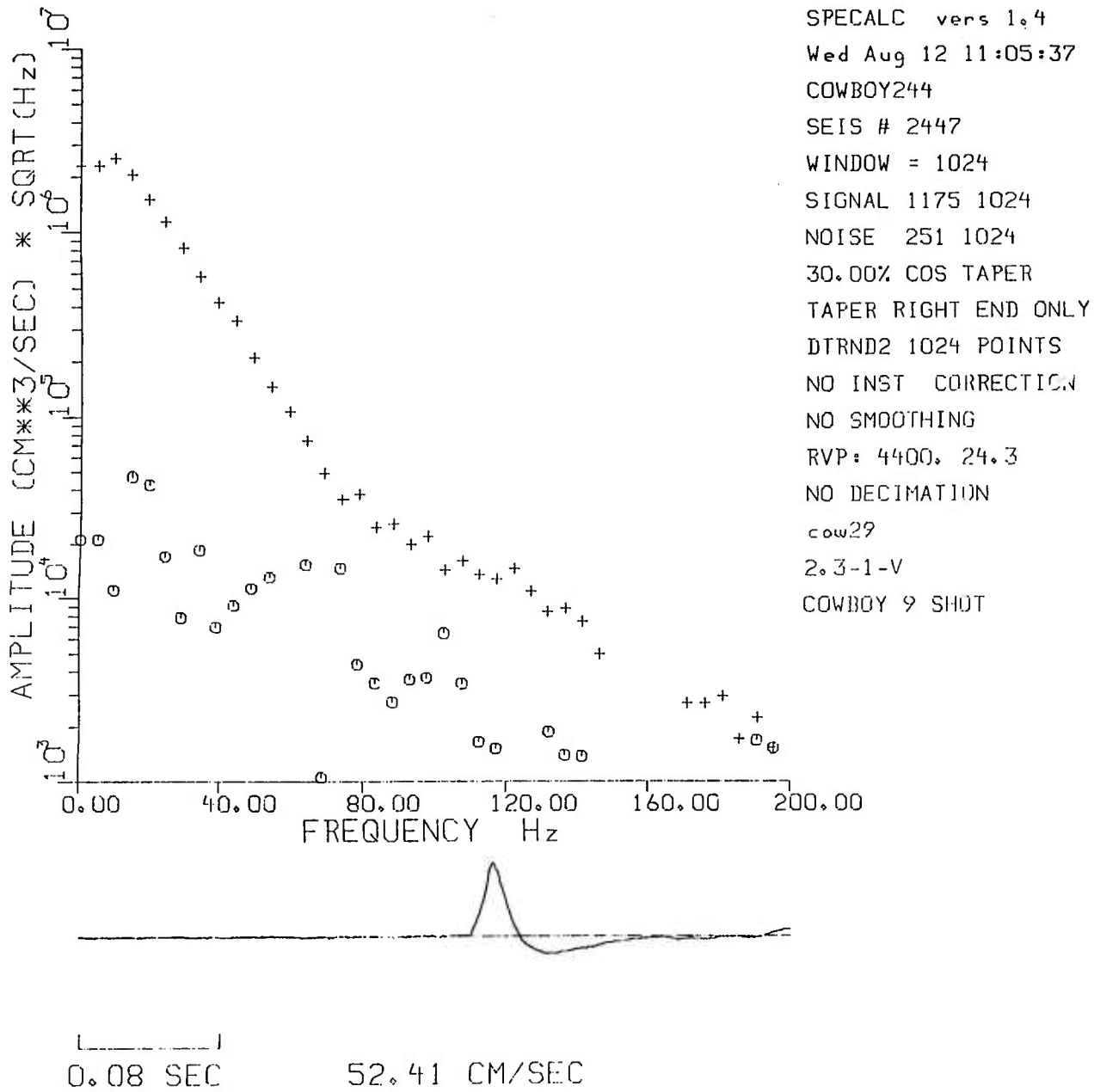

Figure B2. Similar to and for the same shot as in Figure B1 for Cow-29 and a distance of 24.3 m.

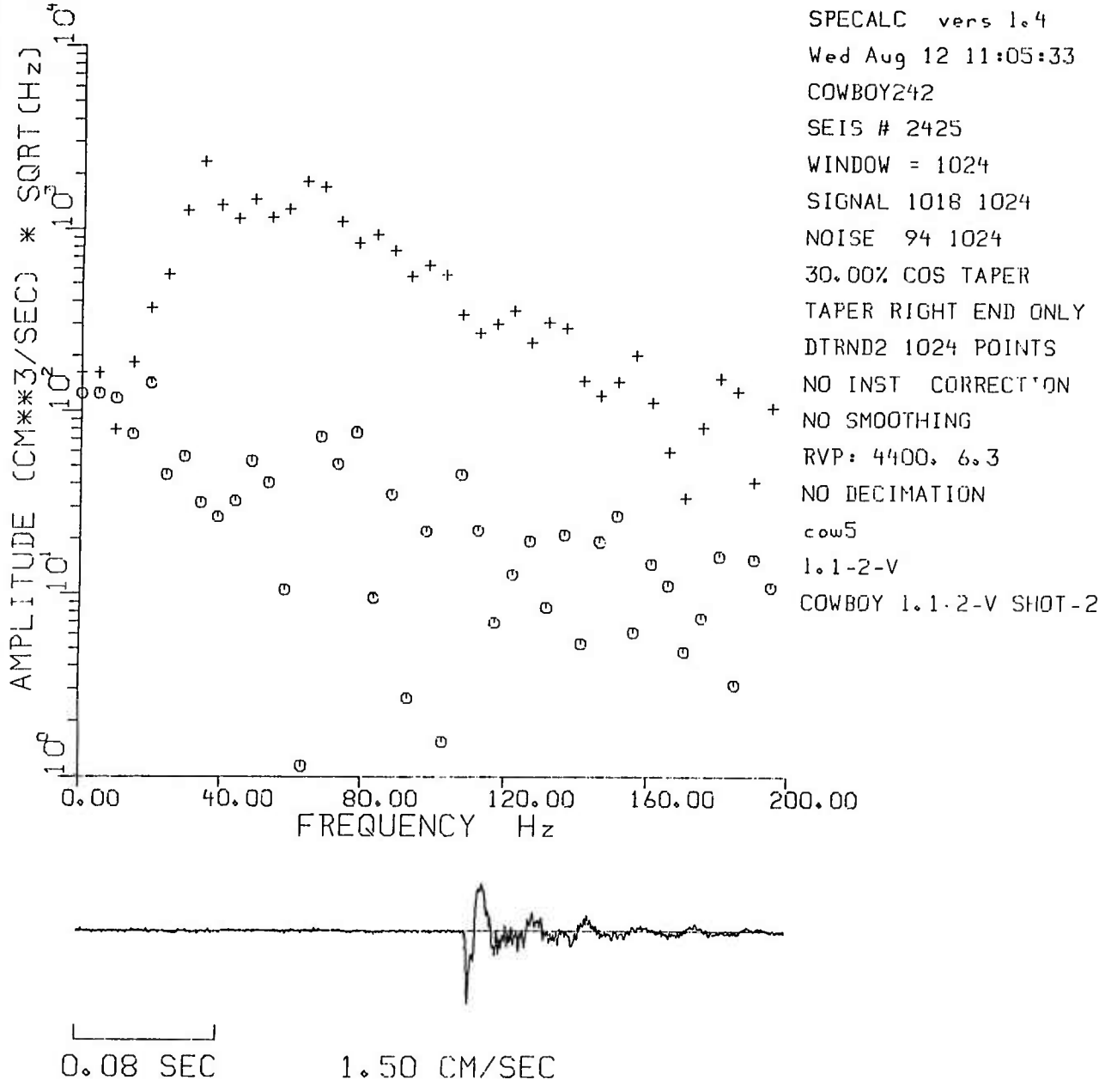

Figure B3. Record Cow-5 (shown at bottom) and the corresponding RVP spectra for Shot No. 2 (20 lbs, decoupled) recorded at a distance of 6.3 m. The lower spectra is for noise preceding the signal and of equal window length.

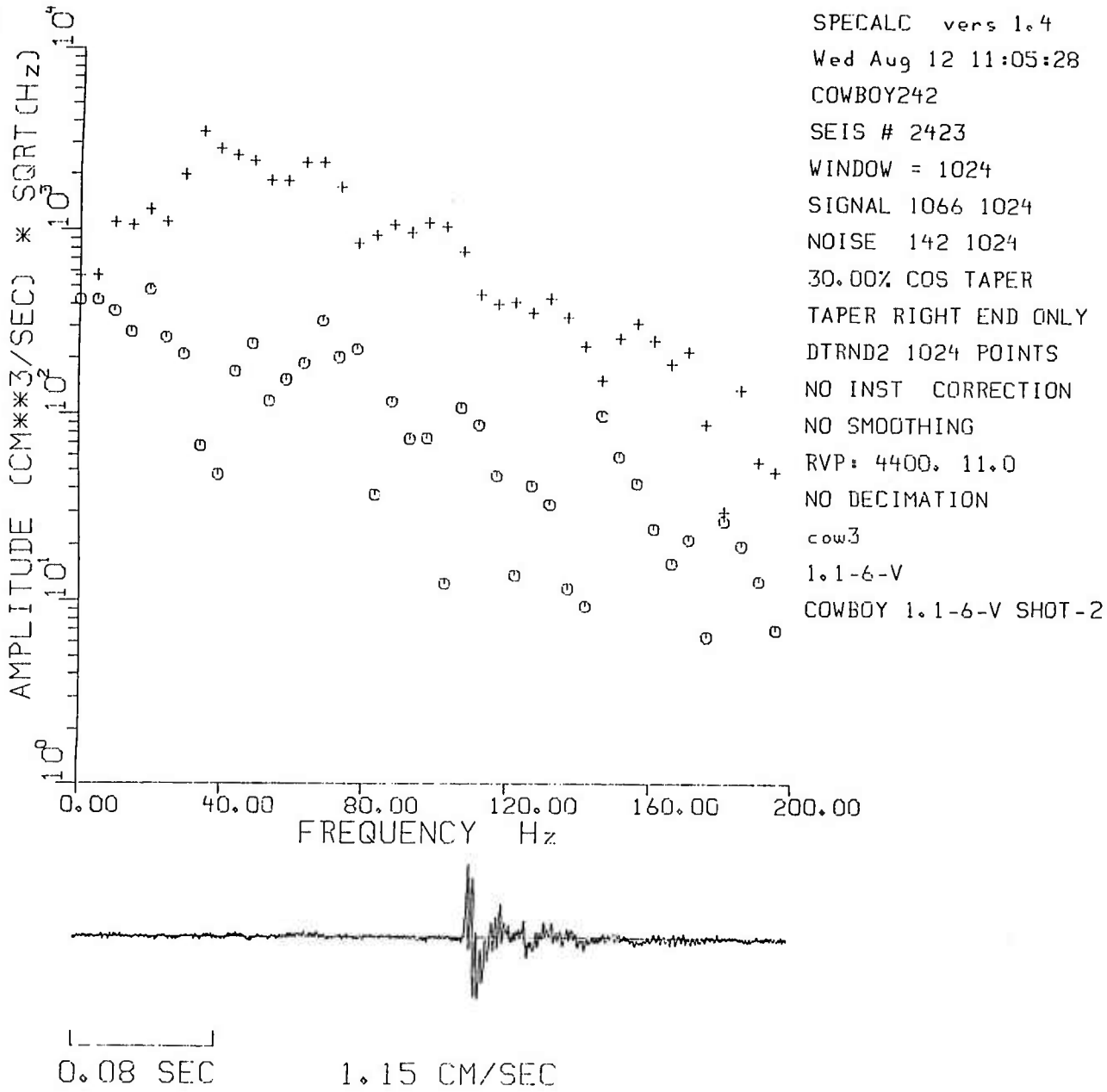

Figure B4. Similar to and for the same shot as in Figure B3 for Cow-3 and a distance of 11.0 m.

are from a decoupled shot (Shot No. 2, 20 lbs in a cavity of 12 ft diameter) recorded at distances of 6.3 and 11.0 m, respectively. The raw trace, with its peak amplitude value, is shown at the bottom of each spectrum. Spectral ratios from the two spectra in Figures B1 and B2, corrected for noise and considering only those points with S/N power ratio of at least 2, are shown in Figure B5 (upper plot), in which the dashed line shows mean (least squares) slope over the frequency range of 1 to 200 Hz. Spectral ratio from the spectrum of Figure B1 and another at a distance of 112.4 m are also shown in Figure B5 (bottom plot). Similar spectral ratios from two decoupled shots are shown in Figure B6, in which the dashed lines again represent the mean slopes over the same frequency range.

The mean spectral slopes can be used to estimate the mean Q, $\overline{Q}$, over a given frequency range. The mean t*, $\overline{t^*}$, is given by (e.g. Der and Lees, 1985)

$$\overline{t^*} = -\frac{1}{\pi}.\frac{d(\ln A)}{df} \qquad \text{(B1)}$$

where A and f represent amplitude and frequency, respectively. If the amplitude ratio (in $\log_{10}$ units) from two receivers at source-receiver distances R_1 and R_2 is plotted versus f (as in Figures B5 and B6) and the mean slope per Hz is s, then

$$\overline{t^*} = 0.733\ s \qquad \text{(B2)}$$

and

$$\overline{Q} = \frac{\Delta}{u\ \overline{t^*}} \qquad \text{(B3)}$$

where $\Delta = R_2 - R_1$ and u is the wave velocity, about 4.4 km/sec for salt (Murphey, 1961). In this manner, data from decoupled shots (Table B1) were used to obtain the four spectral ratios Cow-5/Cow-3, Cow-12/Cow-14, Cow-15/Cow-14, and Cow-23/Cow-26, and the corresponding $\overline{Q}$ values were estimated for frequency ranges of 1 to 100 Hz and 1 to 200 Hz. Similarly, the spectral ratios Cow-30/Cow-29, Cow-30/Cow-29, Cow-72/Cow-76, and Cow-73/Cow-76 were used to derive $\overline{Q}$ values from coupled shots. The results are shown in Figures B7 and B8, in

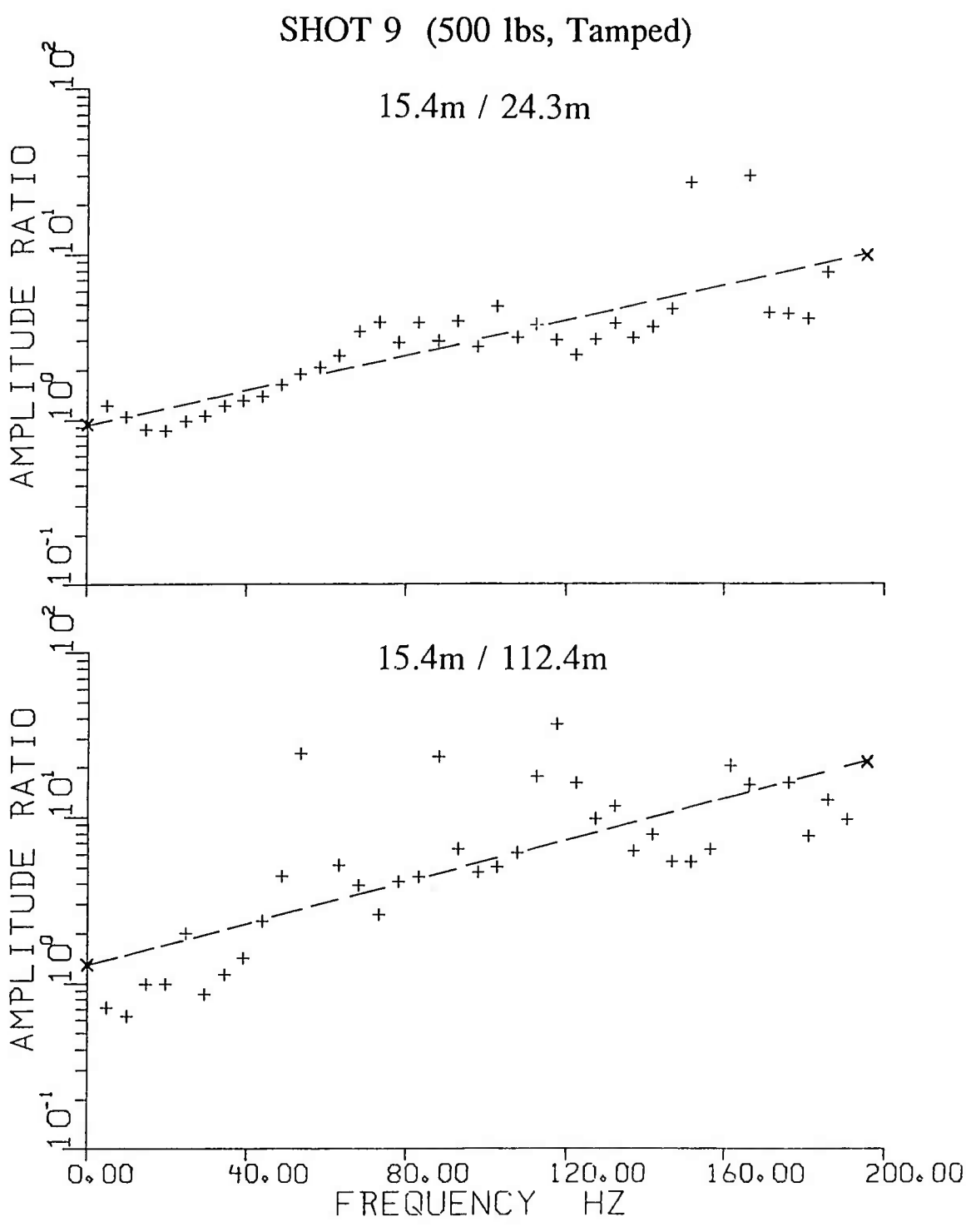

Figure B5. Spectral ratios, corrected for noise, based on RVP spectra derived from Shot 9 at distances of 15.4 and 24.3 m (upper plot) and 15.4 and 112.4 m. Points for which S/N power ratio is less than 2 are not plotted. The dashed line shows mean (least-squares) slope over the frequency range of 1 to 200 Hz.

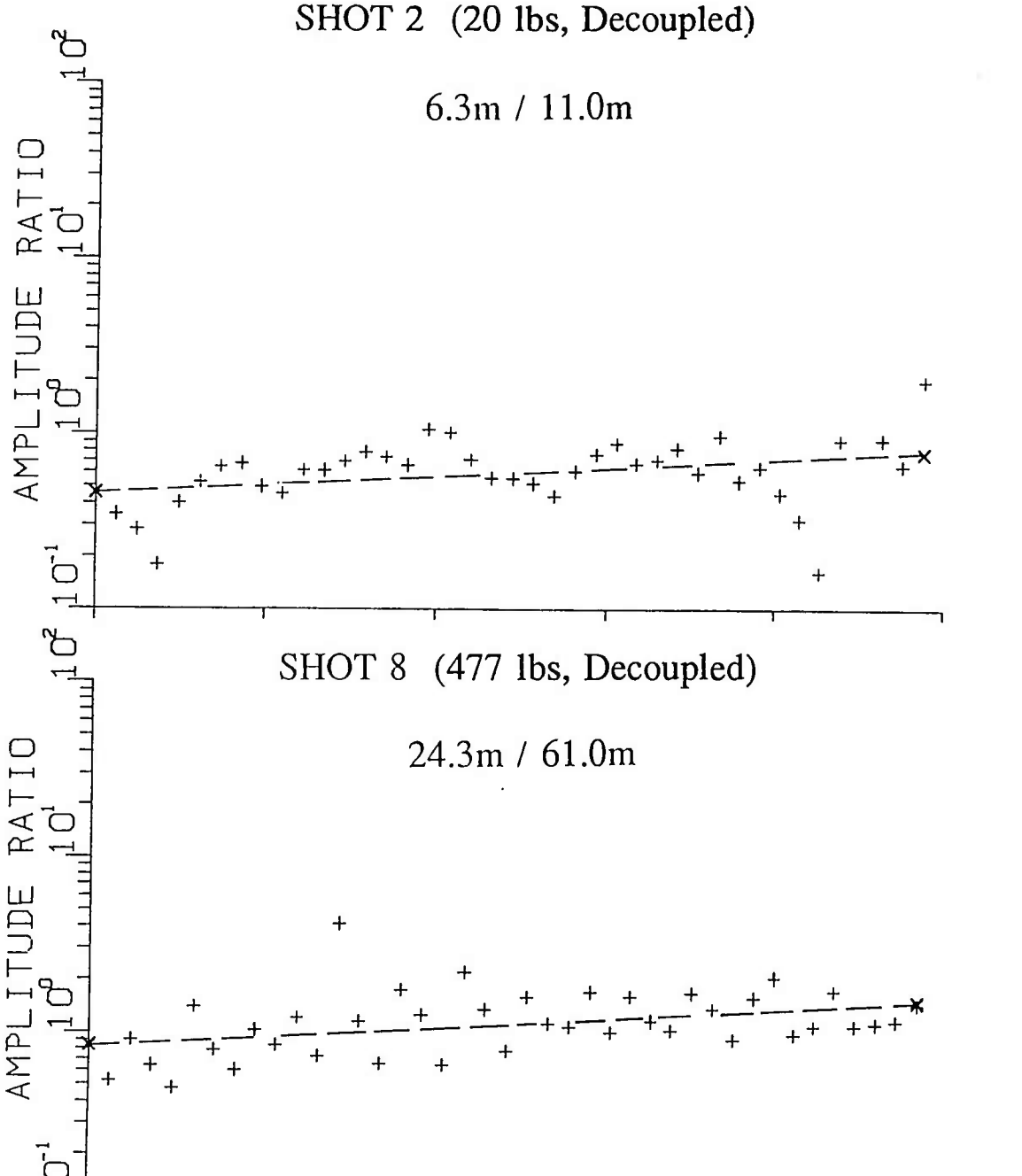

Figure B6. Similar to Figure B5 for Shot 2 (upper plot) and Shot 8.

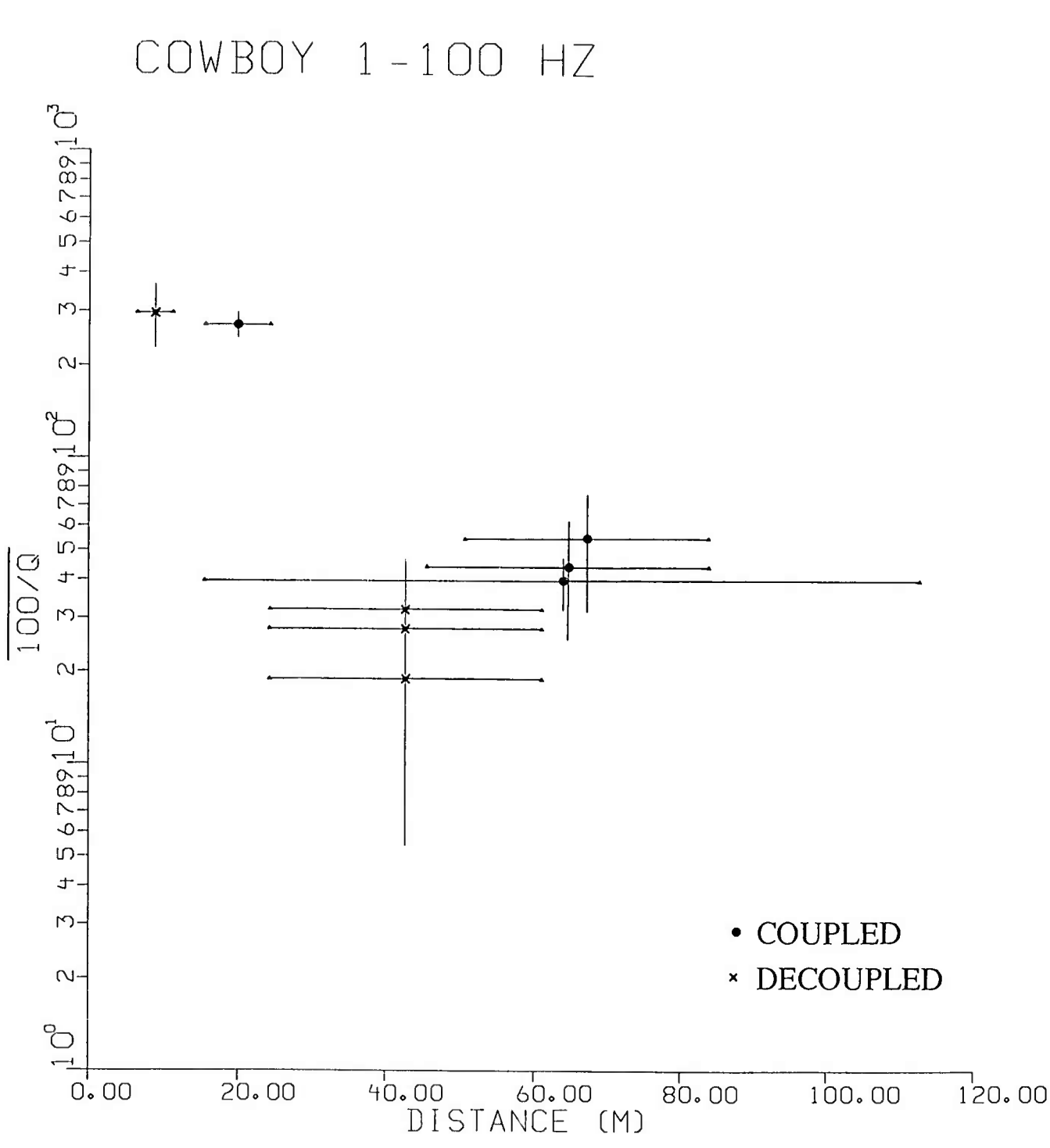

Figure B7. Mean values of 100/Q plotted versus average source-receiver distance for the frequency range of 1 to 100 Hz for both coupled and decoupled shots. The vertical lines represent error bars with one standard deviation whereas the horizontal lines denote the differential source-receiver distance over which mean Q has been computed.

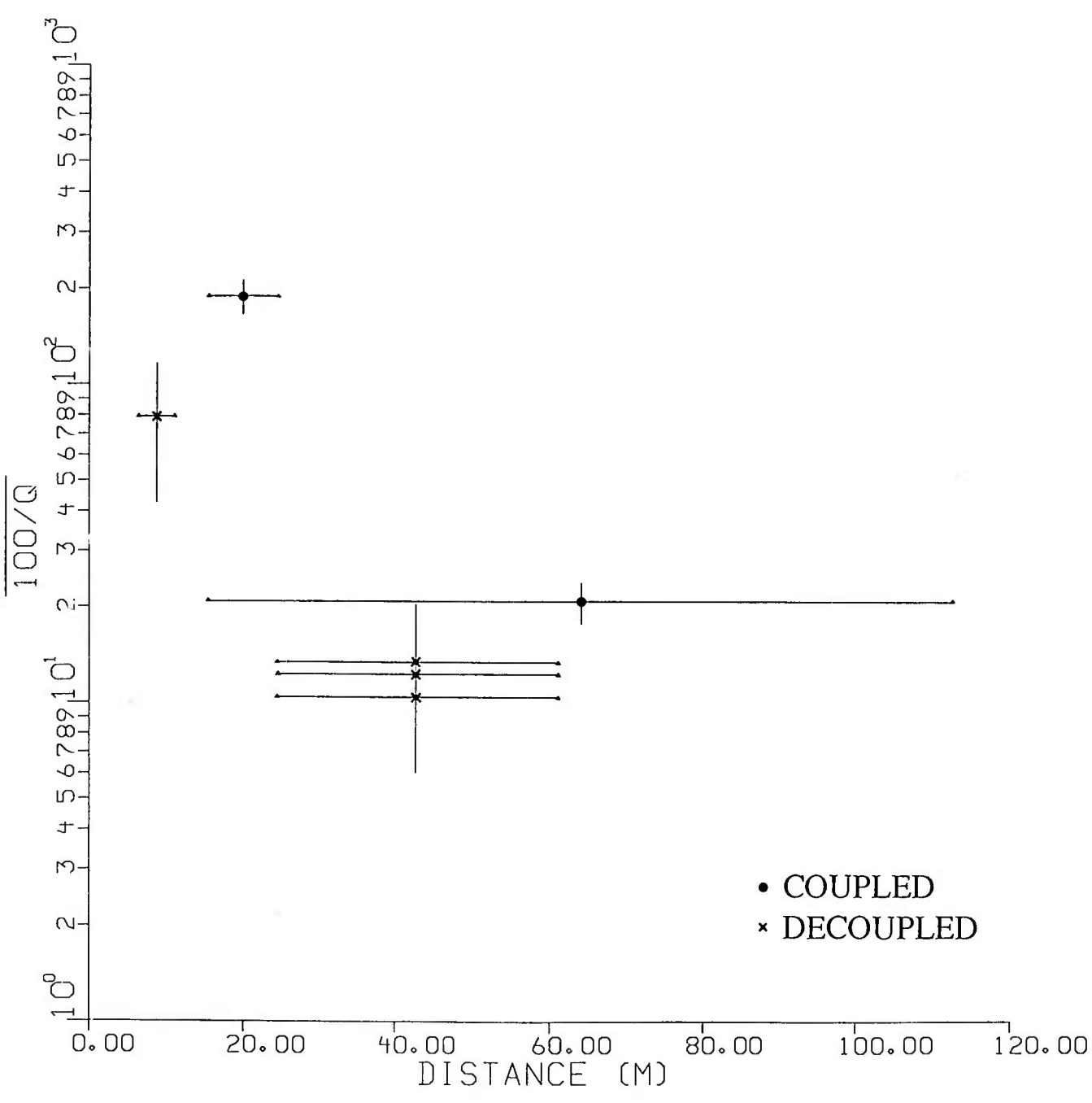

Figure B8. Similar to Figure B7 but for the frequency range of 1 to 200 Hz.

which the mean values of 100/Q are plotted versus source-receiver distance; the vertical lines represent error bars with one standard deviation, whereas the horizontal lines denote Δ. The $\overline{100/Q}$ values are plotted at the mid-point of Δ for both coupled and decoupled shots.

In Gupta et al.'s (1986b) analysis of strong-motion data from Salmon and Sterling to obtain evidence for strain and frequency-dependent attenuation, average 1/Q was measured for each distance range bracketed by the sensor distances. Figure B9, reproduced from their study, shows the mean 100/Q (a measure of attenuation) from Salmon to vary with strain, approximately as $R^{-1/2}$. The data in Figures B7 and B8 are too limited to draw any firm conclusions but appear to be similar to those in Figure B9, with attenuation decreasing with R for both coupled and decoupled shots. At comparable distances, the mean 100/Q values for coupled shots seem to be larger than those for decoupled shots, probably because of larger strain associated with coupled shots. Furthermore, the mean attenuation values for the frequency range of 1 to 100 Hz are larger than those for the frequency range of 1 to 200 Hz, perhaps due to Q increasing with frequency, as also observed in the Salmon data (Gupta et al., 1986b).

Conclusion

Data from both coupled and decoupled shots appear to support our earlier results (Gupta et al., 1986b) suggesting strain and frequency-dependent attenuation. Note, however, that the results here are not only based on very limited data but also suffer from inaccuracies due to spectral slopes being measured over rather small distance range (from about 5 to 100m). Another source of error is the presence of prominent secondary arrivals (such as reflection from the mine roof) within the time window used for spectral analysis, especially at larger source-receiver distances.

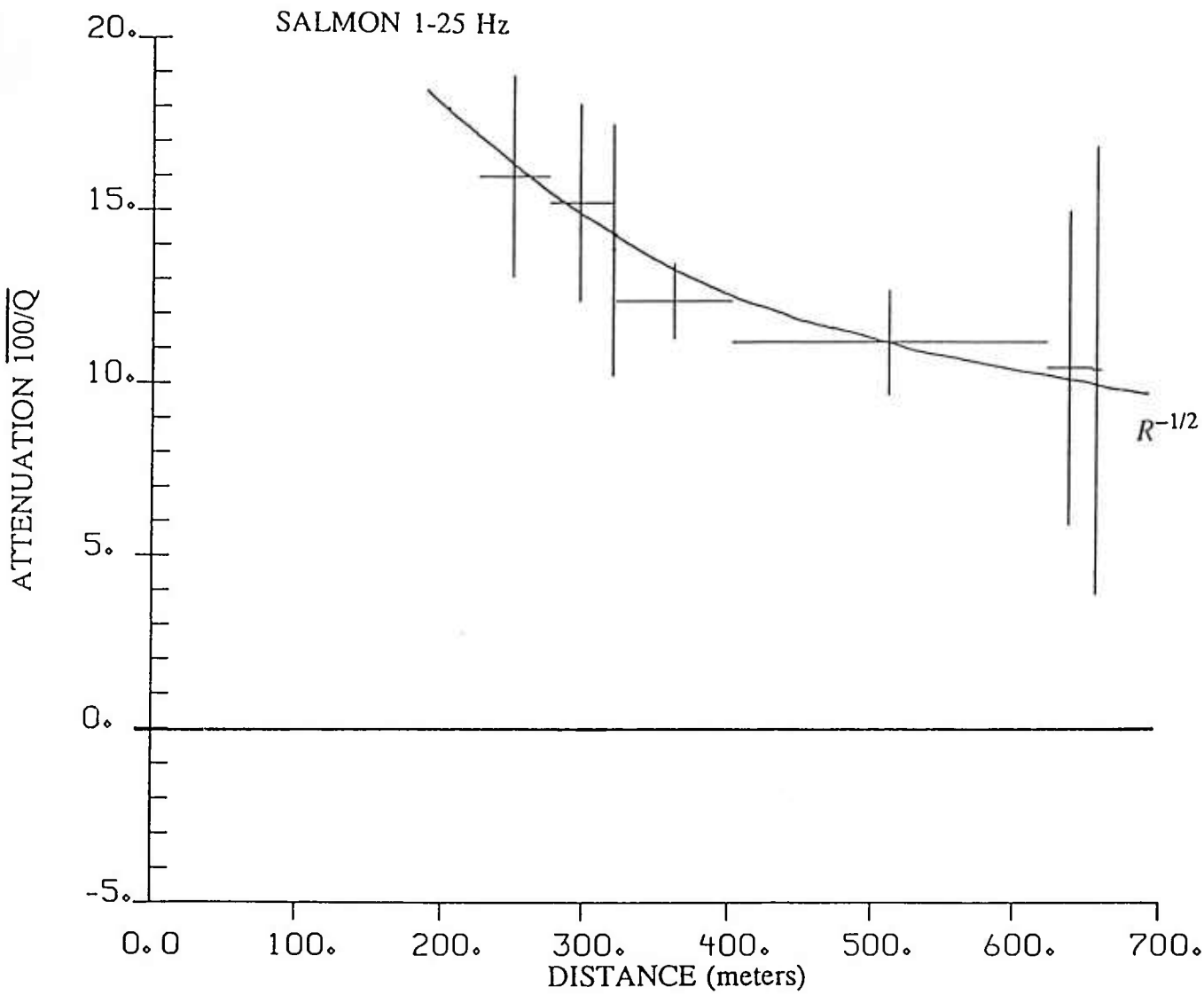

Figure B9. Mean attenuation 100/Q over the frequency range of 1 to 25 Hz versus source-receiver distance, R from Salmon near-field data (after Gupta et al., 1986b). The horizontal bars denote the distance range and the vertical lines represent error bars with one standard deviation. The data are consistent with a $R^{-1/2}$ decay with distance (shown by continuous curve). Note that results in Figures B7 and B8 show variation with distance consistent with that shown above.

C. EFFECT OF SCALED DEPTH ON REGIONAL PHASES

Introduction

Numerous observational studies of regional phases (e.g. Blandford, 1981, 1982; Barker et al., 1981; Pomeroy et al., 1982; Gupta et al., 1982; Gupta and Blandford, 1983; Der et al., 1984; Glaser et al., 1986; Gupta and McLaughlin, 1987) indicate large variations in amplitude and spectra due to factors such as site effects, sensitivity to near-source environment, and propagation path effects. Extreme variability of regional phases from NTS explosions at essentially the same location has been noted by Springer and Denny (1976, especially their Figure 4) and Gupta et al. (1984, see their Figure 11). Theoretical studies based on synthetic seismograms of regional phases (e.g. Bouchon, 1982; Banda et al., 1982; Campillo et al., 1984; Rivers, 1984, Bennett et al., 1987) also suggest that the excitation and propagation of regional phases can be highly variable. In this study, we have tried to isolate the effects of source and near-source parameters, especially depth and yield, by comparing regional phases from shots within the Pahute Mesa region and recorded at a common station.

Effect of Scaled Depth on Spectra of Regional Phases

Scaled depth for nuclear explosions is generally defined as depth(m)/$Y^{1/3}$ where Y is yield in kton. Several studies have indicated that scaled depth is an important parameter directly influencing the spectra and amplitudes of the explosion-generated body and surface waves (e.g. Mueller and Murphy, 1971; Rulev, 1965; and Kisslinger, 1963 for a review of early work). The elastic radius, r, varies as $Y^{1/3}$ so that scaled depth varies as h/r where h is the shot depth. The elastic radius, r, should also vary inversely as rock strength since the nonlinear zone extends to the point where the explosive hoop stress equals the tensile strength of the surrounding rock. This results in larger elastic radii for shots in lower-strength media

(Evernden et al., 1986). Thus r would depend not only on Y but also on medium properties such as density and overburden pressure which are related to the rock strength. For example, Mueller and Murphy (1971) empirically determined that for tuff-rhyolite detonations,

$$\frac{r}{Y^{1/3}} = \frac{2000}{(\rho h)^{1/2.4}} \qquad \text{(C1)}$$

where ρ is the mean overburden (average shot point to surface) density in gm/cc and h is in meters. We shall refer to the quantity h/r as "Effective Scaled Depth" or ESD so that, for tuff-rhyolite shots, ESD may be approximated by

$$ESD = \frac{h}{Y^{1/3}} \cdot \frac{(\rho h)^{1/2.4}}{2000} \qquad \text{(C2)}$$

The first term on the right hand side of the above equation is the scaled depth, whereas the second term may be considered a "correction" for the variation in overburden pressure as the shot depth varies.

If explosions at considerably different depths and in significantly different media are to be compared, physical considerations would suggest the spectral content of the radiated seismic waves to be controlled by the dimensionless quantity h/r or ESD, rather than by the scaled depth $h/Y^{1/3}$. Note that Cisternas' (1964) study of the radiation of elastic waves from a spherical cavity in a homogeneous half space also showed the surface displacement to be dependent on the ratio h/r.

In order to study the effect of variations in scaled depth, we shall now describe some observational results comparing the spectral contents of Pn, Pg, and Lg for explosions with large differences in their shot depth, scaled depth and ESD values. The Pahute Mesa explosions Buteo, Rex, Scotch, and Benham, covering the yield range of 0.7 to 1100 kt, provide unique data for a study of amplitude-yield relations at regional distances (Blandford, 1976). Regional phases from these four and three additional explosions listed in Table C1 were well

recorded at the LRSM station KN-UT (epicentral distance, $\Delta \approx 320$ km). Two of the seven explosions, viz. Cabriolet and Schooner, were cratering shots, so that large ranges of both shot and scaled depths are covered. The ESD values in Table C1 are estimated by using equation (2) and assuming the mean overburden density, ρ, to vary with depth, h, according to the relationship (Ferguson, 1986)

$$\rho = 1.51 + 0.00074\ h. \qquad \text{(C3)}$$

It is interesting to note that time-domain measurements of regional phases from these 7 explosions failed to show any significant differences between the shallowest (cratering) and the deepest and/or the most overburied explosions on amplitude versus yield plots for Pn, Pg, and Lg (Gupta et al., 1985).

TABLE C1

PAHUTE MESA EXPLOSIONS USED IN SPECTRAL ANALYSES

No.	Name	Date	Shot Medium (m)	Shot Depth (m)	Depth of Water Table	Yield+ (kt)	Scaled Depth#	ESD
1	Buteo	12 May 65	tuff	696	660	0.7	784	8.049
2	Rex	24 Feb 66	tuff	671	642	16	266	2.682
3	Duryea	14 Apr 66	rhyolite	544	662	65	135	1.222
4	Scotch	23 May 67	tuff	977	672	150	184	2.262
5	Cabriolet*	26 Jan 68	rhyolite	52	488	2.3	39.4	0.123
6	Schooner*	8 Dec 68	tuff	111	274	35	33.9	0.146
7	Benham	19 Dec 68	tuff	1402	641	1100	136	2.053

+ Values from Springer and Kinnaman (1971) except for Buteo from an estimate, based on LR data, by Blandford (1976).

* cratering explosion

depth(m)/$Y^{1/3}$ where Y is yield in kt.

To isolate source effects, it is important to use common source-receiver paths because of the extreme sensitivity to propagation paths of the regional phases, especially Pn (Langston, 1982) and Lg (Gupta and Blandford, 1983). The seven explosions in Table C1 are all from Pahute Mesa so that the source-receiver paths to KN-UT should not be much different, and the results should be nearly free from propagation path effects. The window lengths used for spectral analysis of Pn, Pg, and Lg on the vertical component records were 6.4, 12.8, and 12.8 sec, respectively, and a 10% cosine taper was used along with 3, 5, and 5 point smoothing of spectra for Pn, Pg, and Lg windows, respectively. Out of these 7 shots, Buteo and Duryea (with their yields differing by a factor of about 100) were detonated in the same hole so that the source-receiver paths are almost identical. A comparison of the relative variations in spectra of the three regional phases for various explosions can be made by an examination of inter-event spectral ratios. Two such ratios Duryea/Buteo and Cabriolet/Buteo for Pn, Pg, and Lg, each corrected for noise, are shown in Figure C1. Cabriolet and Buteo differ in their yield values by a factor of only about 3. For both sets of inter-event spectral ratios, the mean spectral slopes over the frequency range of 1 to 5 Hz are the largest for Pn, the least for Lg, and intermediate between the two for Pg. It seems therefore that the spectra of Pn are the most variable and those of Lg the least variable.

We next obtained the spectral ratios Pn/Lg at the common station KN-UT for the seven explosions listed in Table C1. Results are shown in Figure C2, in which the mean spectral slopes of Pn/Lg over the frequency range of 1 to 5 Hz are plotted versus (a) shot depth, (b) scaled depth, and (c) ESD, all in log units. The three plots show linear trends with correlation coefficient values of 0.726, 0.811, and 0.835, respectively. Assuming the validity of a linear relationship, it seems that the spectral ratio Pn/Lg is influenced the most by ESD, somewhat less by scaled depth, and the least by shot depth. The values of mean slope of the linear trends in the three plots in Figure C2 are also indicated.

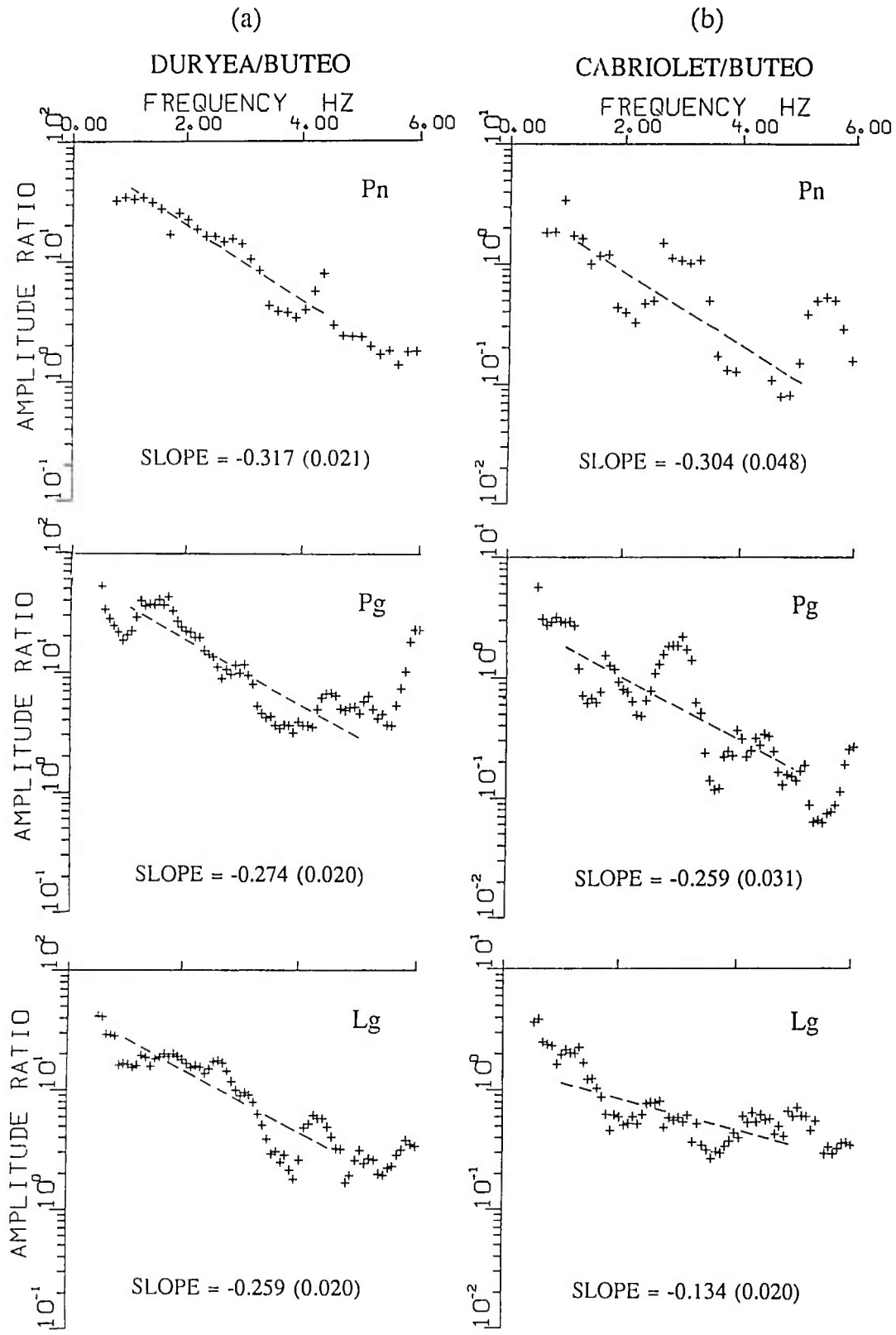

Figure C1. Spectral ratios Duryea/Buteo and Cabriolet/Buteo, corrected for noise, for Pn, Pg, and Lg, recorded at KN-UT. Points for which S/N power ratio is less than 2 are not plotted. The mean (least squares) slope over the frequency range 1 to 5 Hz (dashed line) is indicated (with its standard deviation value in parentheses) for each phase.

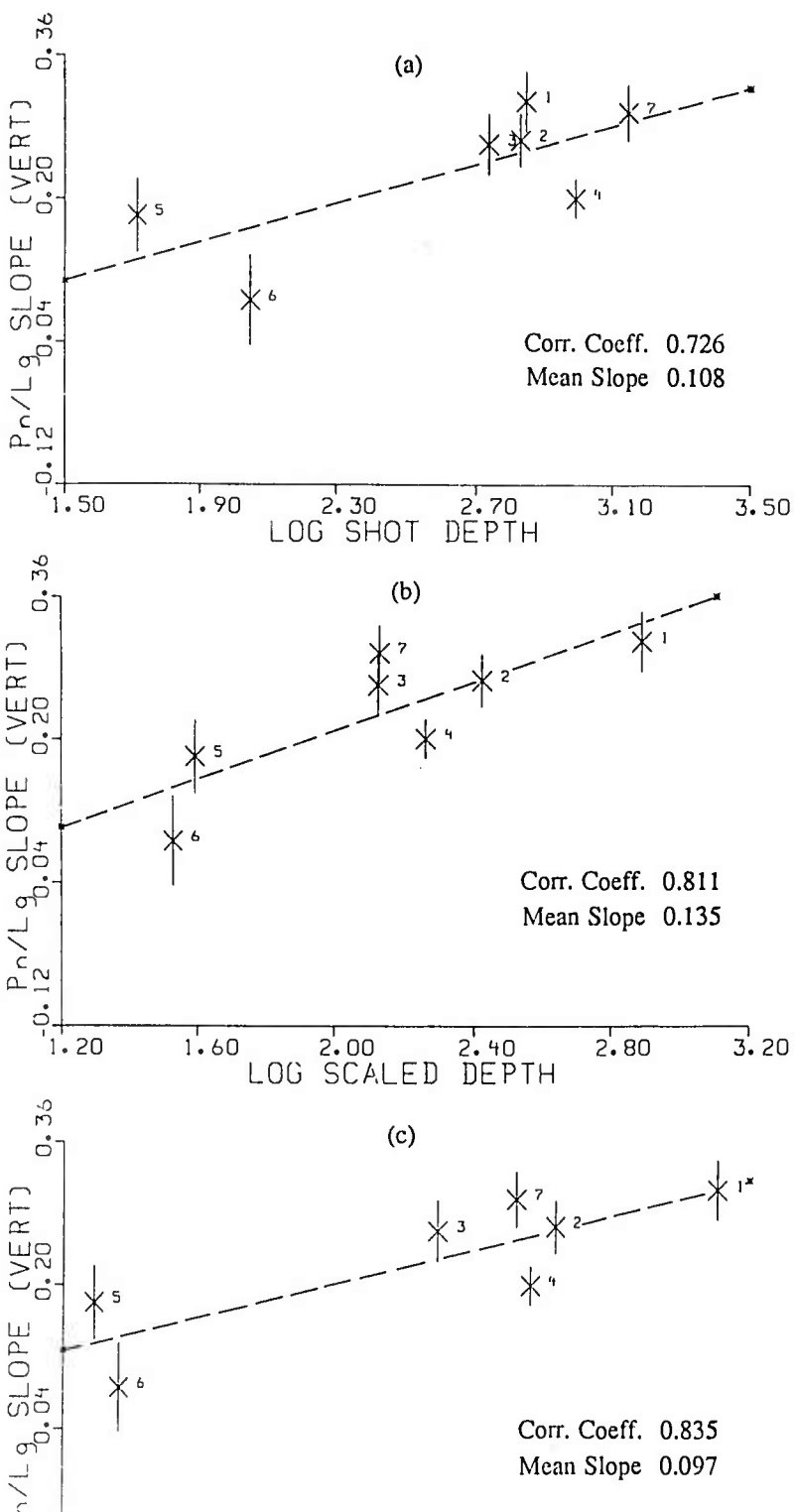

Figure C2. Mean Pn/Lg spectral slope (per Hz) over the frequency range 1 to 5 Hz versus (a) log (shot depth in meters), (b) scaled depth, and (c) log ESD for 7 explosions, numbered as in Table C1. The vertical lines represent error bars with one standard deviation. The correlation coefficient and mean slope value of the least squares linear trend (dashed line) is indicated for each plot.

The spectral ratios Pg/Lg were obtained for 6 shots; Pg for Rex was clipped and could not be used. Plots based on Pg/Lg but similar to those in Figure C2 are shown in Figure C3. The three linear trends with correlation coefficients of 0.849, 0.853, and 0.909, respectively, imply that the spectral ratio Pg/Lg is also influenced the most by ESD, somewhat less by scaled depth and the least by shot depth. The mean slope values of the linear trends in the three plots, indicated in Figure C3, are all considerably smaller than the corresponding values for Pn/Lg in Figure C2. This means that, compared to Pn/Lg, Pg/Lg has a somewhat weaker dependence on shot depth, scaled depth, and ESD.

We also compared the spectral content of individual Pn and Pg windows after correcting for the large differences in the explosion yields. For the latter, we made use of von Seggern and Blandford's (1972) source scaling, in which the source function for a given yield Y is expressed as

$$S(\omega) = Y \frac{\left[A^2(\omega/k)^2 + 1\right]^{1/2}}{\left[(\omega/k)^2 + 1\right]^{3/2}} \Psi(\infty) \qquad \text{(C4)}$$

where $\omega = 2\,\pi\,f$, $\Psi(\infty)$ is a coupling term independent of frequency,

$$k = k_0\,(5/Y)^{1/3} \qquad \text{(C5)}$$

and

$$A = 2B + 1 \qquad \text{(C6)}$$

where B and k_0 are medium-dependent constants. In this model, shot depth is not an independent parameter, but the source function can be varied by assigning different values to the rise time and overshoot parameters k_0 and B, respectively. Considering first the Pn windows for the various explosions, the spectra were corrected for the instrument response and anelastic attenuation by assuming $t^* = 0.1$ sec, the value used by Blandford (1976). A correction for the

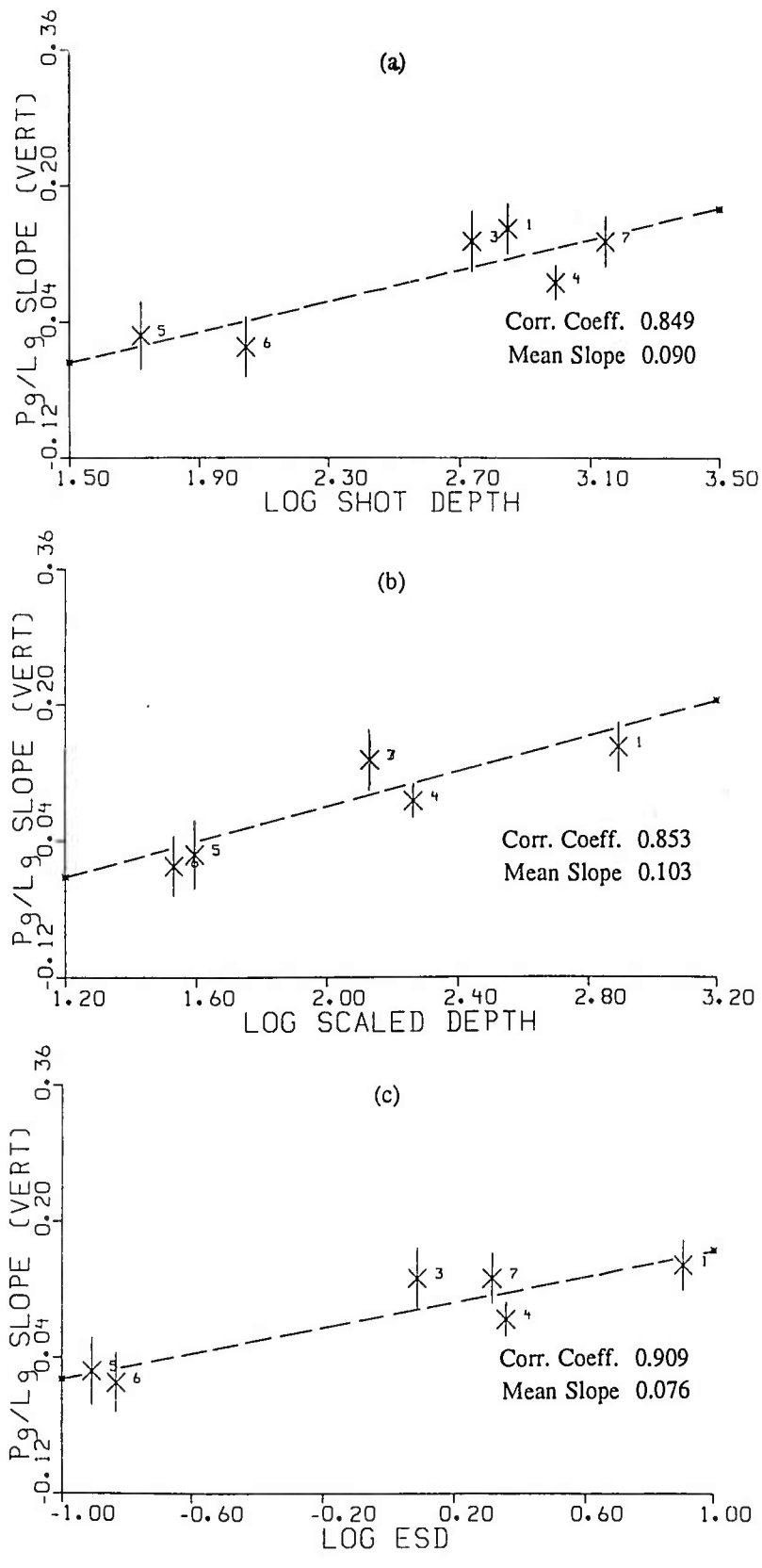

Figure C3. Similar to Figure C2 for the spectral ratio Pg/Lg. Note that the mean slope values of the linear trends in (a), (b), and (c) are smaller than the corresponding values in Figure C2, indicating smaller variation in the spectral slope Pg/Lg as compared to Pn/Lg.

differences in yield was applied by using the source function in equation (C4) to correspond to a tuff reduced displacement potential (RDP), i.e. $k_0 = 12.0$ and $B = 0$. With these three corrections, the Pn spectra become flat if the shot depth and medium did not influence the spectral shapes. Most of the corrected spectra were not flat and their mean spectral slopes indicated nearly linear trends (the results for Duryea and Buteo can be seen in Gupta et al., 1986b, Figure 18). This means that ordinary cube-root scaling (i.e. with fixed values of parameters k_0 and B) fails to model the observed Pn spectra of explosions with large variations in yield and shot depth. Plots of the derived mean spectral slopes (over the frequency range of 1 to 5 Hz) versus the shot depth, scaled depth, and ESD (all in log units) are shown in Figure C4. The least squares linear trends (dashed lines) have correlation coefficients of 0.827, 0.970, and 0.979, respectively, suggesting that the Pn spectra are influenced the most by ESD, somewhat less by scaled depth, and the least by shot depth.

The same corrections (i.e. $t^* = 0.1$ sec and tuff RDP) were also applied to the Pg spectra and the mean spectral slopes over the same frequency range computed. Plots of these slopes versus the shot depth, scaled depth, and ESD are shown in Figure C5. The use of $t^* = 0.1$ sec for Pg may not be justified, but a different value will simply raise or lower all data points by the same amount so that the correlation coefficient and mean slope values, indicated for the three plots in Figure C5, will not change. The linear trends (dashed lines) have correlation coefficients of 0.846, 0.977, and 0.992, respectively, again suggesting the Pg spectra are shaped the most by ESD, somewhat less by scaled depth, and the least by shot depth. A comparison of the mean slope values for the data in Figures 4 and 5 (indicated for each plot) indicates Pn spectral slope to be more variable than the Pg spectra slope.

An examination of the results in Figures 1 through 5 shows internal consistency and the following two results: (1) spectral ratios Pn/Lg, Pg/Lg as well as the spectra of Pn and Pg

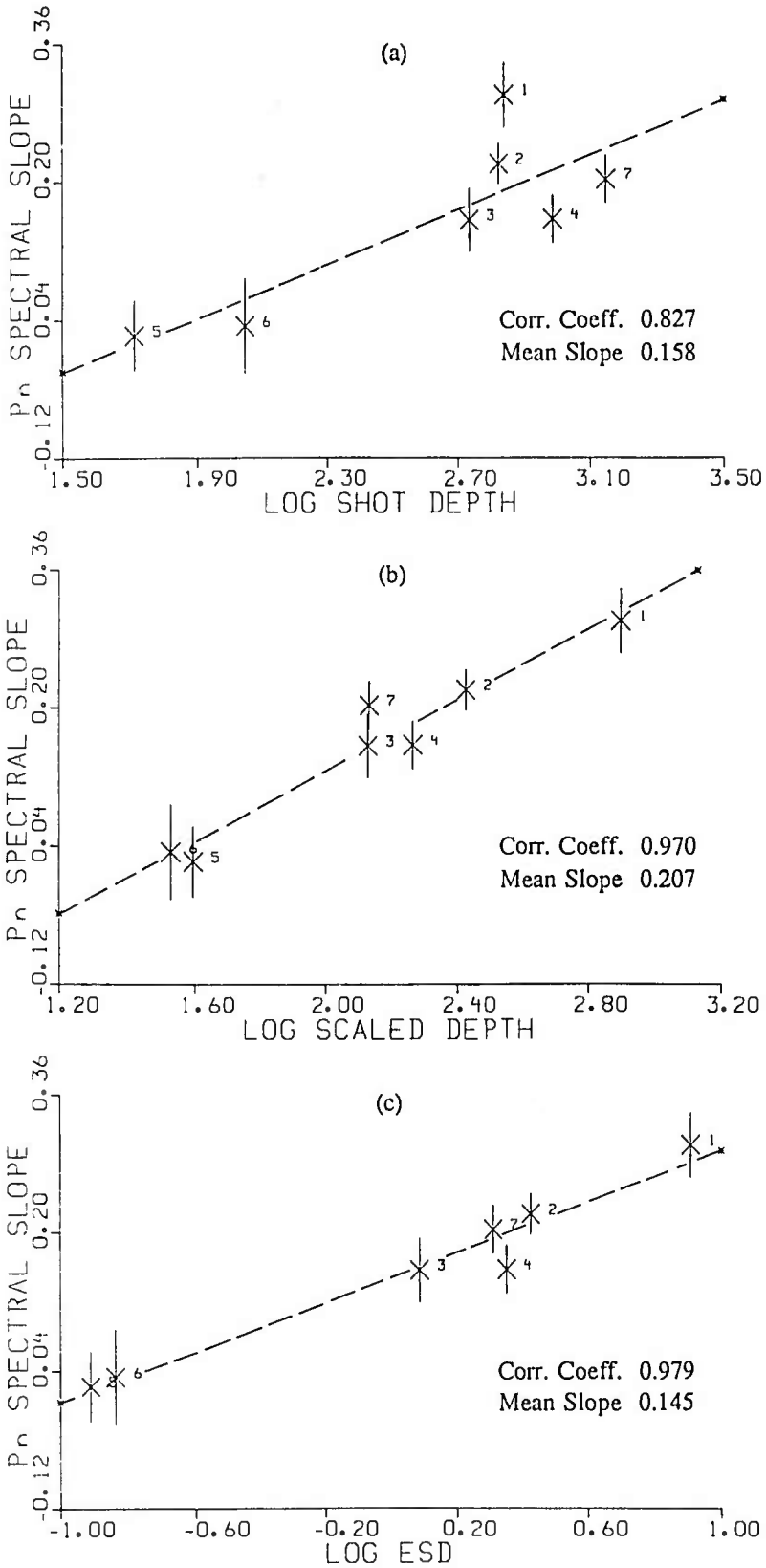

Figure C4. Mean spectral slope for Pn (corrected for noise, yield, and t*) over the frequency range 1 to 5 Hz versus (a) log (shot depth in meters), (b) scaled depth, and (c) log ESD for 7 explosions, numbered as in Table C1. The vertical lines represent error bars with one standard deviation. The correlation coefficient and mean slope value of the least squares linear trend (dashed line) is indicated for each plot.

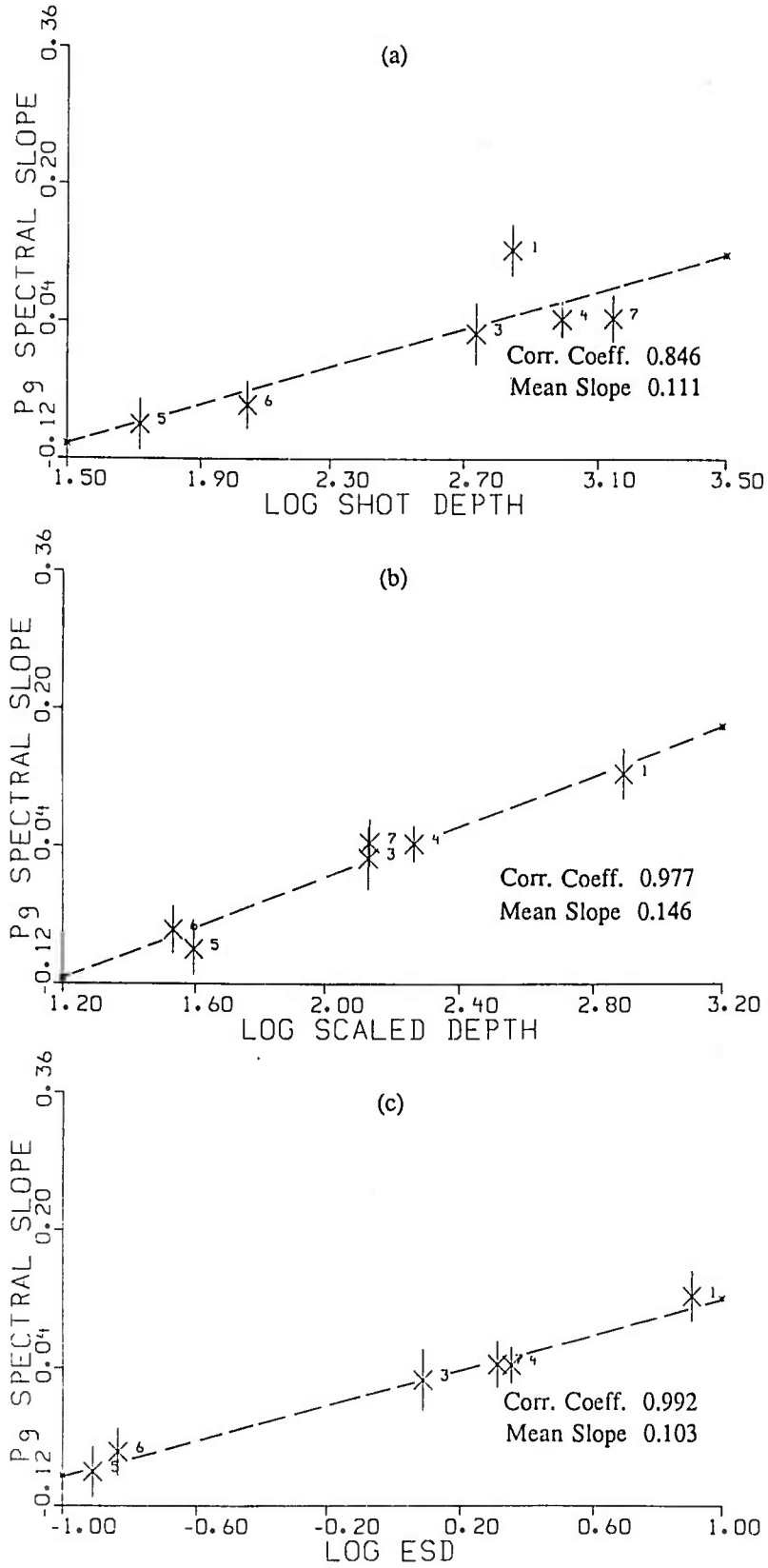

Figure C5. Similar to Figure C4 for Pg. Note that the mean slope values of the linear trends in (a), (b), and (c) are smaller than the corresponding values in Figure C4, indicating smaller variation in the spectra of Pg as compared to Pn.

depend the most on ESD, somewhat less on scaled depth, and the least on shot depth, and (2) the enrichment of higher frequencies due to increased ESD is the largest in the spectra of Pn, somewhat less for Pg, and the least for Lg.

Low-Frequency Asymptote and Deconvolved Pn

The low-frequency asymptote, A_o, and the area under the initial pulse of deconvolved Pn (denoted by Ω_o) are good measures of the explosion yield (Douglas et al., 1987; McLaughlin et al., 1987). A spectral measure of A_o was made by removing the instrument response, correcting for noise, and then least-squares fitting the log-amplitude spectra to a model spectrum with a fall-off rate of f^{-3} (McLaughlin et al., 1987). The amplitude spectrum was assumed to have the form (Boatwright, 1978)

$$A(f) = \frac{A_o}{\sqrt{1 + (f/f_c)^6}} \qquad (C7)$$

where f_c is the corner frequency. The least squares fit to the log-amplitude spectra was determined for the combination of A_o and f_c; the derived values are listed in Table C2. Plots of log (A_o/Y) versus (a) shot depth, (b) scaled depth, and (c) ESD, are shown in Figure C6. Assuming linear trends (dashed lines), it seems that, for a fixed yield, the low-frequency asymptote, A_o, is influenced the most by scaled depth, somewhat less by ESD, and considerably less by shot depth. The values of mean slope of the linear trends in the three plots in Figure C6 are also indicated.

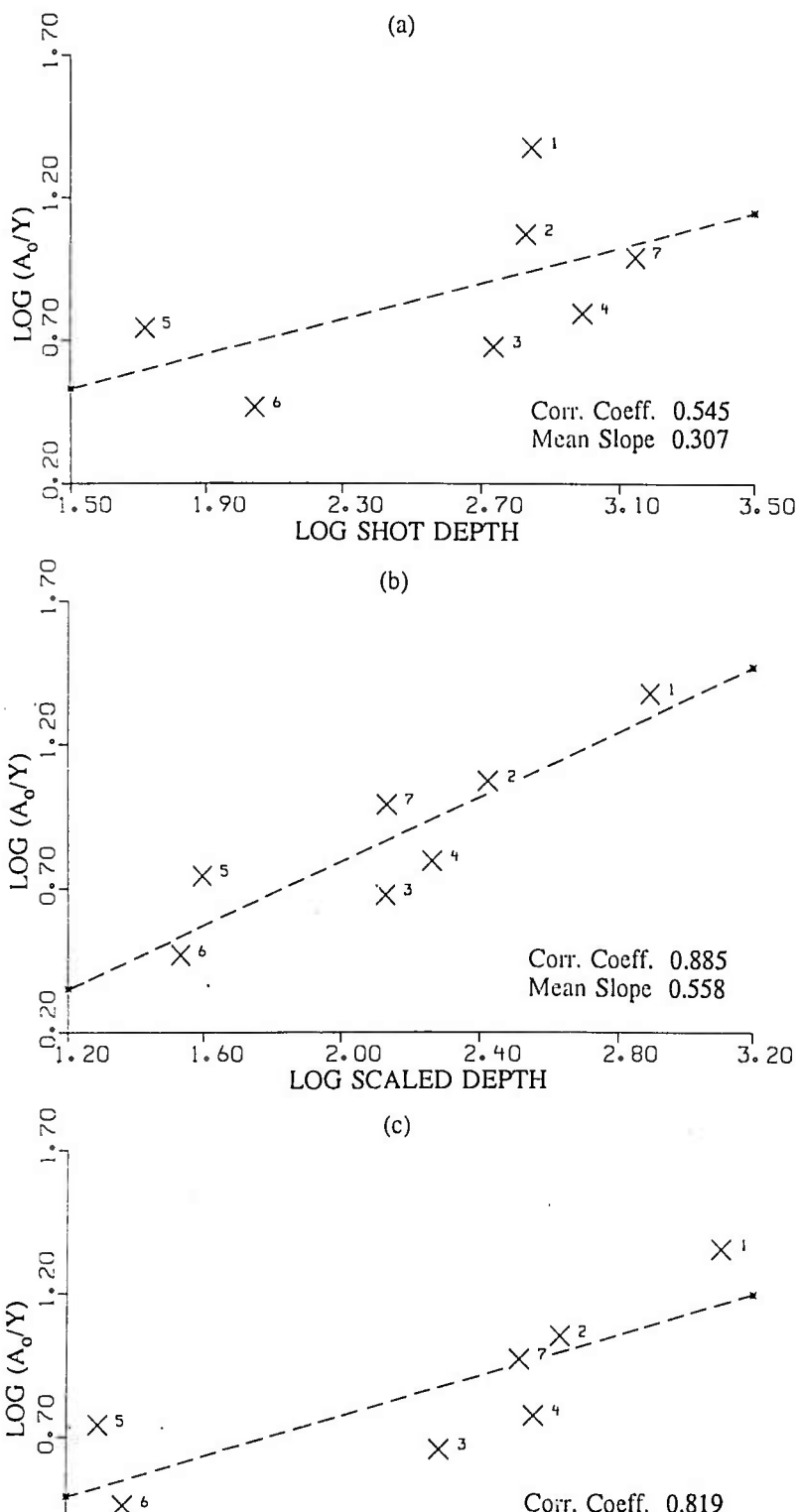

Figure C6. Log (A_o/Y) versus (a) shot depth, (b) scaled depth, and (c) log ESD for 7 explosions, numbered as in Table C1. The correlation coefficient and mean slope value of the least squares linear trend (dashed line) is indicated for each plot.

TABLE C2

VALUES OF A_o, f_c, AND Ω_o FOR PAHUTE MESA EXPLOSIONS

No.	Name	A_o (nm-sec)	f_c (Hz)	Ω_o (nm-sec)
1	BUTEO	16.62	6.64	13
2	REX	189.0	3.15	160
3	DURYEA	310.0	2.68	414
4	SCOTCH	936.9	2.60	1257
5	CABRIOLET	12.77	3.81	11.5
6	SCHOONER	103.0	1.68	142
7	BENHAM	10760	1.89	8627

The Pn arrivals at the LRSM station KN-UT were deconvolved by removal of the instrument response and selection of an optimum bandpass that takes into consideration the ambient noise spectrum (Gupta and McLaughlin, 1987). The values of Ω_o were obtained by measuring the area of the first positive pulse (Table C2). Figure C7 shows plots of log (Ω_o/Y) versus (a) shot depth, (b) scaled depth, and (c) ESD. The three plots have linear trends (dashed lines) suggesting that Ω_o is influenced the least by shot depth and considerably more by scaled depth and ESD. The values of mean slope of the linear trends in the three plots in Figure C7 are also indicated; these are all smaller than the corresponding slopes in Figure C6.

As expected, the two measures A_o and Ω_o are nearly equal (Table C2). A plot (log-log scale) of the area under the initial pulse of deconvolved Pn, Ω_o versus the low-frequency asymptote, A_o, is shown in Figure C8. The near-equivalence of the two measures is attested by the high correlation coefficient and an estimated slope value close to unity.

When comparing contained and cratering explosions, Blandford (1976) observed significant spectral differences between the two types of explosions for both body and surface waves. It is therefore important to examine whether scaled depth and ESD are significant

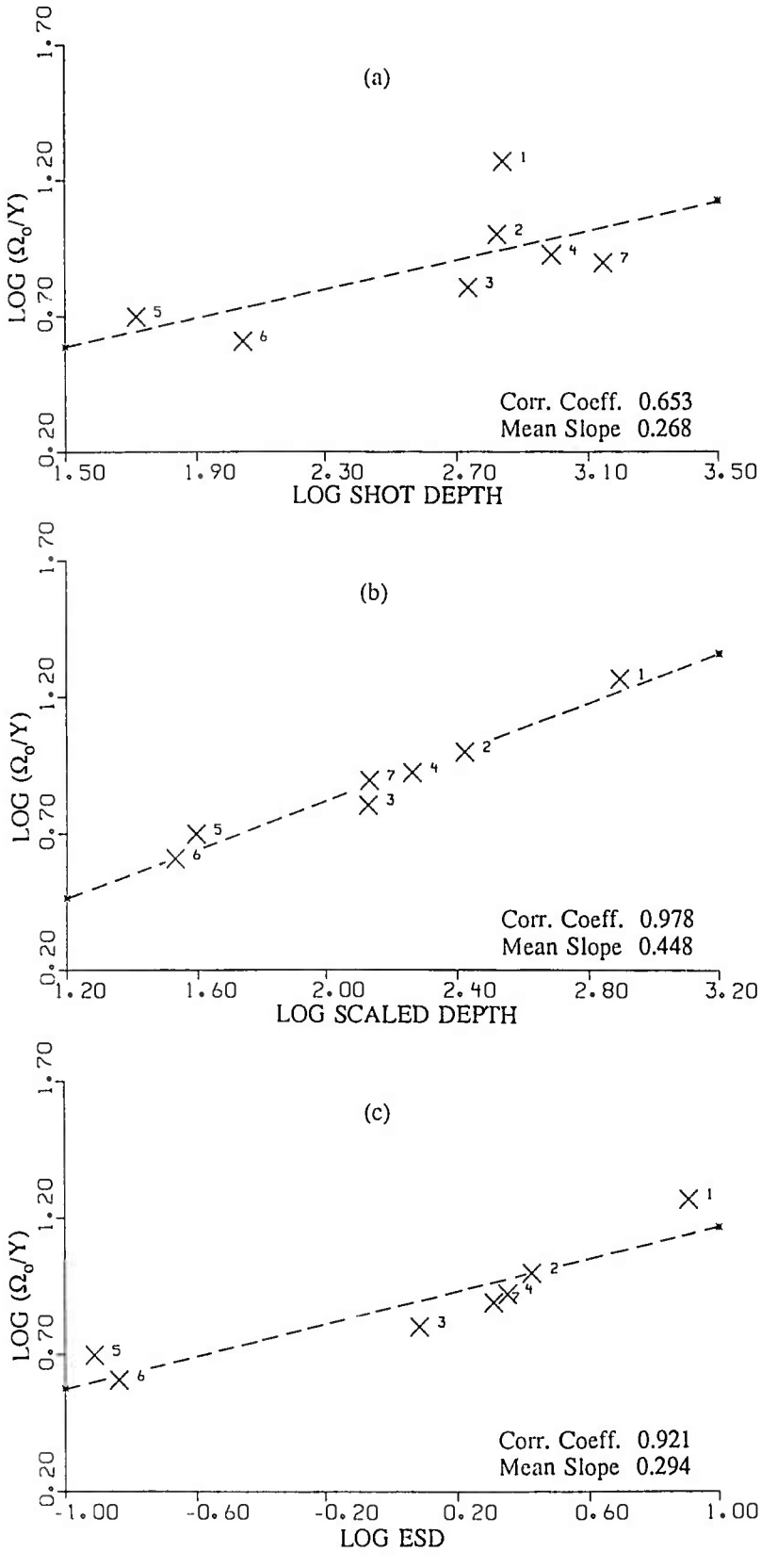

Figure C7. Similar to Figure C6 for log (Ω_o/Y). Note that the mean slope values of the linear trends in (a), (b), and (c) are smaller than the corresponding values in Figure C6, indicating somewhat smaller variation in log (Ω_o/Y) as compared to log (A_o/Y).

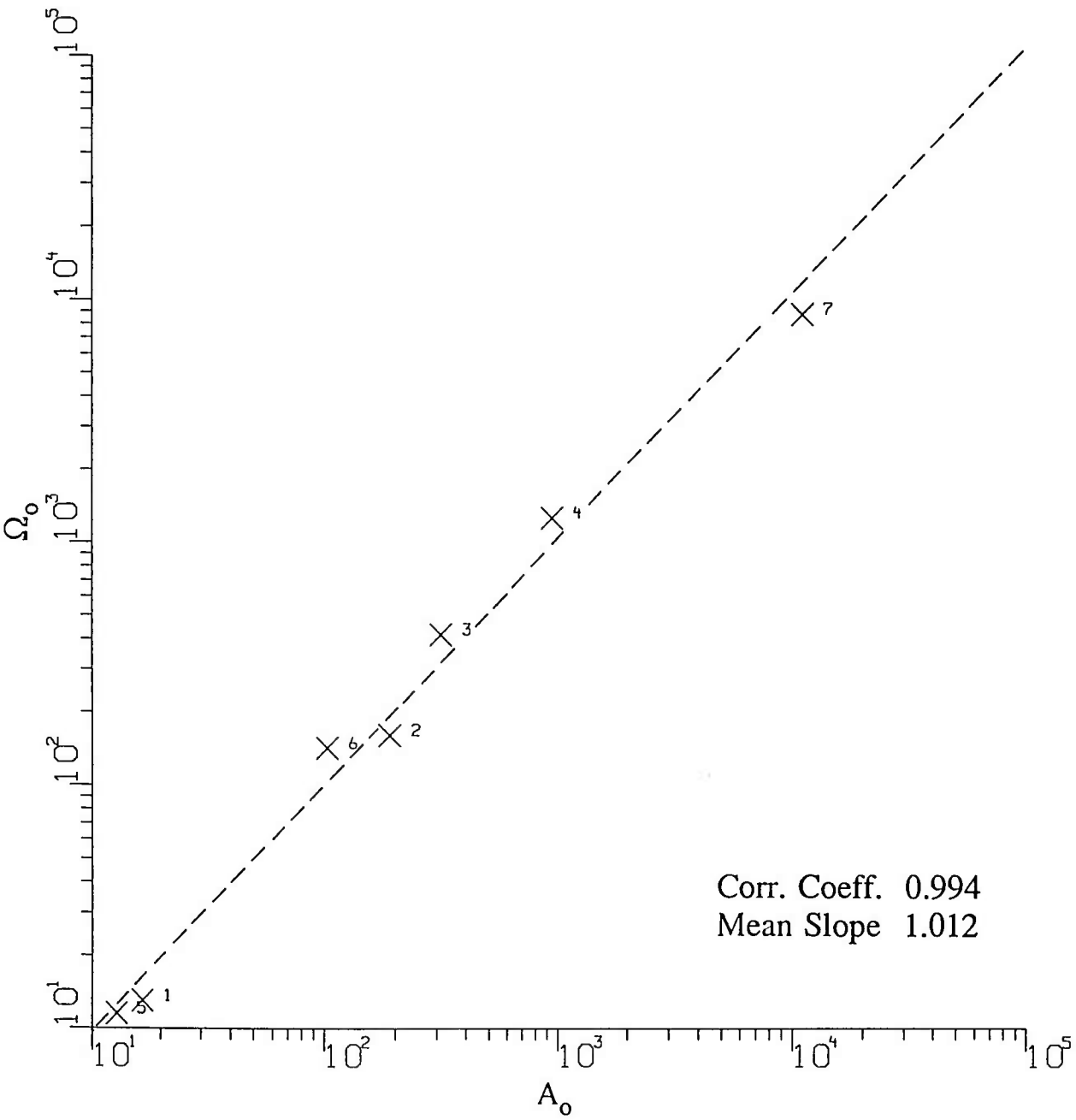

Figure C8. Plot (log-log scale) of the area under the initial pulse of deconvolved Pn, Ω_o, versus the low-frequency asymptote, A_o, both in units of nm-sec. The near equivalence of the two measures is confirmed by the high correlation coefficient value and slope close to unity.

parameters when the two cratering shots are excluded from the data set. The data in Figures C2 and C3 appear to suggest poor correlations for all three (shot depth, scaled depth, and ESD) parameters if only the contained shots are considered. However, the data in the remaining four figures (C4, C5, C6, and C7) strongly indicate the scaled depth and ESD to provide correlations that are considerably better than with shot depth. A comparison of the correlation coefficient values for all 7 shots and for only 5 contained shots is shown in Table C3.

TABLE C3

COMPARISON OF RESULTS WITH AND WITHOUT TWO CRATERING SHOTS

PARAMETER	CORRELATION COEFFICIENT					
	7 SHOTS			5 SHOTS		
	LOG SHOT DEPTH	LOG SCALED DEPTH	LOG ESD	LOG SHOT DEPTH	LOG SCALED DEPTH	LOG ESD
Pn SPECTRAL SLOPE	0.827	0.970	0.979	0.092	0.908	0.928
Pg SPECTRAL SLOPE	0.846	0.977	0.992	0.145	0.983	0.987
LOG (Ω_0/Y)	0.653	0.978	0.921	0.133	0.984	0.994
LOG (A_0/Y)	0.545	0.885	0.819	0.035	0.883	0.938

Comparison with Mueller-Murphy Scaling

By analyzing a large amount of near-field data, Mueller and Murphy (1971) found that the yield, depth of burial, and emplacement medium play dominant roles in defining the seismic-spectrum scaling of underground nuclear explosions. They used source-receiver distances of about 100 km or less and examined the spectra of the entire seismograms. In nearly all cases, S waves (including Lg) dominate over other arrivals. In fact, a comparison of the spectral ratios based on S waves and total seismograms by Murphy (1975) indicated the two

spectral measures to be essentially identical for frequencies greater than 1 Hz.

Our results clearly indicate that the spectral scaling is strongly dependent on the phase type. In other words, the variation with yield of the source spectrum is not the same for Pn, Pg, or Lg phases. For example, in Figure C1, the inter-event spectral ratios of Pn, Pg, and Lg are significantly different for both pairs of shots. In most cases, S waves or Lg dominate the ground motion, so that scaling based on the entire seismogram may not be valid for scaling of Pn or Pg. As an example, let us consider the data from Rex (overburied) and Schooner (cratering), both of which were used in Mueller and Murphy's study. One of their results is reproduced in Figure C9, which shows the pseudo relative velocity (PSRV) spectra (for 5 % damping) of Rex and Schooner based on the horizontal component data at station SE-6 (epicentral distance about 110 km). We obtained the PSRV response spectrum in the manner described in Gupta and McLaughlin (1987); only spectral points with S/N power ratio of at least 2 are plotted. The PSRV spectra from the horizontal radial (R) component data at KN-UT are shown in Figure C10, which shows results from both (a) Pn (6.4 sec window) and (b) total seismogram (denoted by ALL). There is good agreement between the spectra in Figures 9 and 10b, especially for periods longer than 0.2 sec. In both figures, the Schooner and Rex spectra cross each other at a period of about 0.5 sec. The PSRV spectra of Pn (Figure C10a) appear to be quite different from those in Figure C10b, especially for periods longer than 0.5 sec. The spectral ratios Rex/Schooner are probably not significantly different, except that for periods longer than 0.5 sec, the ratio is about 2 for Pn and about 3 for ALL in Figure C10. The results from another pair of events, Buteo (overburied) and Cabriolet (cratering), are shown in Figure C11. The spectra based on the total seismogram (Figures C10b and C11b) appear fairly similar, whereas those for Pn (Figures C10a and C11a) are significantly different. For periods greater than about 0.5 sec, the spectral ratio Buteo/Cabriolet for Pn (Figure C11a) is significantly different from that for the total seismogram (Figure C11b).

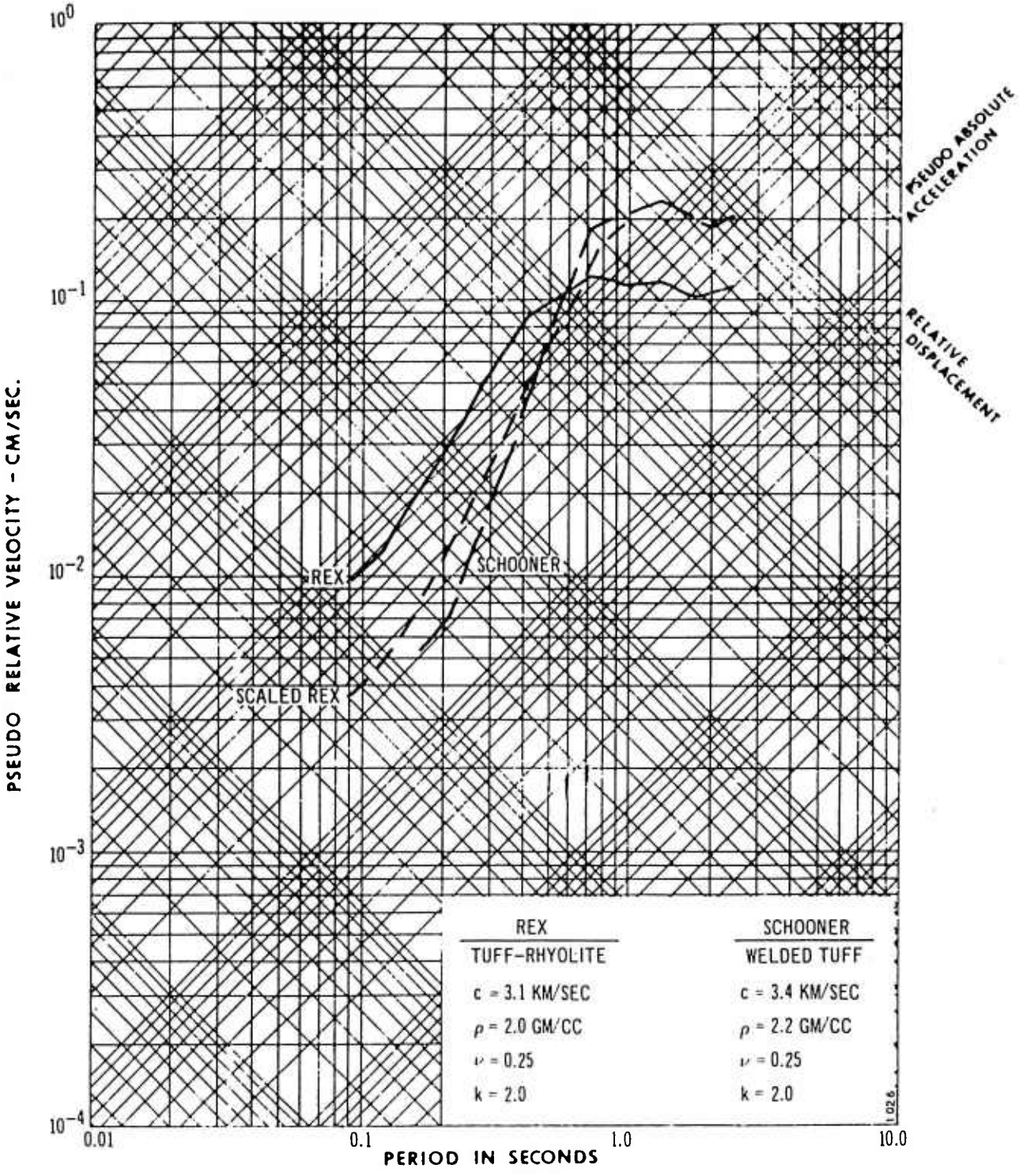

Figure C9. Comparison of Rex (overburied), scaled Rex, and Schooner (underburied) spectra at SE-6, Las Vegas (Horizontal Component), after Figure 11, Mueller and Murphy (1971).

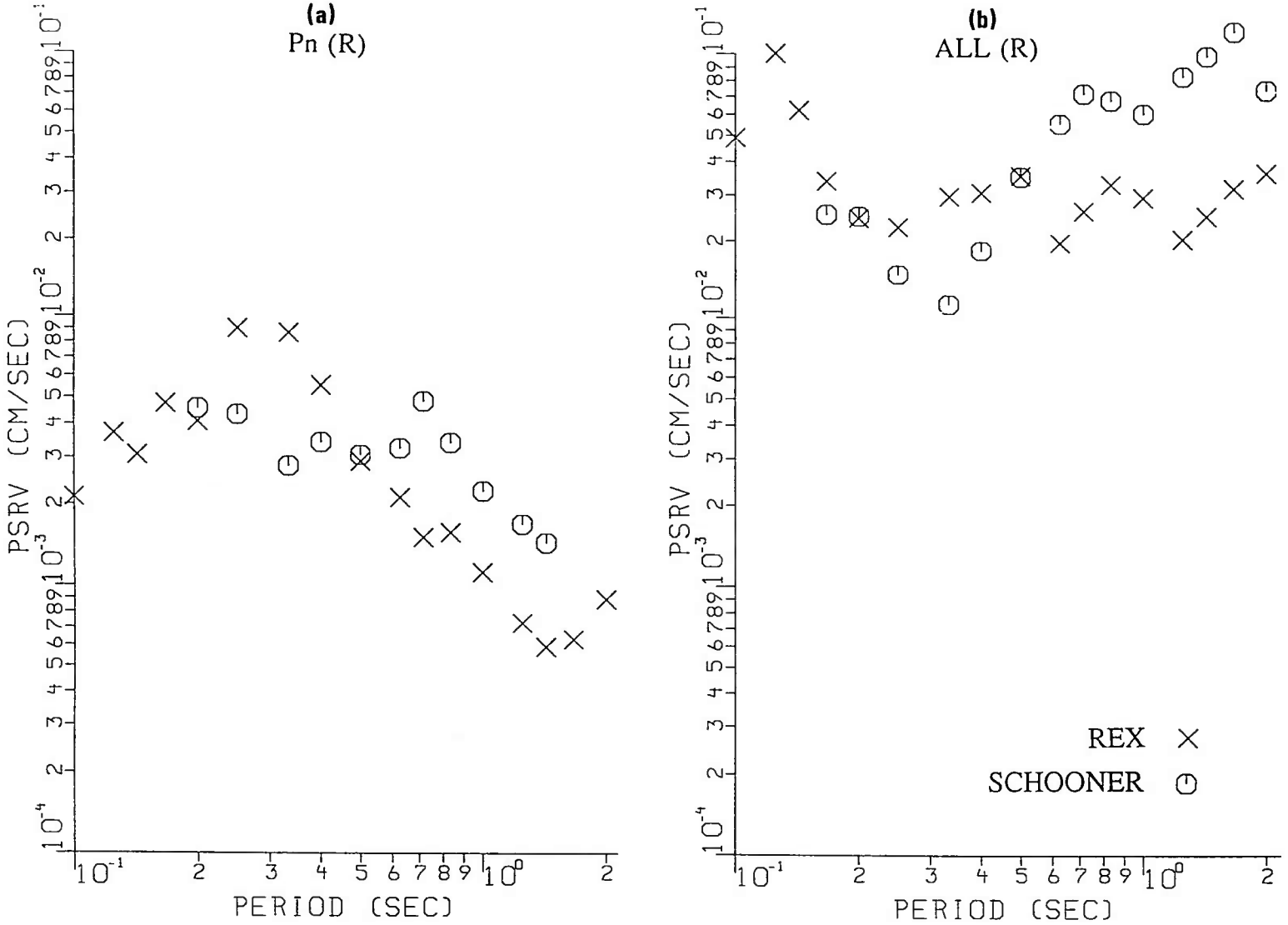

Figure C10. PSRV spectra based on radial component data at KN-UT for (a) Pn (6.4 sec window) and (b) total (ALL) seismogram (102.4 sec window) for Rex and Schooner. Only spectral points with S/N power ratio of at least 2 are plotted.

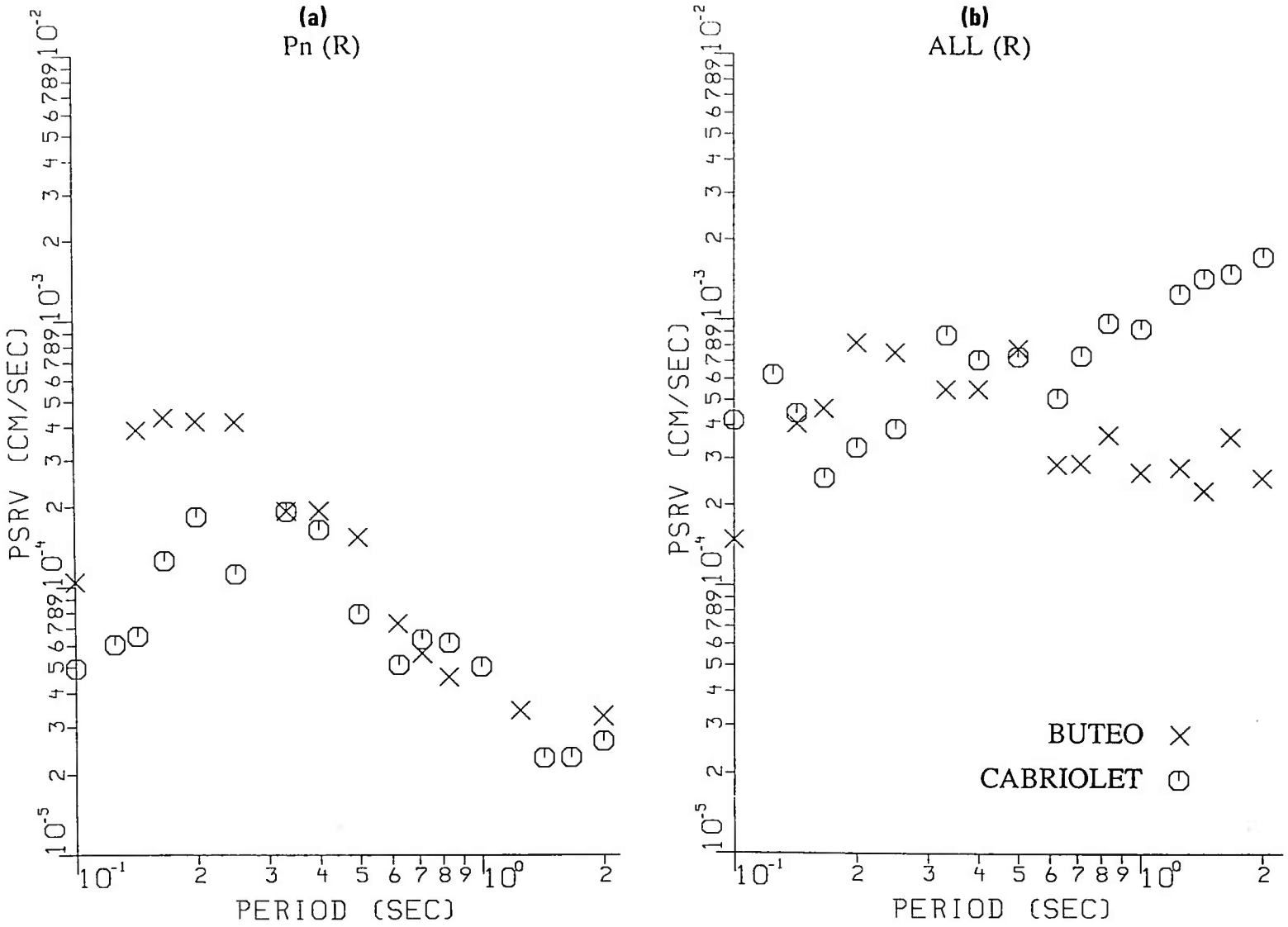

Figure C11. Similar to Figure C10 for Buteo (overburied) and Cabriolet (underburied).

Quite often, horizontal component data are not available and only vertical component records are used. On the vertical component record of Rex, the phase Pg is clipped, so that PSRV spectra similar to those in Figure C10b could not be obtained. Results from the vertical component data from Buteo and Cabriolet at KN-UT are shown in Figure C12. A comparison with Figure C11 suggests that the horizontal and vertical component spectra are by no means identical, although the spectral ratios Buteo/Cabriolet are rather similar.

Discussion and Conclusion

The spectral ratio P/P-coda, obtained from short-period, vertical component records of 20 NTS explosions recorded at teleseismic distances, showed significant correlation with both P-wave overburden velocity, $\bar{\alpha}$, and shot depth (see Figures 4 and 5, Gupta and Blandford, 1987). Assuming that these shots were fired approximately at their scaled depths, equation (2) would suggest that both $\bar{\alpha}$ and h are rough measures of ESD, since $\bar{\alpha}$ and ρ are nearly always well correlated and each increases with depth. Thus, the spectral slope of P/P-coda at teleseismic distances varies with ESD in the same manner as Pn/Lg at regional distances. Moreover, in Gupta and Blandford's (1987) study, most of the spectral variation appeared to be in the initial P waves and P-coda was found to be stable, similar to the results for Pn and Lg spectra in this study. By applying frequency-wavenumber methods to NORESS data from NTS explosions, Dainty (1985) found evidence indicating that the dominant mode of near-source scattering contributing to teleseismic P coda is Lg to P due to shallow heterogeneity. It seems therefore that the spectral variations with ESD in Pn and Lg at regional distances are similar to those of P and P-coda at teleseismic distances.

Flynn (1986) studied effects of source depth on near source seismograms by examining the spectra of P and SV-Rayleigh surface waves from five 115 kg chemical explosions buried at depths ranging from 1.8m (optimum cratering depth) to 11.5 m (fully contained). Energy in

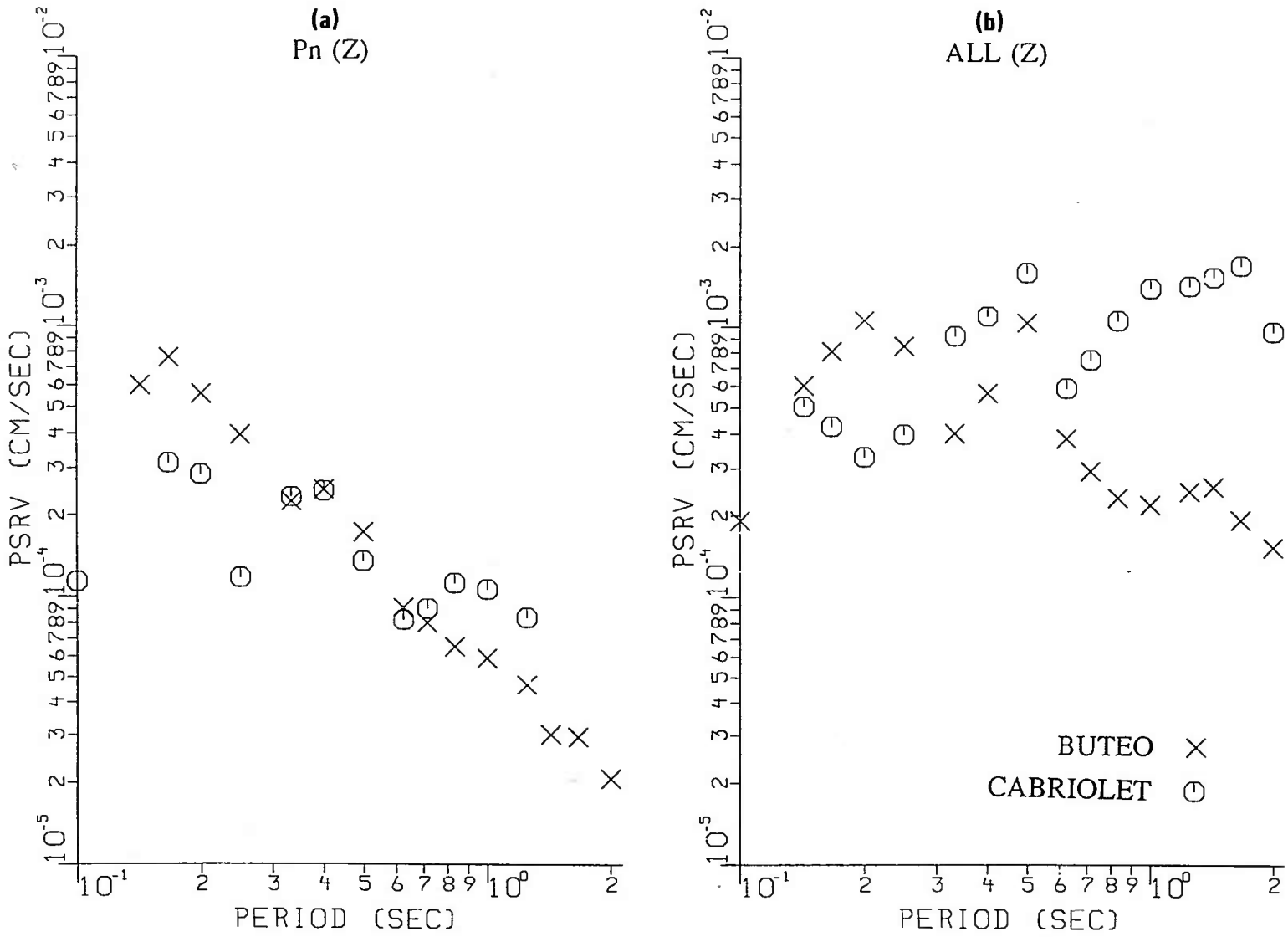

Figure C12. Similar to Figure C10 for Buteo (overburied) and Cabriolet (underburied) but for the vertical (Z) components.

the high frequency band of 10 to 40 Hz, dominated by P waves, was found to increase significantly with source depth whereas energy in the low frequency band of 4 to 12 Hz, consisting mostly of SV-Rayleigh waves, was not a strong function of shot depth. It was concluded that the fully contained source generates more high frequency energy as a result of an increase of coupling over the near-surface source. Our results regarding the influence of scaled depth (or ESD) on the relative excitation of P and Lg as well as on A_o and Ω_o are therefore in good agreement with those of Flynn (1986).

Underground nuclear explosions are generally very complex with both primary and secondary sources of seismic waves (e.g. Stump, 1987; Stump and Reinke, 1987). The idealization of an explosion source as a pressure pulse applied to the walls of a spherical cavity should at best be used to infer only qualitative results. Non-linear effects, known to be important for most nuclear explosions (especially those with shallow scaled depths) also drastically modify the seismic signals (Perl et al., 1979; Rimer et al., 1979; Day et al., 1986). Note that non-linear finite difference modeling of the explosion source indicates strong dependence on scaled depth that differs significantly from that derived by assuming an elastic point source (Day et al., 1986).

Pn arrivals from deeper and/or overburied explosions are richer in high frequencies as compared to their Lg. These results, similar to the earlier results of Blandford (1976) based on observations of Pn and Rayleigh wave spectra, indicate that the scaling laws may be strongly dependent on the phase type. Scaled depth or ESD, a measure of the source size, appears to play an important role in shaping the spectra of various regional phases as well as in determining A_o and Ω_o, both of which are measures of the explosion seismic moment.

D. DECONVOLUTION AND SPECTRAL RATIOS FROM SOVIET SALT SHOTS

Introduction

We first applied the maximum-likelihood multichannel deconvolution method of Shumway and Der (1985) to teleseismic P waves from 10 salt shots in the Astrakhan region of the USSR (Table D1). The deconvolution method utilizes the well known fact that P wave spectra can be decomposed into source and receiver spectral factors; details of the procedure can be found in Shumway and Der (1985) and Der et al. (1987). The multichannel deconvolution approach for estimating source and site region characteristics has several advantages. First, the method utilizes both amplitude and phase information in the frequency domain calculations. Since this is a frequency domain calculation, the maximum available bandwidth can be used, avoiding the ambiguities associated with time domain fitting of narrow frequency band seismic signals. Furthermore, no *a priori* assumptions need to be made about the complexity of either the source or the site spike series, e.g. the presence of pP does not need to be presupposed by providing an initial guess of the pP delay time and amplitude. Therefore, the source functions obtained in the deconvolution process provide a better estimate of the explosion source time functions, especially the presence or lack of secondary arrivals following the direct P wave such as pP or spall.

We also carried out single-station deconvolutions for 4 salt shots of October 16, 1982 recorded at two SRO stations, ANMO and KONO. In order to explore why the last shot in the sequence has a larger magnitude value than the earlier three, we obtained mean amplitude ratios of P and P-coda, spectral ratio slopes of P, and P/P-coda spectral slopes.

Multichannel Deconvolutions

Two sequences of Astrakhan events containing 4 and 6 events on October 16, 1982 and September 24, 1983, respectively (Table D1), were deconvolved from observations at GBA and the four RSTN stations, RSON, RSON, RSNT, and RSSD. From the GBA array data, four common receivers with good S/N were selected. The values of t* for GBA and RSTN were assumed to be 0.15 and 0.2 sec, respectively. Following Borg (1983), the yields of all 10 shots in salt were considered to be 15 kt each; the corresponding von Seggern and Blandford (1972) or "VSB" wavelet was based on this yield value.

TABLE D1

ASTRAKHAN SHOTS DECONVOLVED IN THE STUDY
(Information from the ISC Bulletins)

Event	Origin Time	Location		m_b
		Lat(°N)	Lon(°E)	
1982289a	05:59:57.4	46.77	48.22	5.2
1982289b	06:04:57.4	46.77	48.24	5.2
1982289c	06:09:57.4	46.77	48.22	5.2
1982289d	06:14:57.5	46.75	48.20	5.4
1983267a	04:59:57.2	46.81	48.29	5.2
1983267b	05:04:57.3	46.81	48.27	5.1
1983267c	05:09:57.4	46.84	48.33	5.0
1983267d	05:14:57.4	46.84	48.29	5.2
1983267e	05:19:57.4	46.88	48.30	5.4
1983267f	05:24:57.0	46.80	48.29	5.3

Figure D1 shows source time functions for the four events of October 16, 1982 deconvolved separately from data recorded at GBA (left) and four of the RSTN stations (center). The VSB wavelet has been removed in the deconvolutions. The relatively great depth of these shots can be inferred from the pP delay time of over 1 sec for all four shots. There are also two or three arrivals which consistently show up between the P and pP. These appear to be

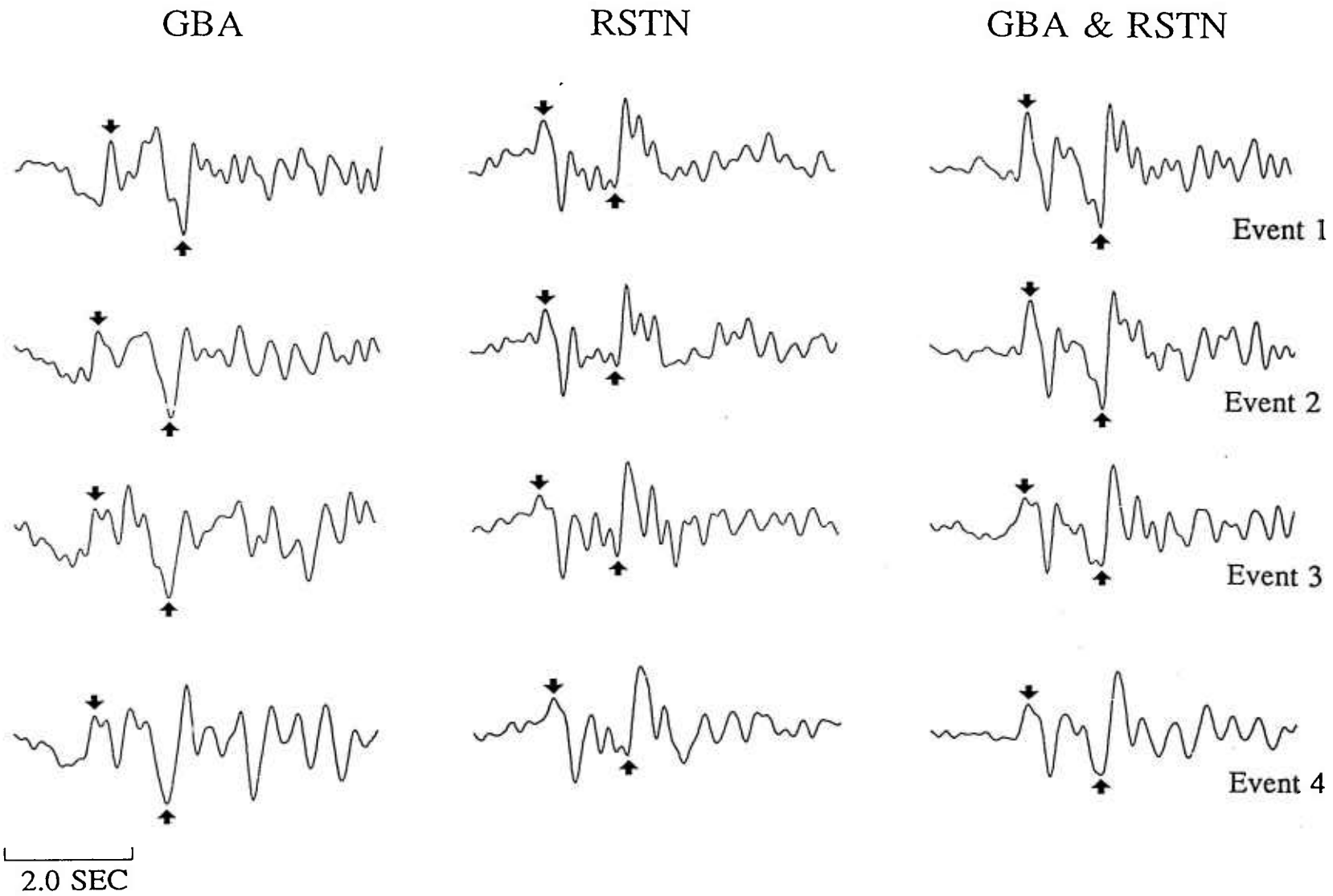

Figure D1. Deconvolved source time functions for the four Astrakhan events of October 16, 1982 recorded at GBA (left) and RSTN (center) and "joint" deconvolutions (right) based on the deconvolved waveforms from both GBA and RSTN. The arrows denote the peaks of P and pP arrivals.

similar to those observed for Salmon, and are interpreted to be reflections from the high impedance contrast layers between the shot point and the surface (Blandford and McElfresh, 1982). This is a distinct possibility because these shots were detonated within an area of salt domes.

The source time functions on the right in Figure D1 are the result of deconvolving the two separate sets of deconvolutions at the left and center. In this case, t* and instrument response were not removed since they had already been removed in the previous deconvolutions. These "joint" deconvolutions contain parts of the source time functions that are common to observations at both arrays and are therefore somewhat more azimuthally averaged and less complex than the other two sets. However, they do still show clear P and pP phases, which incidentally look very much like mirror images of each other.

Figure D2 shows the deconvolved source time functions for the six events of September 24, 1983 as recorded at GBA and obtained with the same parameters as for the four shots in Figure D1. As with the previous set of events, the pP delay time is over 1 sec, and there is an additional arrival or two between the P and pP. The six events are very closely co-located in space and time, so it is probably not surprising that their source functions look so similar.

Figure D3 shows the deconvolved source time functions for all ten Astrakhan events, as recorded at GBA, deconvolved together. Results from the RSTN stations, with the same parameters as for the four shots in Figure D1, are shown in Figures D4 and D5. One shot was not recorded at the RSTN station RSSD. Source deconvolutions from all ten shots recorded at three RSTN stations (Figure D4) are similar to those for 9 shots based on data from the four RSTN stations (Figure D5). Again, the depth and other secondary arrivals are very similar for all events.

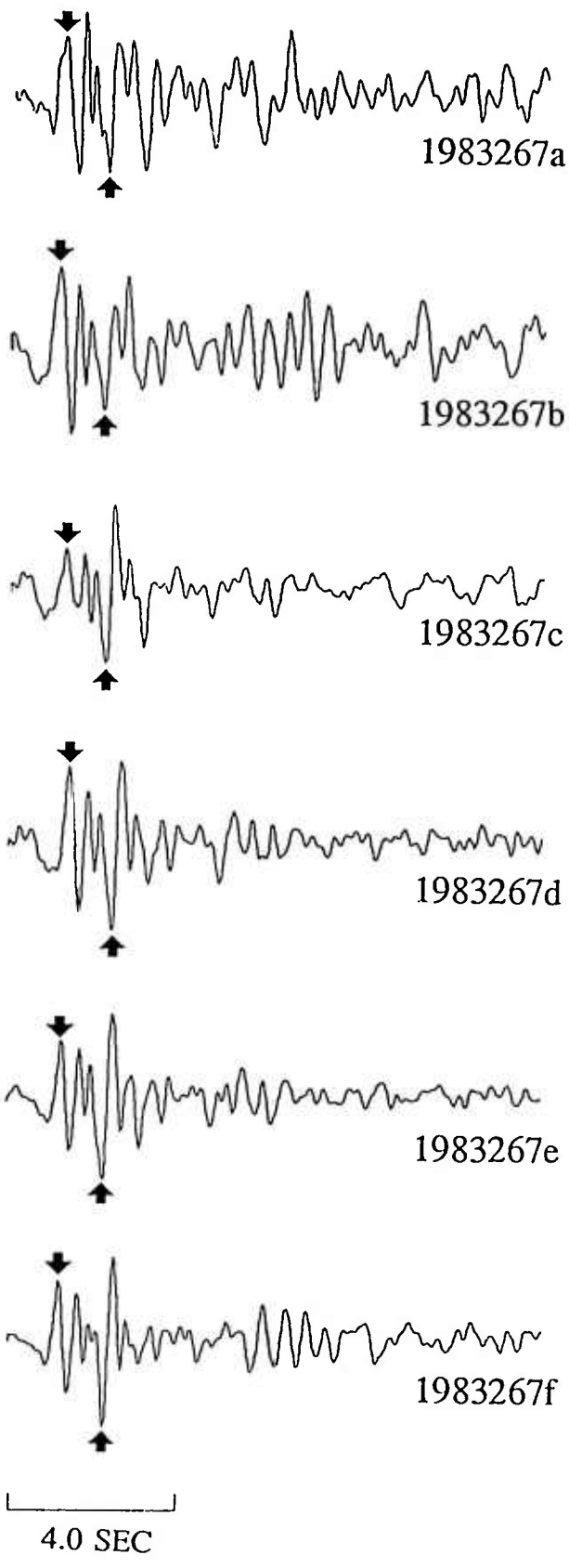

Figure D2. Deconvolved source time functions for the six Astrakhan events of September 24, 1983 recorded at GBA. The arrows denote the peaks of P and pP arrivals.

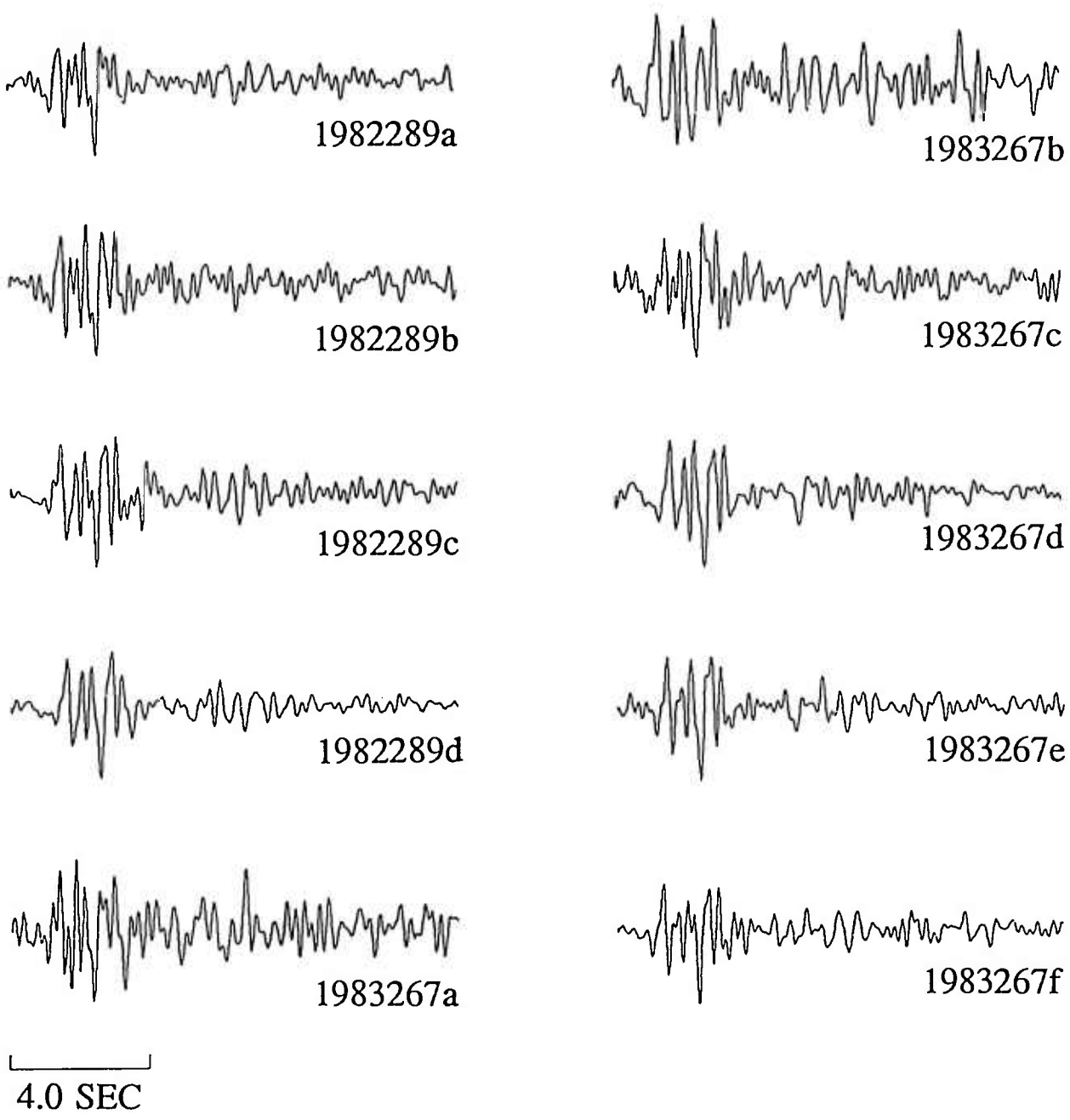

Figure D3. Deconvolved source time functions for the ten Astrakhan events of October 16, 1982 and September 24, 1983 recorded at GBA.

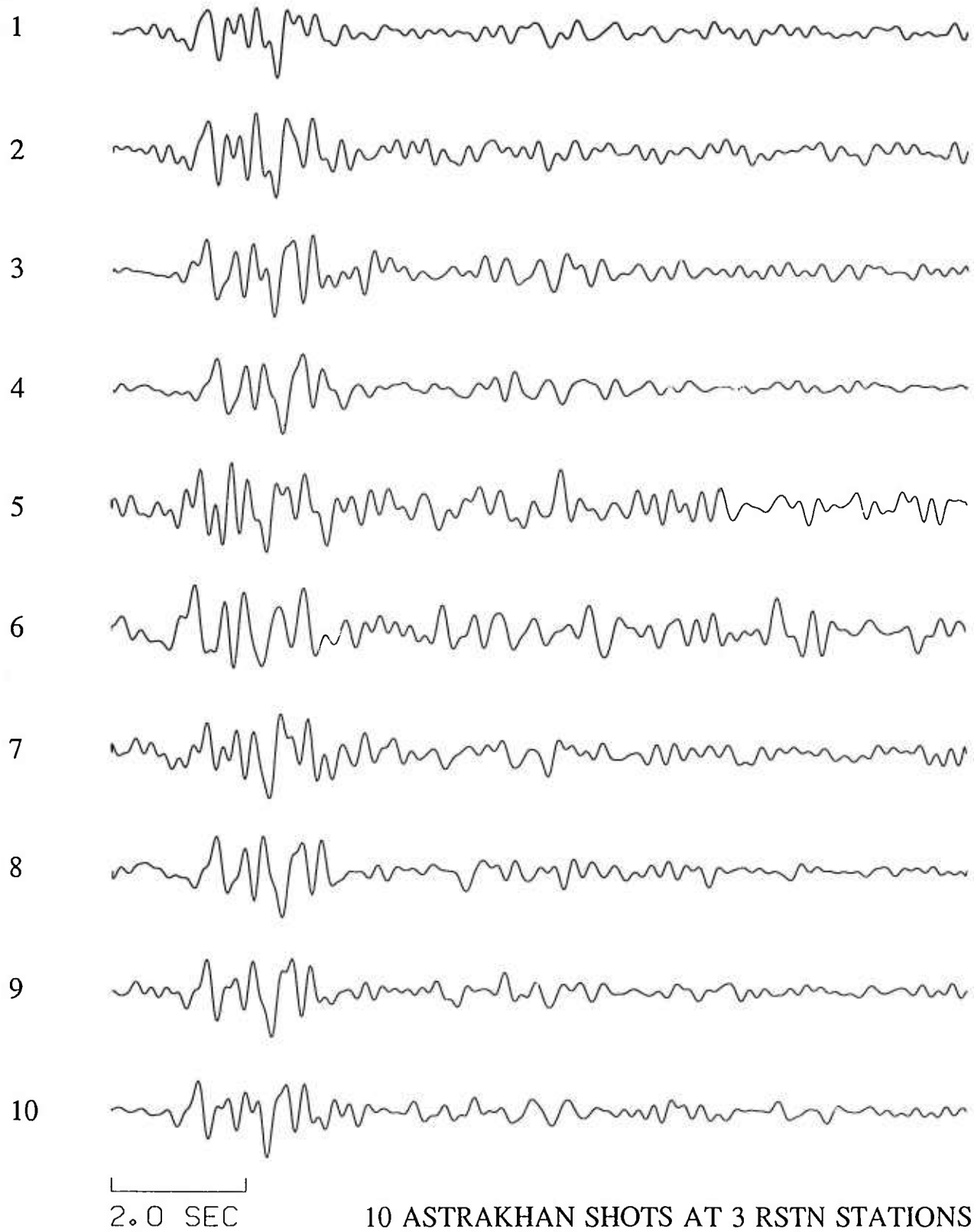

Figure D4. Deconvolved source time functions for the ten Astrakhan events of October 16, 1982 and September 24, 1983 recorded at the three RSTN stations RSON, RSNT, and RSNY.

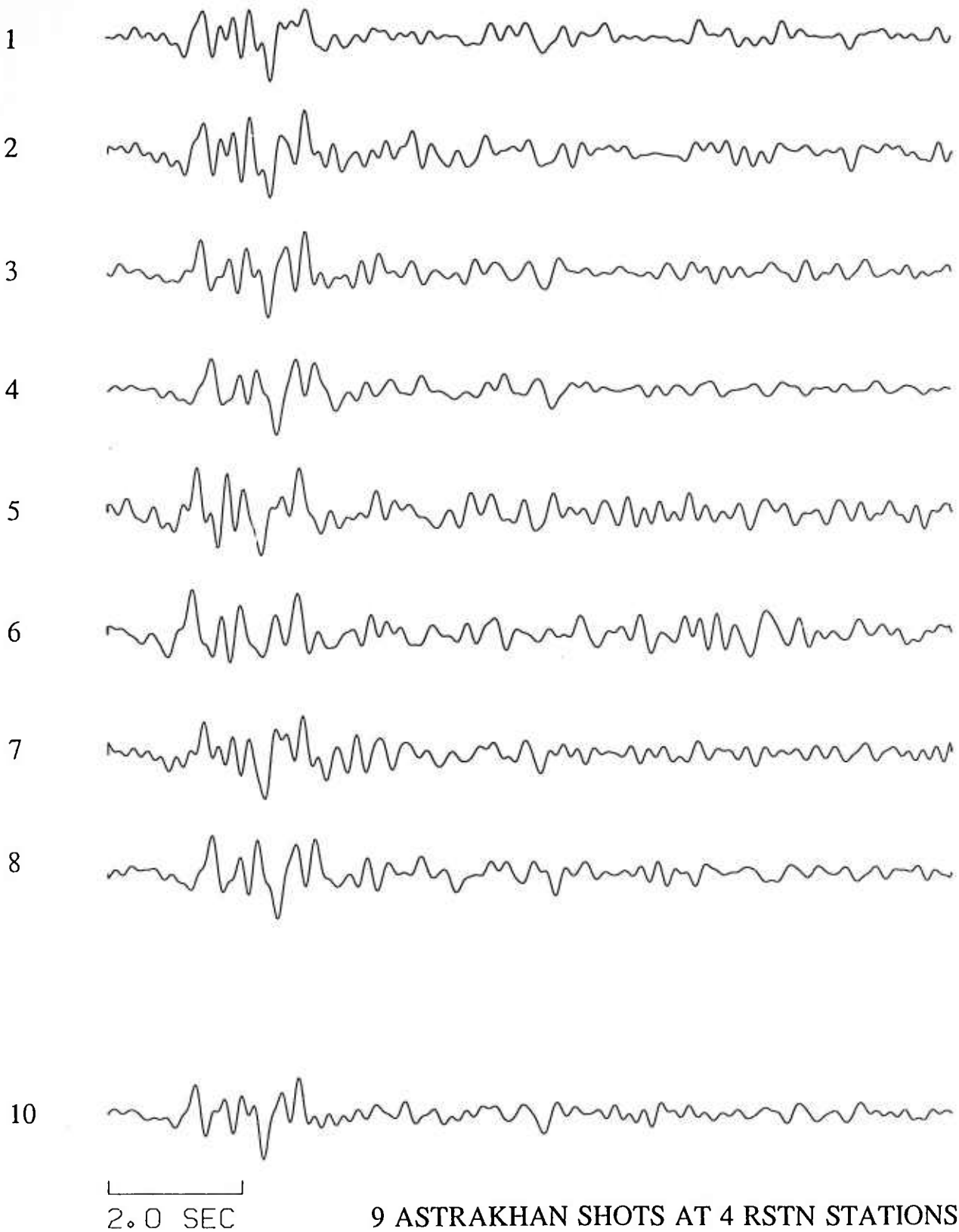

Figure D5. Deconvolved source time functions for nine Astrakhan events (four on October 16, 1982 and five on September 24, 1983) recorded at the four RSTN stations RSON, RSNT, RSNY, and RSSD.

Single Station Deconvolutions

Deconvolution of the four Astrakhan explosions of October 16, 1982 was extended to the teleseismic data from the SRO stations ANMO and KONO at epicentral distances, Δ of approximately 96° and 26°, respectively. The deconvolution is accomplished by removal of the instrument response, correction for the appropriate t*, and selection of an optimum bandpass that takes into consideration both the instrument response and the ambient noise spectra (Gupta and McLaughlin, 1987). We used t* = 0.45 for ANMO and t* = 0.40 for KONO. The results are shown in Figure D6. The first P arrivals at KONO are weak but, because of the triplication in the travel-time curves for the epicentral distance to this station, a second set of P waves corresponding to a later branch of the travel-time curve can be seen. The results are similar to those obtained earlier from the RSTN stations and the GBA array; the pP and P arrivals are again separated by about 1 sec for each of the four shots.

Spectral Ratios of P Waves

Deconvolved waveforms of the four shots of October 16, 1982 are similar and the P and pP arrivals are separated by nearly the same amount, suggesting nearly the same depth for all shots. Yet the magnitude of the last shot in the sequence is 0.2 unit larger than those of the earlier shots (Table D1). In order to explore a possible reason for this, we examined the spectra of P and P-coda for all four shots. We first obtained the mean spectral amplitude ratios of 6.4-sec long P windows (with 10% cosine taper and corrected for noise), averaged over the frequency range of 1 to 5 Hz (the frequency range with generally good S/N), for all inter-event combinations. Results for the six possible inter-event combinations from 4 shots (denoted by E1, E2, E3, and E4, respectively) recorded at the four RSTN stations and four sensors of the GBA array are shown in Figure D7. On the average, the last shot in the sequence is about 0.2 magnitude unit larger than the first three, in agreement with their m_b values. Similar mean

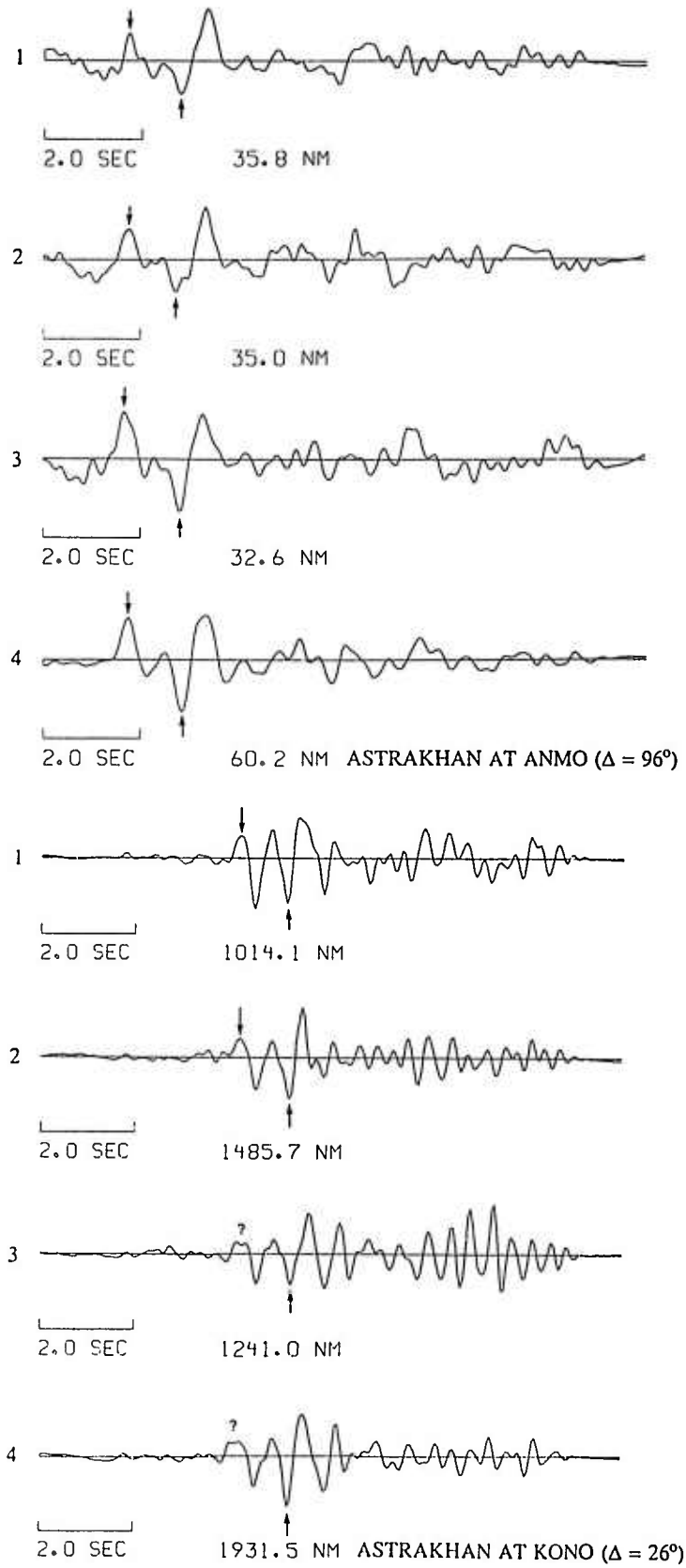

Figure D6. Deconvolved source time functions for the four Astrakhan events of October 16, 1982 recorded at ANMO and KONO. The numbers denote zero-to-peak amplitudes in nanometers. The arrows denote the peaks of P and pP arrivals.

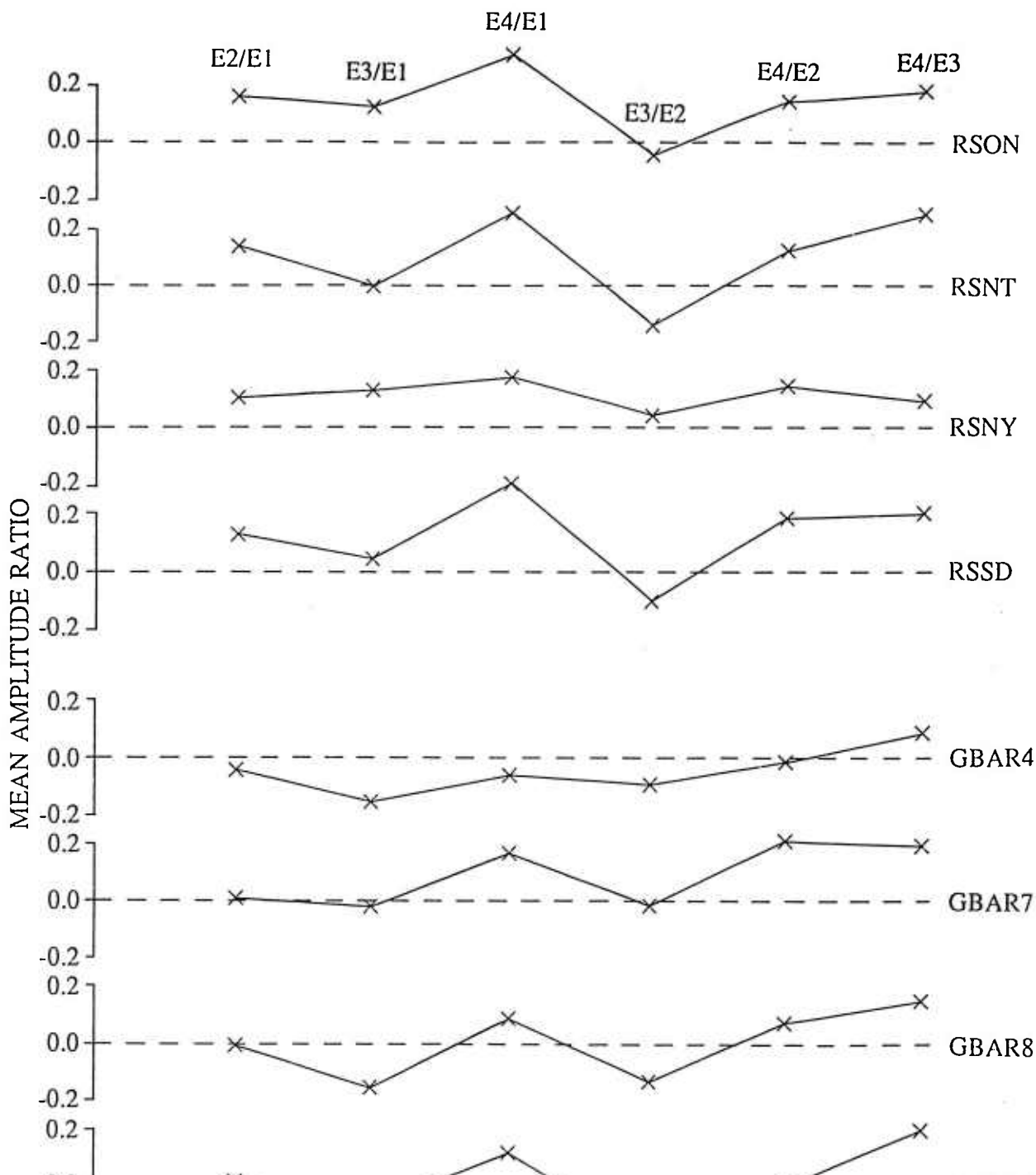

Figure D7. Inter-event mean spectral amplitude ratios of P, in log units and over the frequency range 1 to 5 Hz, for 4 RSTN and 4 GBA sensors. The ratios indicate the fourth event to be, on the average, larger than the first three by about 0.2 unit.

amplitude ratios derived from the spectra of 12.8 sec of P coda (again with 10% cosine taper and corrected for noise), immediately following the 6.4 sec long P window, are shown in Figure D8. The P coda of the last shot appears, on the average, to be about 0.1 magnitude unit larger than those of the first three. A comparison of Figures D7 and D8 shows similar trends but generally smaller variation for P coda than for P.

Inter-event mean spectral slopes of P, with 10% cosine taper and corrected for noise, over the frequency range of 1 to 5 Hz, at both RSTN and GBA, are shown in Figure D9. Each of the spectral ratios E4/E1, E4/E2, and E4/E3 has a mean value of about -0.1/Hz. This "red-shift" in the spectrum of the last shot is significantly larger than that expected on the basis of the 0.2 magnitude unit difference in magnitudes (the latter value is about -0.02/Hz on the basis of theoretical spectra with yields estimated from the m_b values). Thus the last event appears to be rich in low frequency (or depleted in high frequencies) as compared to the first three shots.

We also obtained the P/P-coda spectral slopes for the four shots at the four RSTN stations. Results for the mean slopes, over the frequency range of 1 to 5 Hz, are shown in Figure D10. At each station, the spectral slope value for the last shot is lower than for the first three shots. Results from the GBA array were found to be unreliable due to poor S/N.

In a comparison of P spectra from several shots in close proximity to one another, Aki et al. (1970) observed the later shots to have larger amplitudes and lower frequency content than the first shot. They attributed this to changes in the medium properties due to shock waves from the earlier shot; the inelastic zone from the first shot contained crushed or cracked rocks which, for a later shot, preferentially attenuated the high frequencies and also gave rise to greater displacement. Our results in Figures D7 and D9 are therefore consistent with the possibility that the fourth shot was detonated within the inelastic zone of an earlier shot. Gupta and Blandford (1987) compared the spectra of P and P-coda at teleseismic distances for shots in

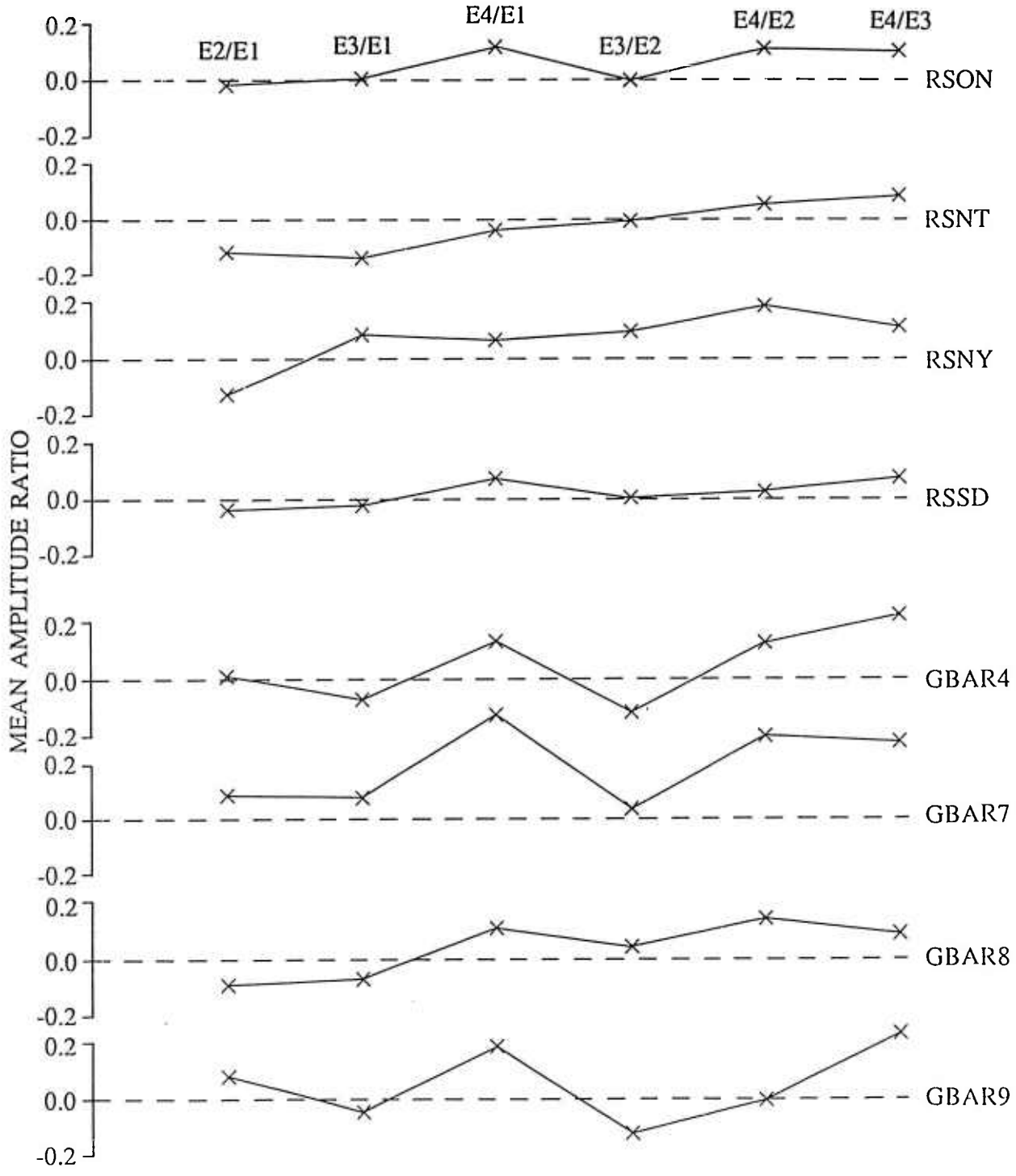

Figure D8. Inter-event mean spectral amplitude ratios of P coda, in log units and over the frequency range 1 to 5 Hz, for 4 RSTN and 4 GBA sensors. The ratios indicate the fourth event to be, on the average, larger than the first three by about 0.1 unit.

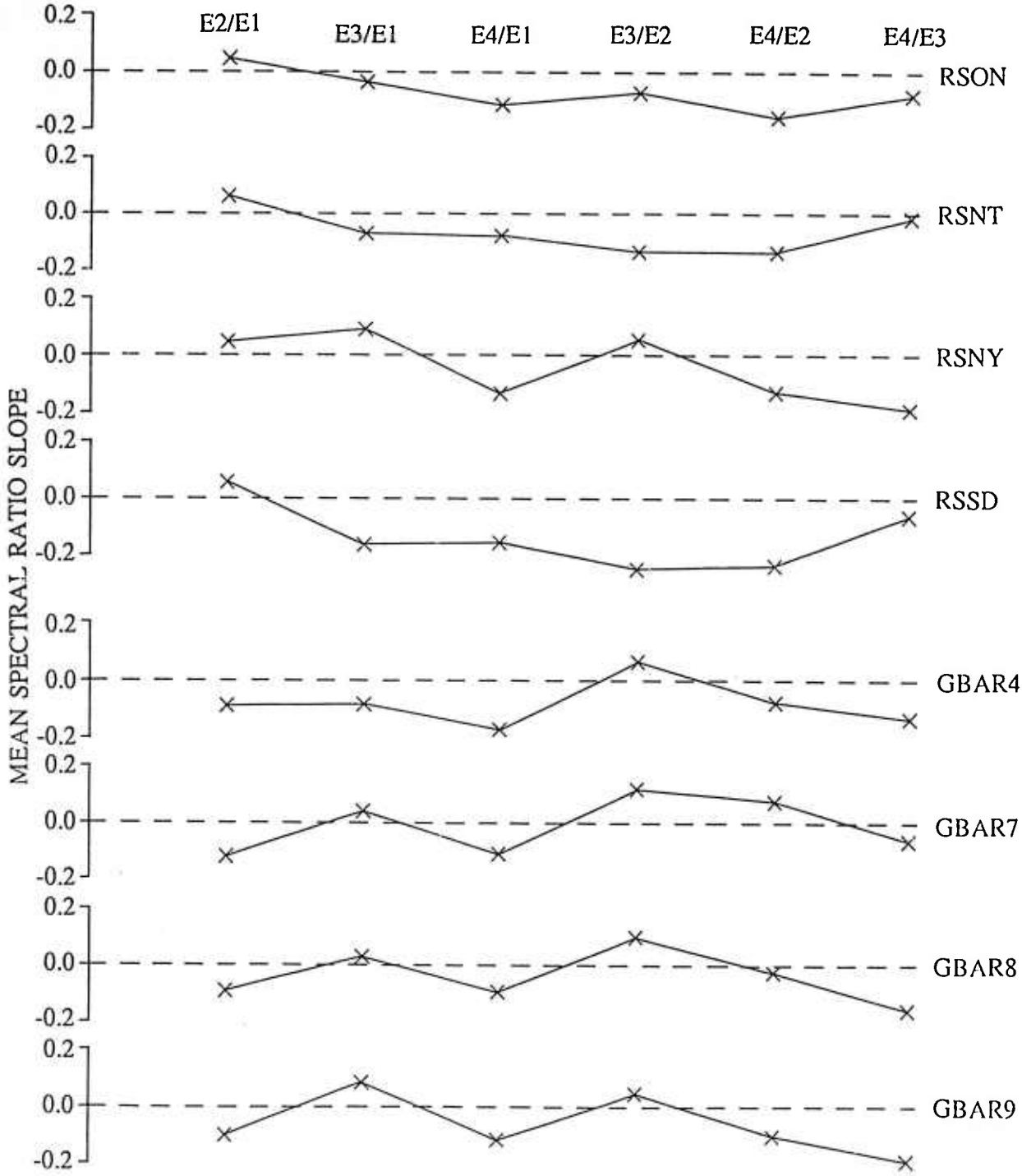

Figure D9. Inter-event mean spectral ratio slopes of P, in log units per Hz and over the frequency range 1 to 5 Hz, for 4 RSTN and 4 GBA sensors. The slope values indicate the fourth event to have, on the average, about 0.1 unit/Hz lower slope than the first three shots.

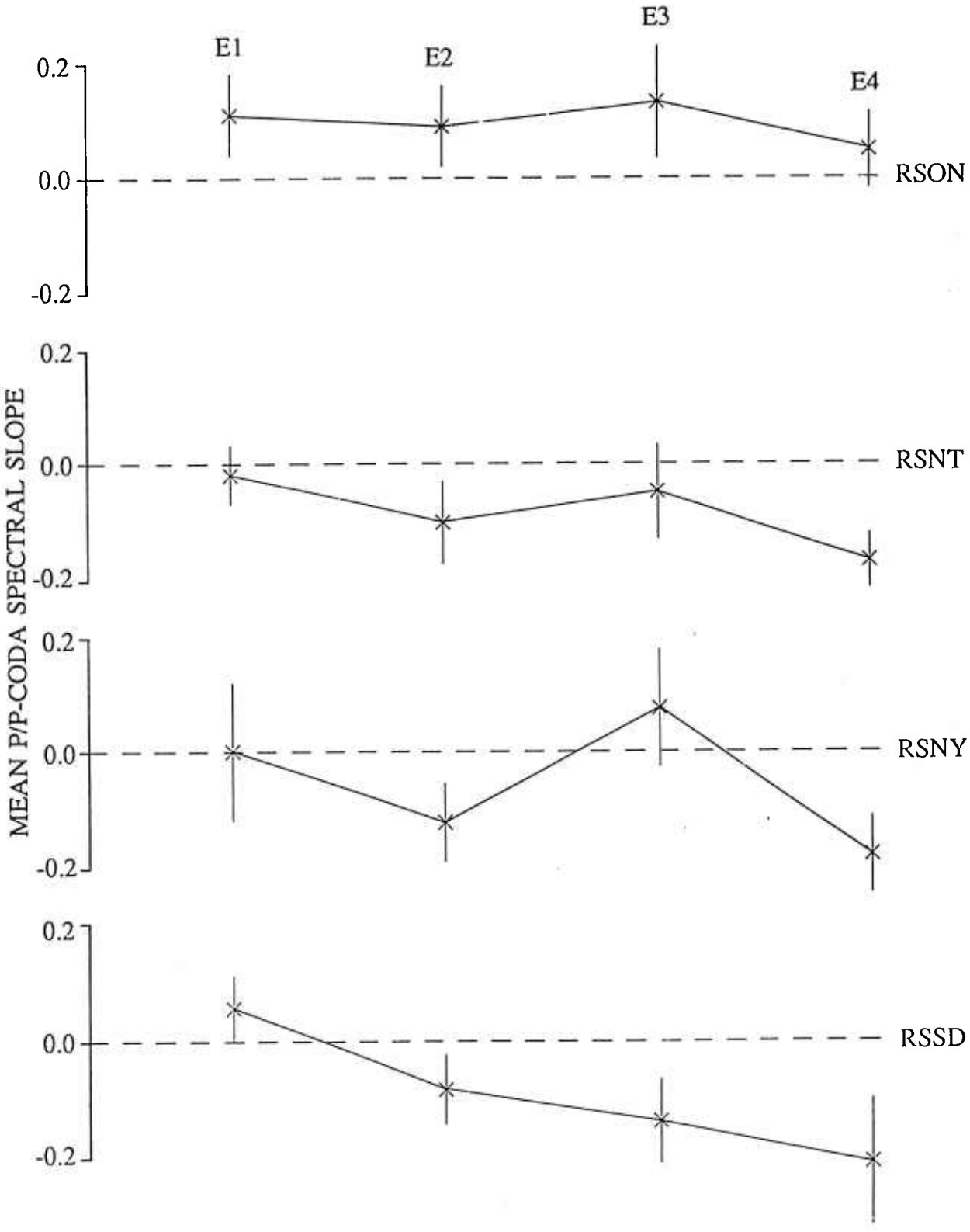

Figure D10. Mean P/P-coda spectral slopes, in log units per Hz and over the frequency range 1 to 5 Hz, for the four shots of October 16, 1982 recorded at the four RSTN stations. The vertical lines represent error bars with one standard deviation. At each station, the fourth shot has a lower spectral slope value than for the first three shots.

various velocity media and found both amplitude and spectral variation in P coda to be considerably smaller than in P, similar to the results in Figures D7 and D8. Furthermore, they found lower P/P-coda spectral slope, as for the fourth shot in Figure D10, to be an indication of lower medium velocity around the shot point. It is therefore quite possible that the yield of the fourth shot was no larger than the three earlier shots but that it was in close proximity of one or more earlier shots.

According to Borg (1983), the four explosions occurred within five minutes of one other, possibly to minimize disturbance at the city of Astrakhan some 30 to 40 km distant, and the yields of these shots were about 15 kt each. The Soviets are known to detonate shots near the cavity of a previous shot (e.g. Nordyke, 1973, Figure 30; Polskov et al., 1980, Figure 2). Therefore, it seems likely that the four shots were of equal yields, fired close to each other, and the last shot was influenced by the fracture zone of an earlier shot.

E. ANALYSIS OF DATA FROM SOVIET SALT SHOTS WITH KNOWN YIELDS

We analyzed teleseismic P arrivals from three USSR salt explosions with known yields and shot depths (Blandford, 1978) as recorded at the LRSM stations NP-NT and RK-ON. Two of these (shots of 22 April 1966 and 1 July 1968) had their epicenters in the Azgir region, approximately 48°N, 48°E, north of the Caspian region. The epicenter of the third (21 May 1968) was at Bukara, approximately 39°N, 65°E. All three explosions were well recorded at the three-component stations NP-NT and RK-ON. The vertical component records of these three salt shots, along with the U.S. salt shot Salmon, are shown in Figures E1 and E2. The analog record of the 1 July 1968 shot at both RK-ON and NP-NT was redigitized, as the earlier waveforms suffered from spikes acquired during the analog to digital conversion.

An examination of the spectra of the three Soviet salt explosions with known yields was made in order to test whether they are consistent with conventional scaling for salt, such as von Seggern and Blandford's (1972) scaling (equations C3, C4, and C5). Of the three Soviet shots, only two (22 April 1966 and 1 July 1968) were very near each other so that the propagation path effects may be considered to be the same. The spectral ratios (1 Jul 68)/(22 Apr 66) for P (6.4 sec windows) and P coda (12.8 sec windows) at both NP-NT and NP-NT are shown in Figure E3. The spectra were obtained with 10 % cosine taper and no smoothing. The spectral ratios were corrected for noise and only points with S/N power ratio of at least 2 are shown. The theoretical spectral ratios, also shown in Figure E3, were obtained by using values of the two medium-dependent constants, k_o and B to be 26 and 0, respectively.

Lyuke et al. (1976) used the von Seggern and Blandford source model to scale successfully the spectra of salt shots recorded at several distances. Their analysis, which included the 1.1 kt shot of 22 April 1966, indicated the best agreement between theory and observation when k_o and B were selected to be 11 and 0, respectively. They also considered the values k_o

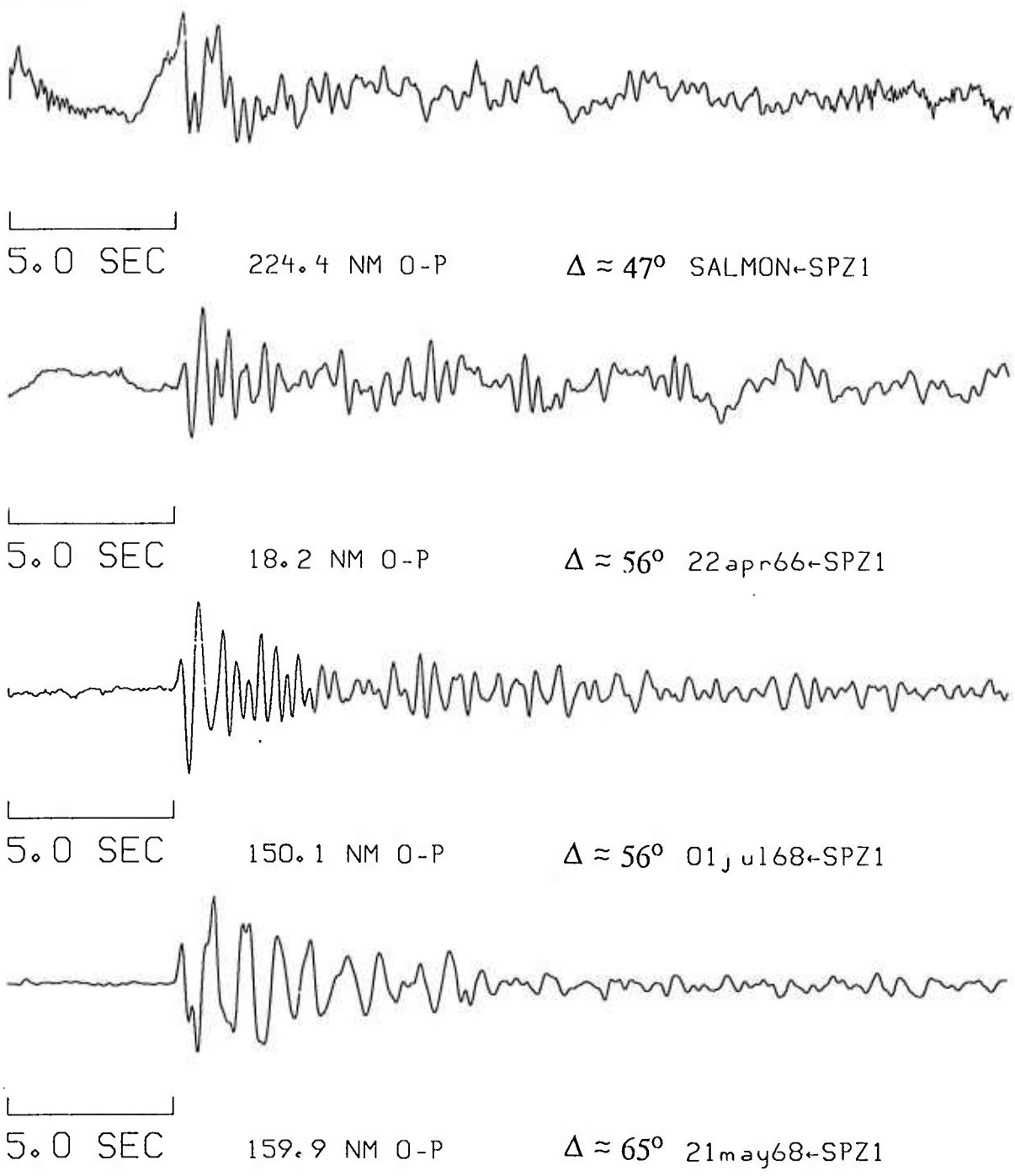

Figure E1. Vertical component records of four salt shots at the LRSM station NP-NT. Δ denotes the epicentral distance in degrees.

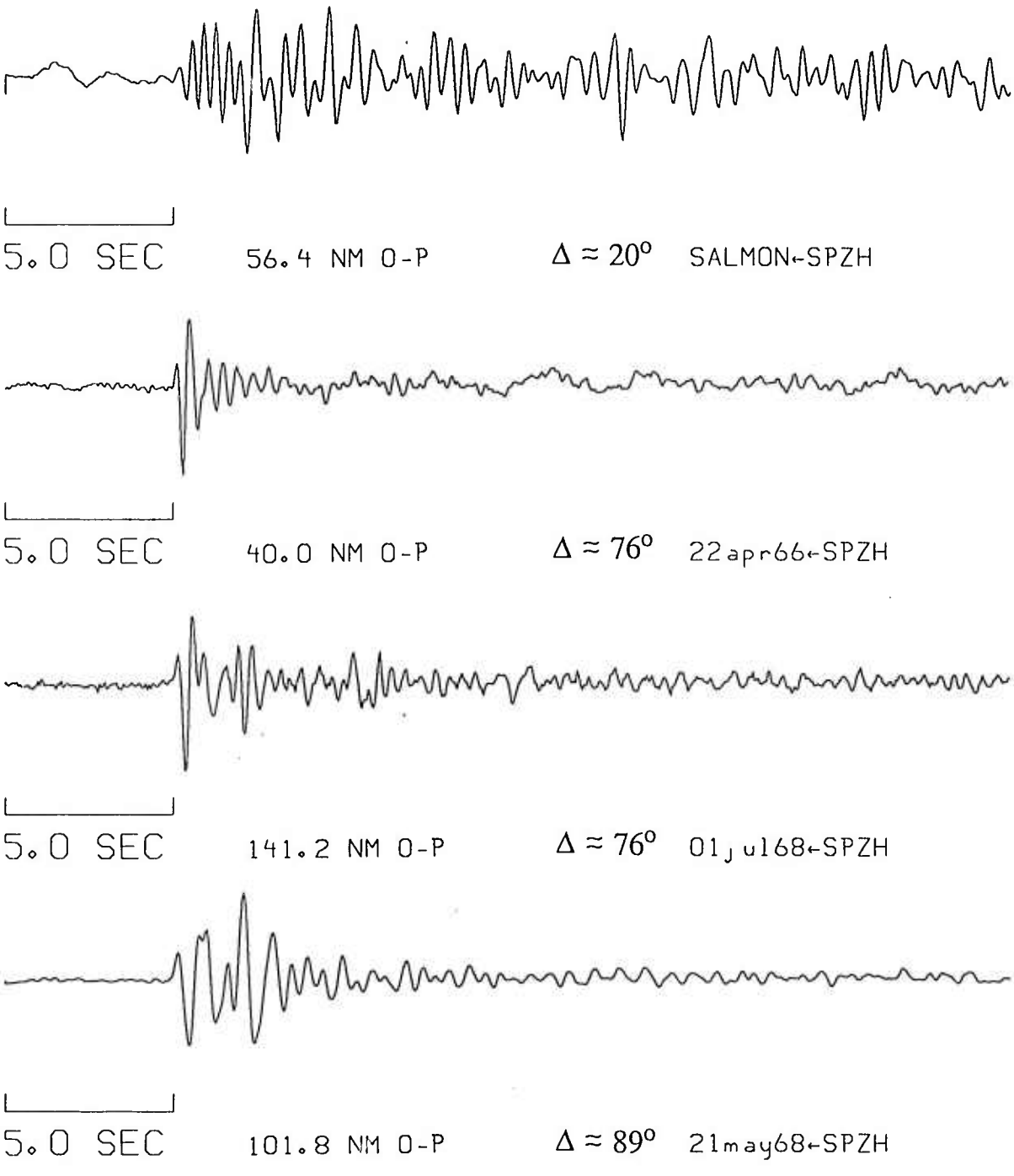

Figure E2. Records of the same four salt shots as in Figure E1 at the LRSM station RK-ON. Δ denotes the epicentral distance in degrees.

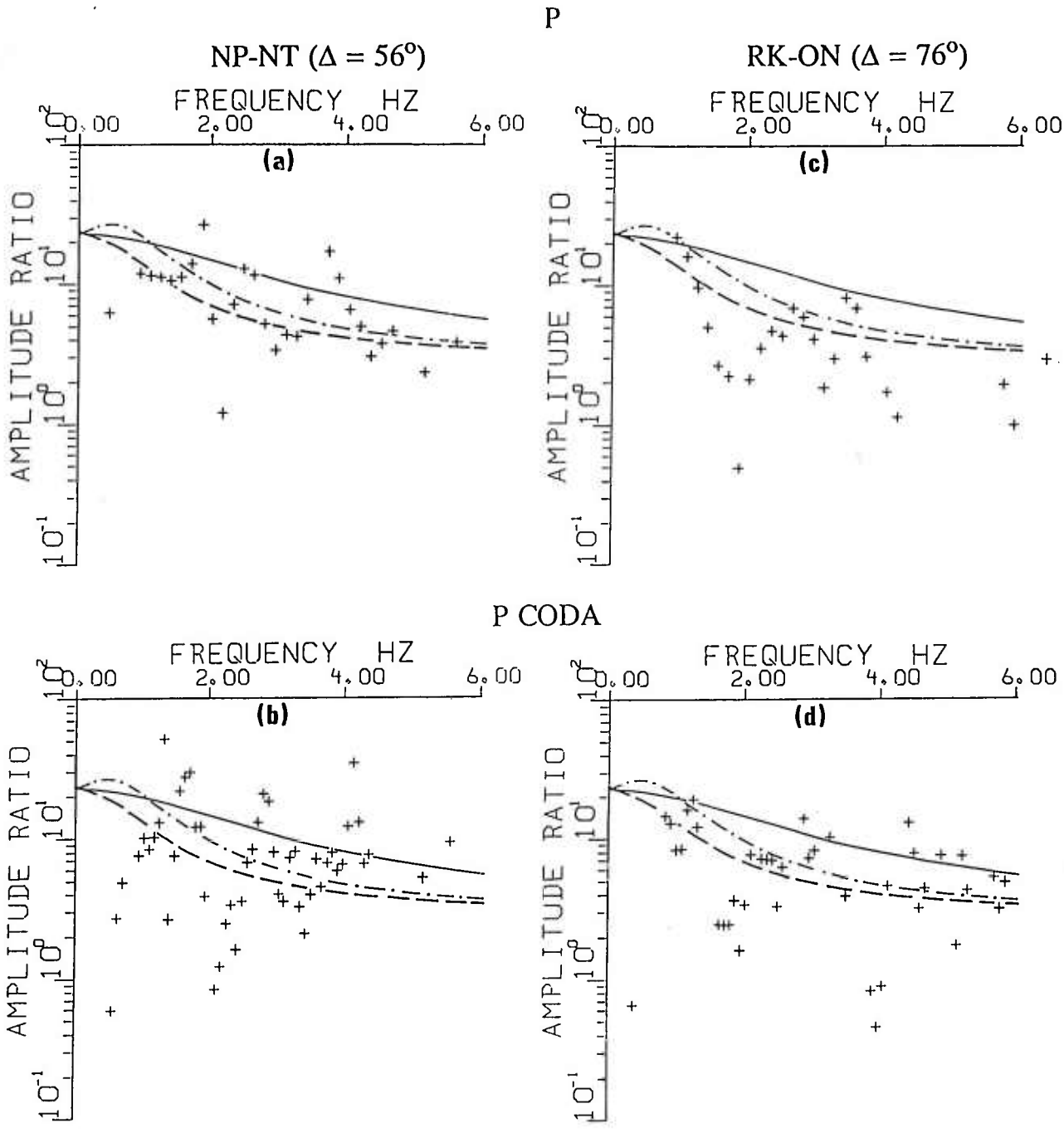

Figure E3. Observed spectral ratios for P and P-coda at stations NP-NT and RK-ON and theoretical spectral ratios

= 11, B = 1. Theoretical spectral ratios for these two sets of values of k_o and B are also shown in Figure E3. Considering all four spectral ratios, the theoretical spectra with k_o = 11 and B = 0 appear to be the closest to the observed data. It seems therefore that for the Soviet salt shots, k_o is considerably smaller than for the U.S. salt shot Salmon. Since the explosion rise time varies inversely as k_o, the Soviet salt is indicated to be "softer" than the Salmon salt. This could be due to the Salmon salt being harder (possibly because of larger depth and overburden pressure) than the USSR salt shot as suggested by a comparison of their physical properties, listed in Table E1.

TABLE E1

COMPARISON OF SALMON AND USSR 1.1 KT SHOT SALT PROPERTIES

Property	SALMON	USSR Shot
Yield	5.3 kt	1.1 kt
Depth	828 m	161 m
Scaled depth	475 m/kt$^{1/3}$	156 m/kt$^{1/3}$
P-wave velocity	4.67 km/sec	4.2 km/sec
Density	2.2 gm/cc	2.15 gm/cc
Young's modulus	4.0 x 10^5 kb	3.2 x 10^5 kb
Reference	Mueller (1969)	Lyuke et al. (1976)

We used the maximum-likelihood multichannel deconvolution method of Shumway and Der (1985), described in Section D, to obtain the deconvolved source terms for the three USSR salt explosions with known yields. Figure E4 shows the deconvolved waveforms which are obtained by making simultaneous use of the vertical and radial component records at the LRSM station NP-NT. The source functions have been corrected for instrumental response and attenuation (by assuming t* = 0.2), but no correction due to differences in yields has been applied. Note that the scaled depths (denoted by S.D. in Figure E4) vary considerably. Only the two deeper (and larger scaled depth) explosions show clear evidence of P and pP arrivals;

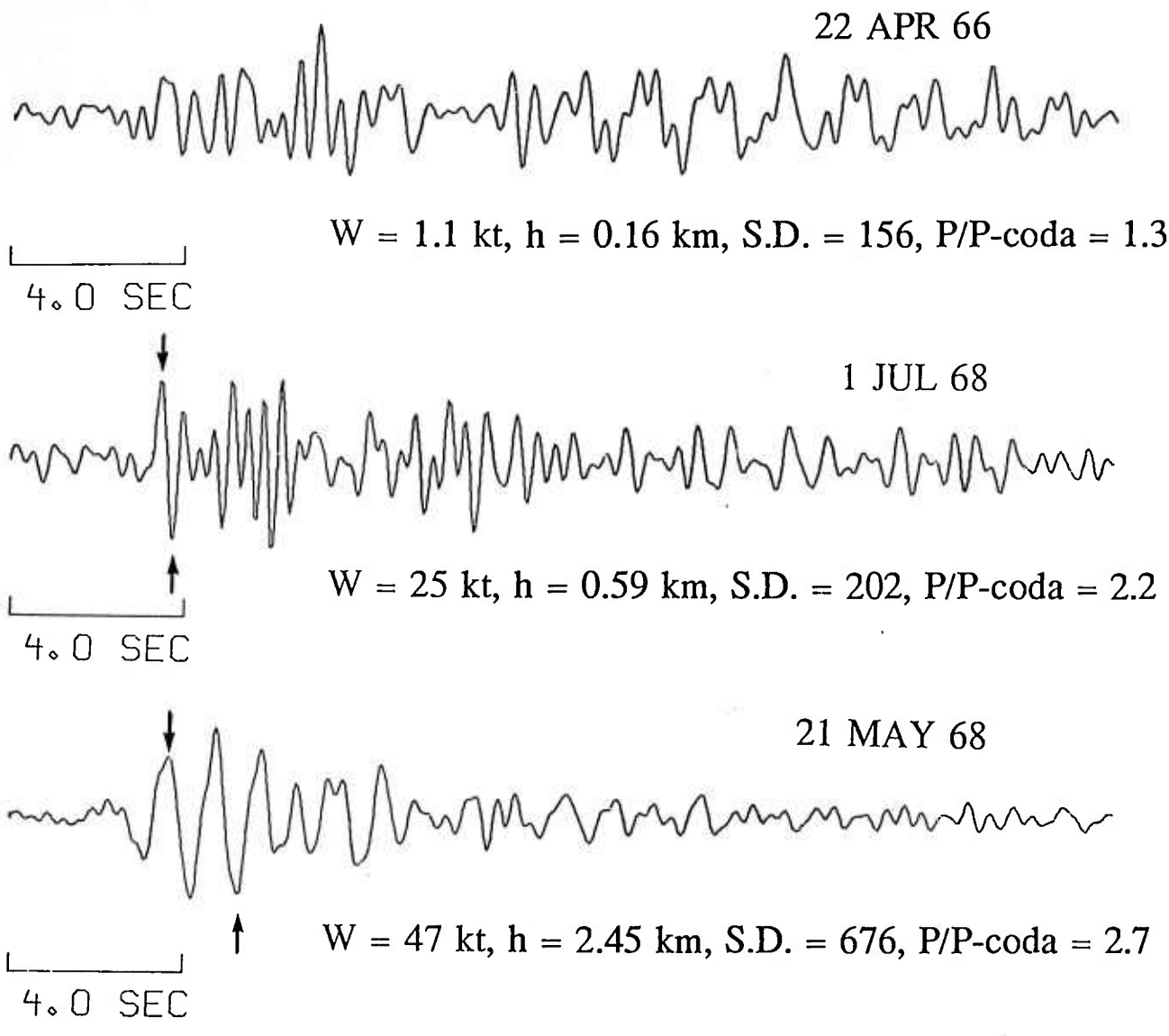

Figure E4. Deconvolved source functions of three USSR salt shots derived from their vertical and radial component records at NP-NT. The arrows denote the peaks on P and pP arrivals. The letters W, h, S.D., and P/P-coda denote yield (kt), shot depth, scaled depth, and average value over the frequency range of 0.5 to 3.0 Hz, respectively.

the pP - P times agree well with the expected values (Blandford, 1978). The average ratio P/P-coda (over the frequency range of 0.5 to 3 Hz) values are also indicated, and they seem to be larger for larger scaled depths, perhaps because an overburied shot is likely to generate less near-source coda than an underburied shot. Note that reciprocal of the average ratio P/P-coda is a measure of the complexity (e.g. Aki, 1982).

REFERENCES

Adams, W. M. and D. C. Allen (1960). Seismic decoupling for explosions in spherical cavities, *UCRL-6086*, Lawrence Radiation Laboratory, University of California, Livermore, California.

Aki, K. (1982). Scattering and attenuation, *Bull. Seism. Soc. Am. 72*, S319-S330.

Aki, K., M. Bouchon, and P. Reasenberg (1974). Seismic source function for an underground nuclear explosion, *Bull. Seism. Soc. Am. 64*, 131-148.

Aki, K., T. DeFazio, P. Reasenberg, and A. Nur (1970). An active experiment with earthquake fault for an estimation of the *in situ* stress, *Bull. Seism. Soc. Am. 60*, 1315-1336.

Aki, K. and P. G. Richards (1980). *Quantitative Seismology*, W. H. Freeman and Company, San Francisco, California.

Banda, E., N. Deichmann, L. W. Braile, and J. Ansorge (1982). Amplitude study of the Pg phase, *J. Geophys. 51*, 153-164.

Barker, B. W., Z. A. Der, and C. P. Mrazek (1981). The effect of crustal structure on the regional phases Pg and Lg at the Nevada Test Site, *J. Geophys. Res. 86*, 1686-1700.

Bennett, T. J., J. R. Murphy, and H. K. Shah (1987). Theoretical analysis of regional phase behavior, *SSS-R-87-8113*, S-CUBED, La Jolla, California.

Blandford, R. R. (1976). Experimental determination of scaling laws for contained and cratering explosions, *SDAC-TR-76-3*, Teledyne Geotech, Alexandria, Virginia.

Blandford, R. R. (1978). Spectral ratios for explosions in salt, *SDAC-TR-78-1*, Teledyne Geotech, Alexandria, Virginia.

Blandford, R. R. (1981). Seismic discrimination problems at regional distances, in *Identification of Seismic Sources - Earthquake or Underground Explosion*, E. S. Husebye and S. Mykkeltveit, Editors, D. Reidel Publishing Co., Dordrecht, Holland, 695-740.

Blandford, R. R. (1982). Seismic event discrimination, *Bull. Seism. Soc. Am. 72*, S 69-S 87.

Blandford, R. R. and T. W. McElfresh (1982). Studies of explosions in salt using teleseismic data (U), *VSC-TR-82-18*, Teledyne Geotech, Alexandria, Virginia.

Blandford, R. R. and J. R. Woolson (1979). Experimental spectral analysis of Salmon/Sterling decoupling, *SDAC-TR-79-3*, Teledyne Geotech, Alexandria, Virginia.

Boatwright, J. (1978). Detailed spectral analysis of two small New York State earthquakes, *Bull. Seism. Soc. Am. 68*, 1117-1131.

Borcherdt, R. D., J. H. Healy, W. H. Jackson, and D. H. Warren (1967). Seismic measurements of explosions in the Tatum salt dome, Mississippi, *Tech. Letter Crustal Studies - 48*, U. S. Geological Survey.

Borg, I. Y. (1983). Peaceful nuclear explosions in Soviet gas condensate fields, *Energy and Technology Review (May 1983)*, 30-33. Lawrence Livermore National Laboratory, Livermore, California, Livermore, California.

Bouchon, M. (1982). The complete synthesis of seismic crustal phases at regional distances, *J. Geophys. Res. 87*, 1735-1741.

Campillo, M., M. Bouchon, and B. Massinon (1984). Theoretical study of the excitation, spectral characteristics, and geometrical attenuation of regional seismic phases, *Bull. Seism. Soc. Am. 74*, 79-90.

Cisternas, A. (1964). The radiation of elastic waves from a spherical cavity in a half space, *Ph. D. thesis*, Caltech, Pasadena, California.

Dainty, A. M. (1985). Coda observed at NORSAR and NORESS, *AFGL-TR-85-0199*, Georgia Tech Research Institute, Atlanta, Georgia.

Day, S. M., N. Rimer, T. G. Barker, E. J. Halda, and B. Shkoller (1986). Numerical study of depth of burial effects on the seismic signature of underground explosions, *SSS-R-86-7398*, S-CUBED, La Jolla, California.

Der, Z. A. and A. C. Lees (1985). Methodologies for estimating t*(f) from short-period body waves and regional variations of t*(f) in the United States, Geophys. J. 82, 125-140.

Der, Z. A., M. E. Marshall, A. O'Donnell, and T. W. McElfresh (1984). Spatial coherence structure and attenuation of the Lg phase, site effects, and interpretation of the Lg coda, *Bull. Seism. Soc. Am. 74*, 1125-1147.

Der, Z. A., R. H. Shumway, and A. C. Lees (1987). Multi-channel deconvolution of P waves at seismic arrays, *Bull. Seism. Soc. Am. 77*, 195-211.

Douglas, A., P. D. Marshall, and J. B. Young (1987). The P waves from the Amchitka Island explosions, *Geophys. J. 90*, 101-117.

Evernden, J. F., C. B. Archambeau, and E. Cranswick (1986). An evaluation of seismic decoupling and underground nuclear test monitoring using high-frequency seismic data, *Rev. of Geophysics 24*, 143-215.

Ferguson, J. F. (1986). Geophysical investigations at Pahute Mesa, Nevada, *DARPA/AFGL Seismic Research Symposium*, 6-8 May 1986, Colorado Springs, Colorado.

Flynn, E. C. (1986). Effects of source depth on near source seismograms, *M. S. Thesis*, Southern Methodist University, Dallas, Texas.

Glaser, R. E., S. R. Taylor, M. D. Denny, and E. S. Vergino (1986). Regional discrimination of NTS explosions and Western U. S. earthquakes: multivariate discriminants, *UCID-20930*, Lawrence Livermore National Laboratory, Livermore, California.

Gupta, I. N. and R. R. Blandford (1983). A mechanism for generation of short-period transverse motion from explosions, *Bull. Seism. Soc. Am. 73*, 571-591.

Gupta, I. N. and R. R. Blandford (1987). A study of P waves from Nevada Test Site explosions: near-source information from teleseismic observations, *Bull. Seism. Soc. Am. 77*, 1041-1056.

Gupta, I. N., J. A. Burnetti, R. A. Wagner, and M. Marshall (1984). Discrimination between quarry blasts, nuclear explosions, and earthquakes, *TGAL-TR-84-1*, Teledyne Geotech, Alexandria, Virginia..

Gupta, I. N. and K. L. McLaughlin (1987). Attenuation of ground motion in the Eastern United States, *Bull. Seism. Soc. Am. 77*, 366-383

Gupta, I. N., K. L. McLaughlin, and R. A. Wagner (1985). Analysis of regional data from cratering and non-cratering nuclear explosions, *TGAL-85-5*, Teledyne Geotech, Alexandria, Virginia.

Gupta, I. N., K. L. McLaughlin, and R. A. Wagner (1986a). Studies in decoupling using Salmon/Sterling and Soviet salt explosions, *TGAL-85-9*, Teledyne Geotech, Alexandria, Virginia.

Gupta, I. N., K. L. McLaughlin, R. A. Wagner, T. W. McElfresh, M. E. Marshall, and R. S. Jih (1986b). Studies in decoupling, *TGAL-86-08*, Teledyne Geotech, Alexandria, Virginia.

Gupta, I. N., D. H. von Seggern, and R. A. Wagner (1982). A study of variations in the horizontal to vertical Lg amplitude ratio in the eastern United States, *Bull. Seism. Soc. Am. 72*, 2081-2088.

Kisslinger, C. (1963). The generation of the primary seismic signal by a contained explosion, *Vesiac State-of-the-Art Report 4410-48-X*, University of Michigan, Ann Arbor, Michigan.

Langston, C. A. (1982). Aspects of Pn and Pg propagation at regional distances, *Bull. Seism. Soc. Am. 72*, 457-471.

Larson, D. B. (1982). Inelastic wave propagation in sodium chloride, *Bull. Seism. Soc. Am. 72*, 2107-2130.

Lyuke, E. I., S. K. Daragan, and V. E. Peregontseva (1976). Forecasting the seismic wave spectra of large underground detonations from the spectra of small preliminary detonations, *Izvestiya, Earth Physics (English Edition) 12 (no. 2)*, 103-109.

McLaughlin, K. L., M. E. Marshall, R. A. Wagner, I. N. Gupta, T. W. McElfresh, and A. C. Lees (1987). A study of explosion source functions and amplitudes using available far-field seismic data, *TGAL-87-06*, Teledyne Geotech, Alexandria, Virginia.

Mueller, R. A. and J. R. Murphy (1971). Seismic characteristics of underground nuclear detonations, Part I. Seismic spectrum scaling, *Bull. Seism. Soc. Am. 61*, 1675-1692.

Murphey, B. F. (1961). Particle motions near explosions in halite, *J. Geophys. Res. 66*, 947-958.

Murphy, J. R. (1975). Analysis of near-field ground motion spectra from earthquakes and explosions, *Semi-annual Technical Report (ARPA Order No. 1827)*, Computer Sciences Corporation, Falls Church, Virginia.

Perl, N., F. J. Thomas, J. Trulio, and W. L. Woodie (1979). Effect of burial depth on seismic signals, Vol. 1, *PSR Rept. 815*, Pacific Sierra Research Corp., Santa Monica, California.

Polskov, M. K., L. J. Brodov, L. V. Mitronova, D. Michon, R. Garotta, P. C. Layotte, and F. Coppens (1980). Utilisation combinee des ondes longitudinales et transversales en sismique reflexion, *Geophysical Prospecting 28*, 185-207.

Pomeroy, P. W., W. J. Best, and T. V. McEvilly (1982). Test ban treaty verification with regional data - a review, *Bull. Seism. Soc. Am. 72*, S 89-S 129.

Rimer, N., J. T. Cherry, S. M. Day, T. C. Bache, J. R. Murphy, and A. Maewal (1979). Two-dimensional calculation of Piledriver, analytic continuation of finite difference source calculations, analysis of free field data from Merlin and summary of current research, *SSS-R-79-4121*, Systems, Science, and Software, La Jolla, California.

Rivers, D. W. (1984). Effect of crustal structure on Lg, *SDAC-TR-80-7B*, Teledyne Geotech, Alexandria, Virginia.

Rulev, B. G. (1965). The energy in a Rayleigh surface wave from explosions in different kinds of rock, *Izvestiya, Earth Physics (English Edition), No. 4*, 233-241.

Shumway, R. H. and Z. A. Der (1985). Deconvolution of multiple time series, *Technometrics 27*, 385-393.

Springer, D. L. (1966). Calculation of first-zone P wave amplitudes for Salmon event and for decoupled sources, *J. Geophys. Res. 71*, 3459-3467.

Springer, D. L. and M. D. Denny (1976). Seismic spectra of events at regional distances, *UCRL-52048*, Lawrence Livermore Laboratory, Livermore, California.

Springer, D., M. Denny, J. Healy, and W. Mickey (1968). The Sterling experiment: decoupling of seismic waves by a shot-generated cavity, *J. Geophys. Res. 73*, 5995-6011.

Springer, D. L. and R. L. Kinnaman (1971). Seismic source summary for U. S. underground nuclear explosions, 1961-1970, *Bull. Seism. Soc. Am. 61*, 1073-1098.

Stump, B. R. (1987). Mathematical representation and physical interpretation of a contained chemical explosion in alluvium, *Bull. Seism. Soc. Am. 77*, 1312-1325.

Stump, B. R. and R. E. Reinke (1987). Experimental seismology: *in situ* source experiments, *Bull. Seism. Soc. Am. 77*, 1295-1311.

Thornbrough, A. D., E. S. Ames, and H. L. Hawk (1960). Instrumentation Systems - Project Cowboy, *SC-4470(RR)*, Sandia Corporation, Albuquerque, New Mexico.

von Seggern, D. H. and R. R. Blandford (1972). Source time functions and spectra for underground nuclear explosions, *Geophys. J. 31*, 83-97.

Warren, D. H., J. H. Healy, and W. H. Jackson (1966). Crustal seismic measurements in southern Missouri, *J. Geophys. Res. 71*, 3437-3458.

DISTRIBUTION LIST
FOR UNCLASSIFIED REPORTS
DARPA-FUNDED PROJECTS
(Last Revised: 3 Mar 1988)

RECIPIENT	NO. OF COPIES
DEPARTMENT OF DEFENSE	
DARPA/GSD ATTN: Dr. R. Alewine and Dr. R. Blandford 1400 Wilson Boulevard Arlington, VA 22209-2308	2
DARPA/PM 1400 Wilson Boulevard Arlington, VA 22209-2308	1
Defense Intelligence Agency Directorate for Scientific and Technical Intelligence Washington, D.C. 20301	1
Defense Nuclear Agency Shock Physics Washington, D.C. 20305-1000	1
Defense Technical Information Center Cameron Station Alexandria, VA 22314	12
DEPARTMENT OF THE AIR FORCE	
AFGL/LWH ATTN: Dr. J. Cipar and Mr. J. Lewkowicz Terrestrial Sciences Division Hanscom AFB, MA 01731-5000	2
AFOSR/NPG ATTN: Director Bldg. 410, Room C222 Bolling AFB, Washington, D.C. 20332	1

AFTAC/DA 1
ATTN: STINFO Officer
Patrick AFB, FL 32925-6001

AFTAC/TT 3
Patrick AFB, FL 32925-6001

AFWL/NTESG 1
Kirtland AFB, NM 87171-6008

DEPARTMENT OF THE NAVY

NORDA 1
ATTN: Dr. J.A. Ballard
Code 543
NSTL Station, MS 39529

DEPARTMENT OF ENERGY

Department of Energy 1
ATTN: Mr. Max A. Koontz (DP-52)
International Security Affairs
1000 Independence Avenue
Washington, D.C. 20545

Lawrence Livermore National Laboratory 2
ATTN: Dr. J. Hannon and Dr. M. Nordyke
University of California
P.O. Box 808
Livermore, CA 94550

Los Alamos Scientific Laboratory 2
ATTN: Dr. K. Olsen and Dr. T. Weaver
P.O. Box 1663
Los Alamos, NM 87544

Sandia Laboratories 1
ATTN: Mr. P. Stokes
Geosciences Department 1255
Albuquerque, NM 87185

OTHER GOVERNMENT AGENCIES

Central Intelligence Agency 1
ATTN: Dr. L. Turnbull
OSI/NED, Room 5G48
Washington, D.C. 20505

U.S. Arms Control and Disarmament Agency 1
ATTN: Dr. M. Eimer
Verification and Intelligence Bureau, Rm 4953
Washington, D.C. 20451

U.S. Arms Control and Disarmament Agency 1
ATTN: Mrs. M. Hoinkes
Multilateral Affairs Bureau, Rm 5499
Washington, D.C. 20451

U.S. Geological Survey 1
ATTN: Dr. T. Hanks
National Earthquake Research Center
345 Middlefield Road
Menlo Park, CA 94025

U.S. Geological Survey 1
ATTN: Dr. R. Masse
Global Seismology Branch
Box 25046, Stop 967
Denver Federal Center
Denver, CO 80225

UNIVERSITIES

Boston College 1
ATTN: Dr. A. Kafka
Western Observatory
381 Concord Road
Weston, MA 02193

California Institute of Technology 1
ATTN: Dr. D. Harkrider
Seismological Laboratory
Pasadena, CA 91125

Columbia University 1
ATTN: Dr. L. Sykes
Lamont-Doherty Geological Observatory
Palisades, NY 10964

Cornell University 1
ATTN: Dr. M. Barazangi
INSTOC
Snee Hall
Ithaca, NY 14853

Harvard University 1
ATTN: Dr. J. Woodhouse
Hoffman Laboratory
20 Oxford Street
Cambridge, MA 02138

Massachusetts Institute of Technology 3
ATTN: Dr. S. Soloman, Dr. N. Toksoz, and Dr. T. Jordan
Department of Earth and Planetary Sciences
Cambridge, MA 02139

Southern Methodist University 1
ATTN: Dr. E. Herrin
Geophysical Laboratory
Dallas, TX 75275

State University of New York at Binghamton 1
ATTN: Dr. F. Wu
Department of Geological Sciences
Vestal, NY 13901

St. Louis University 2
ATTN: Dr. O. Nuttli and Dr. R. Herrmann
Department of Earth and Atmospheric Sciences
3507 Laclede
St. Louis, MO 63156

The Pennsylvania State University 1
ATTN: Dr. S. Alexander
Geosciences Department
403 Deike Building
University Park, PA 16802

University of Arizona 1
ATTN: Dr. T. Wallace
Department of Geosciences
Tucson, AZ 85721

University of California, Berkeley 1
ATTN: Dr. T. McEvilly
Department of Geology and Geophysics
Berkeley, CA 94720

University of California Los Angeles 1
ATTN: Dr. L. Knopoff
405 Hilgard Avenue
Los Angeles, CA 90024

University of California, San Diego 1
ATTN: Dr. J. Orcutt
Scripps Institute of Oceanography
La Jolla, CA 92093

University of Colorado 1
ATTN: Dr. C. Archambeau
CIRES
Boulder, CO 80309

University of Illinois 1
ATTN: Dr. S. Grand
Department of Geology
1301 West Green Street
Urbana, IL 61801

University of Michigan 1
ATTN: Dr. T. Lay
Department of Geological Sciences
Ann Arbor, MI 48109-1063

University of Nevada 1
ATTN: Dr. K. Priestley
Mackay School of Mines
Reno, NV 89557

University of Southern California 1
ATTN: Dr. K. Aki
Center for Earth Sciences
University Park
Los Angeles, CA 90089-0741

DEPARTMENT OF DEFENSE CONTRACTORS

Applied Theory, Inc. 1
ATTN: Dr. J. Trulio
930 South La Brea Avenue
Suite 2
Los Angeles, CA 90036

Center for Seismic Studies 2
ATTN: Dr. C. Romney and Mr. R. Perez
1300 N. 17th Street, Suite 1450
Arlington, VA 22209

ENSCO, Inc. 1
ATTN: Mr. G. Young
5400 Port Royal Road
Springfield, VA 22151

ENSCO, Inc. 1
ATTN: Dr. R. Kemerait
445 Pineda Court
Melbourne, FL 32940

Gould Inc. 1
ATTN: Mr. R. J. Woodard
Chesapeake Instrument Division
6711 Baymeado Drive
Glen Burnie, MD 21061

Pacific Sierra Research Corp. 1
ATTN: Mr. F. Thomas
12340 Santa Monica Boulevard
Los Angeles, CA 90025

Rockwell International 1
ATTN: B. Tittmann
1049 Camino Dos Rios
Thousand Oaks, CA 91360

Rondout Associates, Inc. 1
ATTN: Dr. P. Pomeroy
P.O. Box 224
Stone Ridge, NY 12484

Science Applications, Inc. 1
ATTN: Dr. T. Bache, Jr.
P.O. Box 2351
La Jolla, CA 92038

Science Horizons 2
ATTN: Dr. T. Cherry and Dr. J. Minster
710 Encinitas Blvd.
Suite 101
Encinitas, CA 92024

Sierra Geophysics, Inc. 2
ATTN: Dr. R. Hart and Dr. G. Mellman
11255 Kirkland Way
Kirkland, WA 98124

SRI International 1
ATTN: Dr. A. Florence
333 Ravensworth Avenue
Menlo Park, CA 94025

S-Cubed, A Division of 1
Maxwell Laboratories Inc.
ATTN: Dr. S. Day
P.O. Box 1620
La Jolla, CA 92038-1620

S-Cubed, A Division of
Maxwell Laboratories Inc.
ATTN: Mr. J. Murphy
11800 Sunrise Valley Drive
Suite 1212
Reston, VA 22091 — 1

Teledyne Geotech
ATTN: Dr. Z. Der and Mr. W. Rivers
314 Montgomery Street
Alexandria, VA 22314 — 2

Woodward-Clyde Consultants
ATTN: Dr. L. Burdick and Dr. J. Barker
556 El Dorado St.
Pasadena, CA 91105 — 2

NON-U.S. RECIPIENTS

National Defense Research Institute FOA 290
ATTN: Dr. O. Dahlman
Box 27322
S-10254 Stockholm, Sweden — 1

Blacknest Seismological Center
ATTN: Mr. P. Marshall
Atomic Weapons Research Establishment
UK Ministry of Defence
Brimpton, Reading, Berks. RG7-4RS
United Kingdom — 1

NTNF NORSAR
ATTN: Dr. F. Ringdal
P.O. Box 51
N-2007 Kjeller
Norway — 1

OTHER DISTRIBUTION

To be determined by the project office — 9